University of Stuttgart

Institute of Geodesy

Coherency Analysis between SGs at BFO and Strasbourg

Master Thesis

GEOENGINE

at University of Stuttgart

Ying ZHANG

Stuttgart, Dec. 2013

Supervisors: Dr. Rudolf Widmer-Schnidrig
University of Stuttgart

Prof. Dr.-Ing. Nico Sneeuw
University of Stuttgart

Erklärung der Urheberschaft

Ich erkläre hiermit an Eides statt, dass ich die vorliegende Arbeit ohne Hilfe Dritter und ohne Benutzung anderer als der angegebenen Hilfsmittel angefertigt habe; die aus fremden Quellen direkt oder indirekt übernommenen Gedanken sind als solche kenntlich gemacht. Die Arbeit wurde bisher in gleicher oder ähnlicher Form in keiner anderen Prüfungsbehörde vorgelegt und auch noch nicht veröffentlicht.

Ort, Datum   Unterschrift

Acknowledgment

First I want to express deepest gratitude to Dr. Rudolf Widmer-Schnidrig, my supervisor for offering this master thesis topic and tutoring me! He has helped through all stages of this thesis. Without his patient guidance and continuous encouragement, I would not come to these exciting results. Thanks to Prof. Nico Sneeuw for providing valuable recommendations. Prof. Nico Sneeuw's attitude to science and research inspires and encourages me to get through the difficulties.

Thanks to Mrs. Severine Rosat (EOST, Strasbourg) for providing the GGP data and the hydrological data of Strasbourg. Thanks to Mr. Jean-Paul Boy (EOST, Strasbourg) for calculating GGP loadings. Thanks to Mr. Hartmut Wziontek (BKG, Leipzig) for providing the easy to use polar motion calculation program. Mr. Franz Barthelmes (GFZ, Potsdam) helped calculating the gravity disturbances of the two stations from GRACE measurements. Mr. Qiang Chen has helped me with learning LaTex. Mr. Balaji Devaraju has given me some helpful suggestions on hydrological corrections.

Thanks to my parents for bringing me up and financing my study in Stuttgart. It is of challenge for a Chinese family to support their child to study abroad. My parents' hard working would always encourage me spare no pains in my life.

Thanks to all staffs working or has worked for Master program GEOENGINE. They are Prof. Dr.-Ing. Wolfgang Keller, Prof. Dieter Fritsch, Prof. Dr.-Ing. Alfred Kleusberg, Dr.-Ing. Michael Cramer, Dr. Matthias Weigelt, Mr. Matthias Roth, Dr.-Ing. Friedrich W. Krumm. Without their work, I would not be able to solve these problems in my thesis.

The two years in Stuttgart have taught me a lot, not only the knowledge from the university. In the end, I would like to thank again all the people who have helped me with finishing the thesis and living here!

Abstract

The twin satellite GRACE mission has provided high-precision, spaceborne measurements of the Earth time-varying gravity field. Independent validation of the GRACE derived gravity field models using superconducting gravimeters (SGs) has been discussed controversially in the literature, since SGs provide gravity observations at a stationary point with high-precision and low instrumental drift. To evaluate whether ground based gravity observations can be used to validate GRACE gravity field models we compare 3 years of continuous SG data from the Strasbourg Observatory (ST) and the Black Forest Observatory (BFO). These two stations are only 57.5 km apart which is twelve times smaller than the shortest resolved wavelength (about 700 km) in the weekly GRACE gravity field models. Thus, since GRACE derived models predict essentially the same temporal gravity field variations for both ST and BFO we require high correlation between ST and BFO at periods longer than one week. A lack of correlation at these long periods would point to more local sources of these gravity variations and would make a GRACE validation impossible, if BFO and ST are representatives of typical GGP stations. The coherence between the residuals of the two stations ranges from 0.65 to 0.9 at periods from 15 days to 30 days. We further investigate the local hydrology of the SG stations which may not be embodied in the GRACE predictions. Local hydrological signals are known to be a major signal in gravity residuals at period longer than 1 day. We inspect locally recorded precipitation and global hydrological models data in this context. The difference of residuals between the two stations is enlarged after correcting for the local hydrological effects. Correcting for the local hydrological effects using GLDAS model or ERA-interim does not improve the coherence from 15 days to 30 days significantly. The trends of SG residual variations before correcting for local hydrology agree well with GRACE predictions. We suggest more sophisticated measuring and modelling of local hydrology to better estimate the hydrological effect.

Key words: coherence, SG, GRACE, BFO, ST, hydrology

Contents

List of Figures

List of Tables

Chapter 1

Introduction

1.1 Purpose of research

Gravity data from space borne observations and terrestrial observations have provided valuable information about mass distribution and transportation. The GRACE satellite mission with twin satellites launched in March 2002, are producing accurate measurements of Earth's gravity field which have led to discoveries about gravity and Earth's natural systems. Spaceborne gravity measurements have applications varying from evaluating the speed of ice sheet melting, the ocean current and the magma activities deep inside Earth. Scientists are pushing the boundary of GRACE applications, and many new fields involving mass transportation are developed with the help of GRACE data. But single datasets from GRACE can not ensure the data accuracy, since there is no constraint nor parallel observation which can act as a reference for the GRACE data. Potentially, terrestrial observations combining Superconducting Gravimeters (SGs) and Absolute Gravimeters (AGs) provide a unique opportunity to validate GRACE data. SG is the only instrument which can provide accurate long term relative gravity measurements suitable for GRACE validation. AG can help evaluating the drift of SG.
The local hydrological gravity effect is an obstacle in this comparison. Typically, the very local hydrological effect from a diameter of 100 m around the gravimeter has the order of 10 nm/s^2. The magnitude of local effects depends on local hydrological situation and local topography. As the short wavelength hydrology (100 m area) would not have a significant influence on space borne measurements, considering the long distance to the satellites orbiting at an altitude of 500 km, therefore the local hydrological effect has to be corrected before comparing with GRACE data. The local hydrological situation and topography was carefully investigated at Strasbourg Observatory (ST), but a lack of information at Black Forest Observatory (BFO) will make us turn to global hydrological models, in order to make the comparison of the hydrologically corrected results from two stations possible.

1.2 Gravity

The gravity, or the gravity of earth, denoted g, refers to the acceleration of a mass on or near its surface. The SI unit of gravity is meter per second squared (symbol: m/s^2). As our research focuses on the tiny time variation, we adopt nanometer per second squared (symbol: nm/s^2), which equals to 10^{-9} m/s^2. The gal, named after Italian astronomer Galileo Galilei, (symbol Gal) is another unit used extensively in the science of gravimetry. The gal is defined as 1 centimeter per second squared (1 cm/s^2). The milligal (mGal) and microgal (μGal) refer respectively to one thousandth and one millionth of a gal. So we have a relation between the two most commonly used gravity units in the field of SG, 1 nm/s^2 = 0.1 μGal = 10^{-9} m/s^2. The gravity of earth has an approximate value of 9.8 m/s^2. This means that, ignoring other effects, the speed of an object falling close to the Earth's surface will increase by about 9.8 m/s every second. However, the absolute value of earth's gravity is of no interest in this thesis, only the time variation of gravity is investigated. The rotation of the Earth, that produces the centrifugal force would also contribute to the acceleration. The centrifugal force will be considered in the part of polar motion effect.

1.3 GRACE satellite mission

The Gravity Recovery And Climate Experiment (GRACE), a joint mission of National Aeronautics and Space Administration (NASA) and the German Aerospace Center (DLR), has been producing encouraging results of Earth's gravity field since its launch in March 2002. Since gravity is determined by mass distribution, by measuring gravity from space, GRACE allows to constrain the mass distribution around the Earth and see signatures of mass variations over time. GRACE data is an important tool for studying Earth's climate change, ocean and geology. The GRACE satellites were launched on March 17, 2002. As of November 2012 the crafts would decommission in 2015 or 2016. GRACE is a Earth observation project whose primary task is

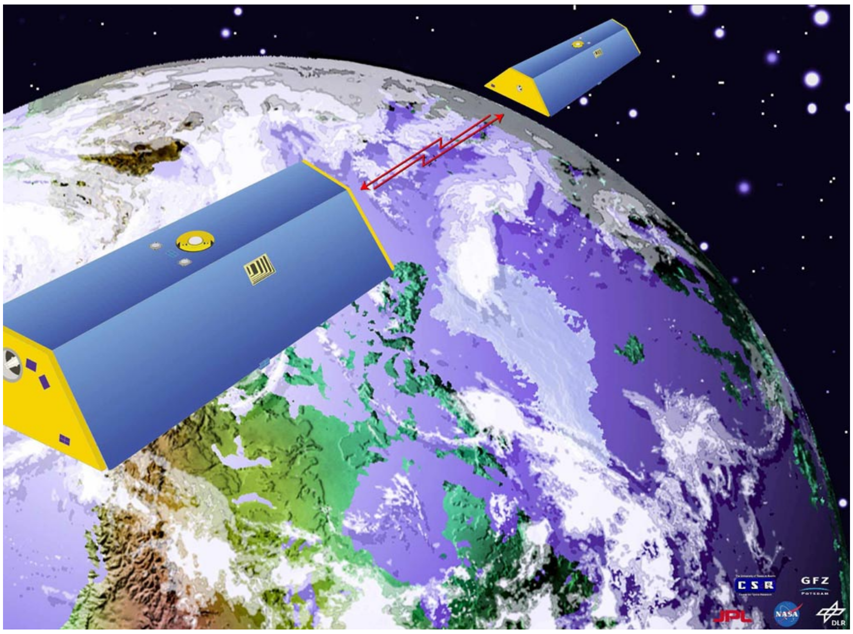

Figure 1.1: Artist's concept of GRACE (http://www.jpl.nasa.gov/missions/web/grace.jpg). A microwave ranging system is used to measure the distance of two satellites.

measuring gravity field. A microwave ranging system is used to measure the distance of two satellites orbiting about 500 km above Earth. The averaged distance between the two satellites is about 220 km. The distance measuring system has resolution as small as 10 micrometres. The two GRACE satellites circle Earth 15 times a day. They give variations in Earth's gravitational force every 1 minute. When the first satellite flies over an area of stronger gravity, it is pulled slightly ahead of the following satellite. The result is the distance between the satellites increases. When the first satellite passes the anomaly, it slows down again; at the same time the following spacecraft accelerates. By measuring the varying distance between the two satellites and combing the data with the measurements from the GPS receivers on board, a varying map of the Earth's gravity field can be constructed. The accelerometers on board can be used as a check for the result given by ranging system. The downloaded data is post processed in ground stations. Additional optical corner reflectors on satellites are used to help laser ranging from ground stations.

1.4 The attenuation of gravity anomaly

A localized mass anomaly has strong attraction on a SG nearby. According to law of universal gravitation, the gravitation force attenuates with the rate of r^2, thus the localized mass anomaly may have limited influence on the space gravity measurement. In this part, the attenuation of gravity anomaly with increasing distance from Earth's surface is investigated. The gravitation force of a localized mass anomaly (or mass variation) can be estimated in the following way. Two cases are considered here: case 1: The heaviest rain in the measuring period of three years at ST has amount of 100 mm in one week. The water mass is $\mathrm{d}m = h \cdot \pi r^2 \cdot \rho_{water}$ ($h = 100$ mm, $r = 20$ km, $\rho_{water} = 1000$ kg/m^3). Case 2, a rock mountain close to ST with height of 200 m and foot radius of 1000 m, $\mathrm{d}m = 1/3 \cdot h \cdot \pi r^2 \cdot \rho_{rock}$ ($h = 200$ m, $r = 1$ km, $\rho_{rock} = 2670$ kg/m^3). Using law of universal gravitation $\mathrm{d}a = G \cdot \mathrm{d}m/r^2$, the gravitational acceleration in the vertical direction can be calculated. Figure 1.2 shows the gravitational accelerations at the altitude of GRACE satellites for a mass at Strasbourg in the case where GRACE is above ST or above BFO. The calculation results are shown in table 1.1.

	a_{ST}	a_{BFO}	$a_{ST} - a_{BFO}$
case 1: rain	0.0335	0.0328	0.0007
case 2: rock mountain	0.1493	0.1459	0.0034

Table 1.1: *The gravitational acceleration of a mass anomaly at ST as observed at the height of GRACE satellites either above ST or above BFO (unit: nm/s^2).*

It is clear that the difference of 0.0007 nm/s^2 or 0.0034 nm/s^2 is far below the accuracy of GRACE derived gravity field. It can be inferred from this calculation that a mass anomaly at the Earth's surface with magnitudes of case 1 and case 2 which surely affects the ground gravity measurement (SG) can be negligible at the height of GRACE satellites. GRACE satellites can give stable estimation of Earth's gravity field up to the spherical harmonic degree of 60, which corresponds to 668 km (res $= 2\pi a/60$) on Earth's equator (447 km at latitude of 48°N). The distance between the two stations is 57.5 km, which is 7 times less than the shortest resolved length. To meet the resolution of 57.5 km at 48°N, a gravity model of 470 degree should be applied. The gravity outside the Earth can be expressed by spherical harmonics (Hager, 2002):

$$U(r,\theta,\varphi) = -\frac{GM}{a}\sum_{l=0}^{\infty}\sum_{m=0}^{l}[A_{lm}\cos m\varphi + B_{lm}\sin m\varphi]P_{lm}(\cos\theta) \tag{1.1}$$

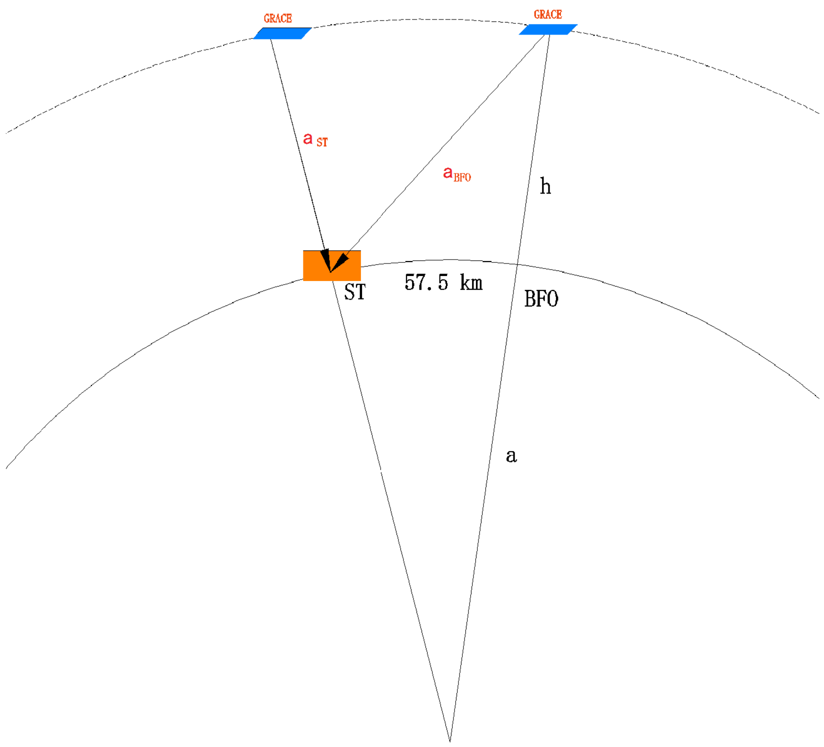

Figure 1.2: *The gravitation force of a mass anomaly at ST as observed when GRACE is either above ST or above BFO. a_{ST} and a_{BFO} are the gravitational accelerations.*

where $Y_{lm}(\theta,\varphi) = [A_{lm}\cos m\varphi + B_{lm}\sin m\varphi]P_{lm}(\cos\theta)$ is the spherical harmonics. $U(r,\theta,\varphi)$ is the gravitational potential outside the mass distribution.
For the gravity, it becomes:

$$g(r,l) = (l+1)(\frac{a}{r})^{l+1}U(l)\hat{\boldsymbol{r}} \tag{1.2}$$

l is the degree of spherical harmonics and r is the distance from the evaluating point to Earth's center. The attenuation of gravity outside Earth's surface is shown in figure 1.3. At the height of 500 km, the gravity is only 1/100 of the gravity on the Earth's surface when degree equals to 60. When the degree reaches 470 (corresponding to the Earth's surface resolution of 57.5 km), the gravity would be $4/10^{16}$ of the gravity at the Earth surface. Figure 1.4 shows the gravity anomaly based on 360 degree gravity field model eigen-gl04c calculated by the on-line Java applet of GFZ http://icgem.gfz-potsdam.de/ICGEM/. The gravity anomaly at BFO is 42.72 mGal and for ST it is 0.99 mGal. In the left part of figure 1.4, there is contrast of the Rhine Graben area (Northwest part of the $2^\circ \times 2^\circ$ area), the Black Forest area (the area around BFO with color from red to white) and the swiss part of the Jura Mountains with negative gravity anomaly (Southeast corner). There is strong coherence between gravity anomaly and the topography in this $2^\circ \times 2^\circ$ area. Considering the attenuation of the gravity with increasing height as shown in figure 1.3, the difference of 40 mGal at the Earth's surface almost vanishes at height of GRACE satellites.

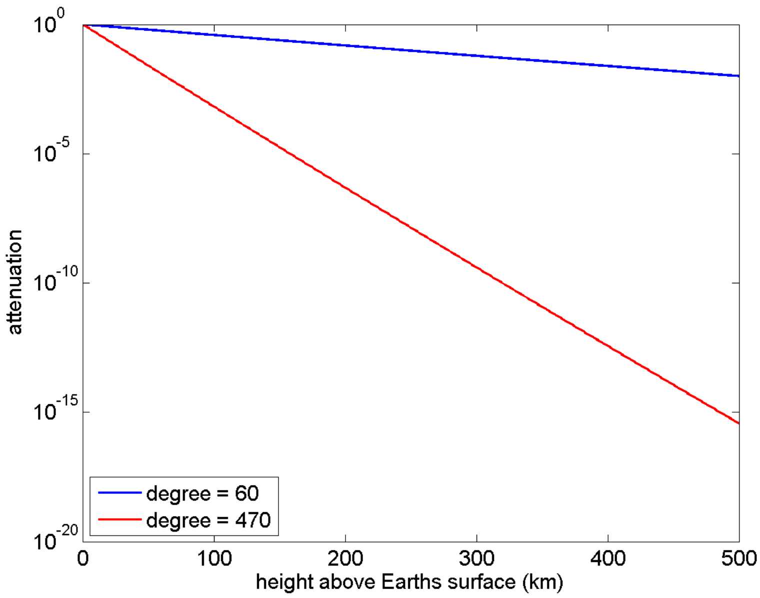

Figure 1.3: *The attenuation of gravity with increasing height. At spherical harmonics degree 60, the amplitude of the harmonic is only 1/100 of the gravity on the Earth's surface (blue line). When the degree reaches 470, the amplitude is $4/10^{16}$ of the gravity at the Earth surface (red line).*

From the analysis above, we can say: GRACE derived models predict essentially the same temporal gravity field variations for both ST and BFO.

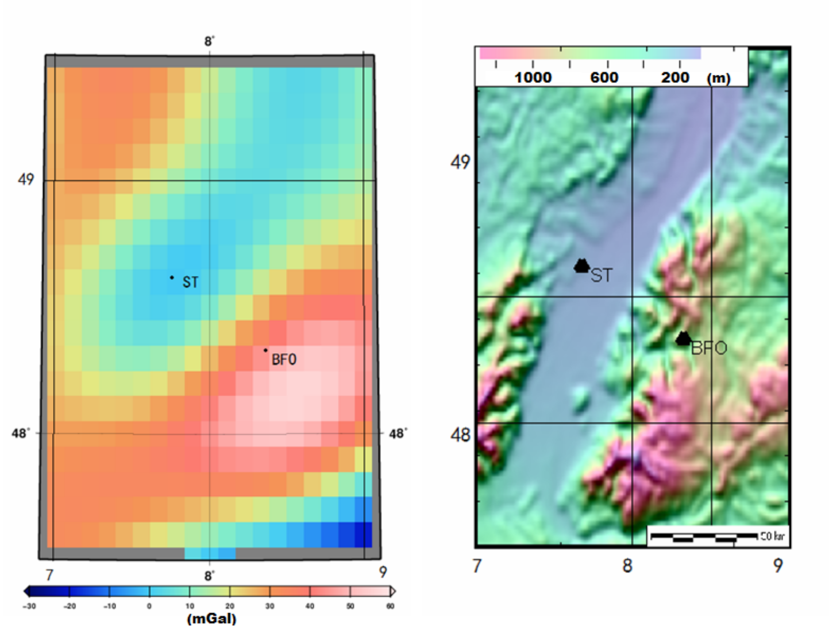

Figure 1.4: The gravity anomaly field of the Rhine Graben area. The left figure is the gravity anomaly calculated using 360 degree gravity field model eigen-gl04c. The right figure shows the topography of the same area. Note the strong coherence between the gravity anomaly and the topography.

Chapter 2

Superconducting Gravimeters

2.1 A brief history of SG

The development of SG can be classified into 4 stages: (1)the experimental type at University of California at San Diego; (2)the first commercial TT models; (3)the compact models; (4)the new OSG models. The first superconducting gravimeter was designed by Goodkind and Prothero in 1960s. It is the first gravimetric instrument with realisation of superconductivity. Within half a century development of SG, the instrument has been improved in all aspects, even though the general principle of levitating a metal sphere using magnetic forces is unchanged. The early research using SG by the team of Goodkind focused on tidal analysis (Prothero and Goodkind, 1972), ocean tide loading (Warburton et al., 1975) and atmospheric effect on gravity measurement (Warburton and Goodkind, 1977).
The achievement of Goodkind's team attracted the interest of other scientist including Paul Melchior, Rudolf Brien and Bernd Richter. Goodkind was asked to develop commercial models to support SG measurements at other sites. The company GWR Instruments was formed in 1979 by Richard Warburton and Richard Reineman, and is still the sole manufacturer of commercial SGs. In 1981, a GWR TT 30 was installed in the basement of Royal Observatory of Brussels (ROB). The cooling method is simply inserting liquid Helium into the dewar. Unlike some later models using compressors to reduce the radiation on the belly, this model was completely quiet. But the disadvantage was the vast consumption of liquid Helium. This was not affordable in Germany, since at that time, Helium was quite expensive in Germany. Rudolf Brien and Bernd Richter purchased a SG with refrigerator system for Bad Homburg Observatory. This model is called TT40, and was installed in 1981. The cold head of the refrigerator system was directly attached to the dewar, which caused vibration noise on the gravity measurements. This was later solved using a new designed frame to hold the cold head (Schubert and Price, 2007). Four years later, a second SG (TT60) was installed at Bad Homberg. Since the parallel measurements of these two SGs gave highly correlated results (Richter, 1990), the quality of SG measurements were confirmed.
GWR Instruments reduced the size of dewar and developed a compact model SG in 1993. Table 2.1 shows the continuous reduction of SG size and Helium consumption. Figure 2.1 is a picture of the compact instrument C026 installed at Strasbourg in 1996. In this model, a separate frame is introduced to support the cold head. A rubber gasket is placed between coldhead and dewar to prevent air from entering the dewar and Helium from leaving the dewar.
The new GWR OSG, Observatory Superconducting Gravimeter gives the best long term gravity measurements and has also dual sphere design models.

	TT70 SG	Compact SG (ST)	Dual-sphere OSG (BFO)
Height	150 cm	105 cm	114 cm
Diameter	80 cm	66 cm	42 cm
Weight	150 kg	90 kg	60 kg
Helium Consumption(per year)	200 l	100 l	0 l
'Belly' volume	200 l	125 l	35 l

Table 2.1: *A comparison of Model TT70, compact SG at Strasbourg and dual-sphere OSG-056 at BFO*

Figure 2.1: *The compact instrument C026 installed at Strasbourg Observatory (http://eost.unistra.fr/observatoires/gravimetrie/instruments/)*

2.2 SG principles

The most commonly used gravimeter are the spring gravimeters. A spring is used to support the test mass. A change in gravitation force generates a signal (nowadays usually electronic signal) as output. The LCR (La Coste&Romberg) and Scintrex spring gravimeter use this principle. The irregular and relative large drift of spring gravimeters usually cause problems for research on phenomena with periods greater than 14 days. In practice, the spring gravimeter should be brought back to the starting point of measurement or to a gravimetric reference point to evaluate the drift.
The principle of SG is the same as spring gravimeter except the spring is replaced by a magnetic levitation structure. The components to produce the levitating force are placed in stable low temperature environment to ensure the stability. Figure 2.2 shows the the major components of a SG: the superconducting sphere, the superconducting coils, the feedback system, the superconducting shield and the vacuum can.

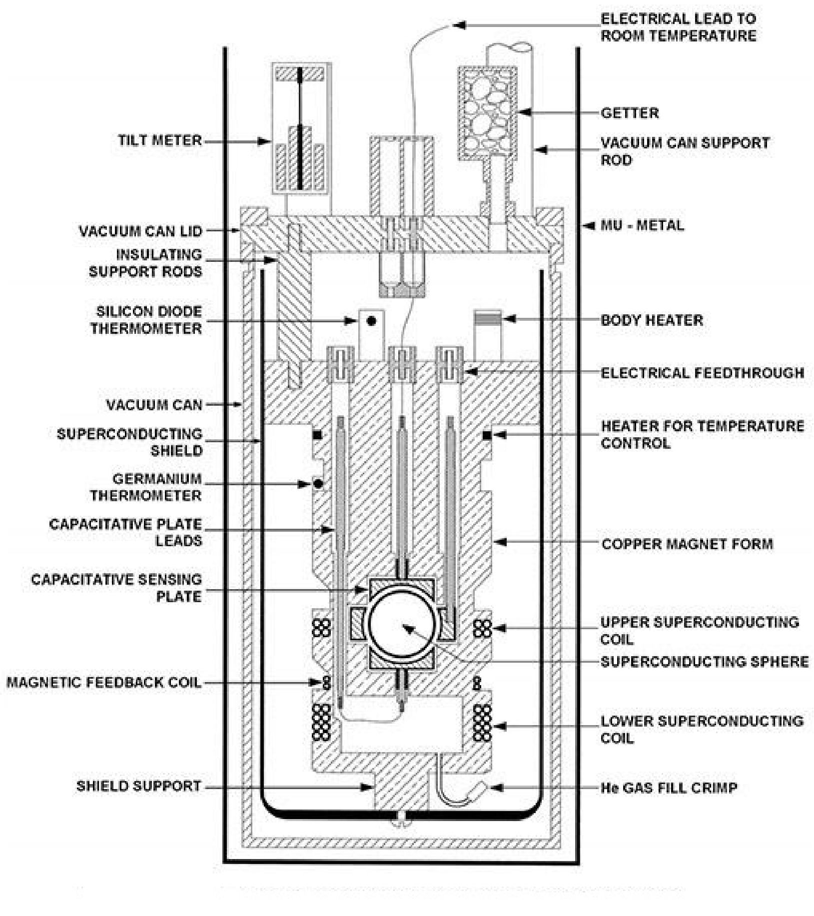

Figure 2.2: *Schematic of single sphere SG sensor showing arrangement of the sphere, coils, vacuum can, and shielding (GWR Instruments, 2011)*

The high sensitivity is realized by using two coils structure. Figure 2.3 shows the relative position of coils, sphere and capacitative sensing plates (GWR Instruments, 2011). The

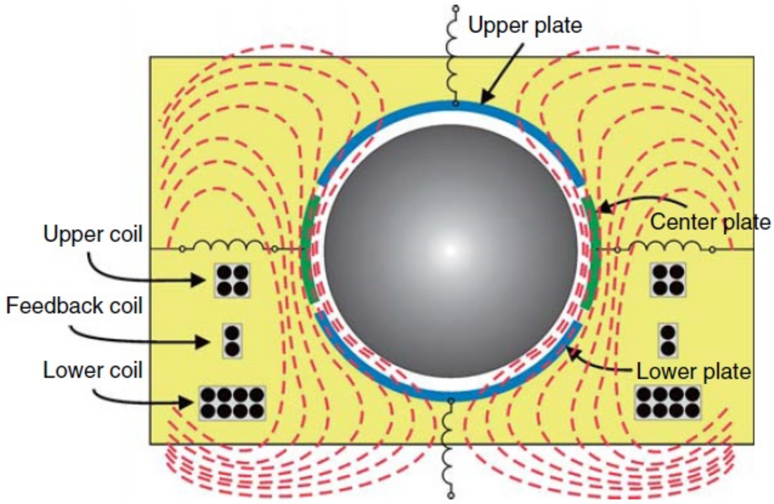

Figure 2.3: The diagram of Gravity Sensing Unit (GSU) (GWR Instruments, 2011). The high sensitivity is realized by using two coils structure. The hemispherical capacitor plates sense the motion of the sphere.

magnetic field is mainly generated by the lower coil and the upper coil. The upper coil is just below the center of the superconducting sphere and the lower coil is aligned with the upper one with distance of 2.5 cm. The current in these two coils can be adjusted independently. The lower coil determines the main part of upwards force to balance the downwards gravity force. The upper coil is used to determine the gravity gradient, which is similar to the concept of 'spring constant'. The gradient is made very small, so that the instrument is very sensitive to the change of gravity. Since the gravitation force changes continuously, the levitation force should also be adjusted constantly to balance the sphere. With hemispherical capacitor plates the motion of the sphere is sensed. The current in the feedback coil is adjusted to keep the surface centered. This feedback current is proportional to changes in gravity, thus to measure the current can reflect the change of gravity indirectly.
To reduce the influence of Earth's magnetic field on the inner structures, a superconducting cylinder inside the vacuum can and a μ-metal shield outside cover the superconducting conponents. The sensor and superconducting shield are installed in a vacuum can, which is surrounded by the liquid helium bath at about 4.2 K (Schubert and Price, 2007). Note that niobium (the material of both coils and sphere) has a superconducting temperature of 9.2 K. The environmental temperature lower than superconducting temperature ensures the superconductivity of the system. A feedback system inside the vacuum can keep the stability of temperature.
For other gravity measurement methods, it is required that the sensitive axis of the instrument is aligned with the direction of gravity. To design a tilt compensation system, we first need to understand the different response of the sensor when the gravimeter is inclined, comparing to spring gravimeter. In spring gravimeter, the test mass moves in the direction of instrument axis. When the sensor is tilted by an angle of θ, the instrument measures the component of gravity in the direction of its axis, which is $g \cos \theta$, where g is the real value of gravity. The error (the difference from the real value) is $g \cos \theta - g \approx -g\theta^2/2$. The error of tilting sensor affects the output of SG in another way. One thing need to mention here is that, the force direction of levitation coils is along the sensor axis and in contrast, the direction of gravity is invariably

the direction of plumbline. When the sensor is perfectly leveled, $g_{\text{output}} = g_{\text{levitation}} = g_{\text{sphere}}$. Because the direction of $g_{\text{levitation}}$ is aligned with g_{sphere}, according to Newton's Law, these two forces exerted on the sphere must be equal. When the sensor is tilted by an angle of theta (again the angle between the plumbline and the sensor axis), the downward gravity attraction keeps unchanged and the component of original $g_{\text{levitation}}$ in the direction of plumbline is $g\cos\theta$, which is weaker than the original force of $g_{\text{levitation}}$. To compensate this effect, the levitation force $g_{\text{levitation}}$ must be enlarged to keep the plumbline direction component of levitation force unchanged. The levitation force should be enlarged to $g/\cos\theta$, so that the plumbline direction component of levitation force is $(g/\cos\theta)\cdot\cos\theta = g$. The two tiltmeters on the top of the vacuum detect the tilt and controls the current into the two levelers on two of the feet. The different characters of SG and spring gravimeter when tilted can be summarized as: tilting of a spring gravimeter leads to smaller gravity readings, while tilting of a SG leads to larger gravity readings.

2.3 Single-sphere design and dual-sphere design

2.3.1 The problematic offsets

Of the two SGs used in this research, the instrument at Strasbourg Observatory is a single-sphere SG and the one at BFO (Black Forest Observatory) is a dual-sphere SG. The very large offsets (amounts to a few hundreds μGal) happen generally with certain cause, like earthquakes. The middle size offsets (a few μGal) happen more likely without any certain cause and usually in random time interval. The small size offsets (less than 1 μGal) happen continuously and it is relative easy to detect and correct such kind of small offsets especially those happen within a short time. To correct the raw data, a pre-determined threshold is used to classify the offsets: all offsets larger than the threshold must be corrected in a proper way, and on the other side, the offsets smaller than this threshold is left out. The determination of the threshold is usually done in an arbitrary way, and moreover, it is problematic to determine an optimal threshold. For example, a sudden precipitation process may cause a step of a few μGal in the gravity residual, that could not be distinguished from other arbitrary offsets without any cause.

2.3.2 Advantages of dual-sphere design

Based on the assumption that offsets without any external cause would not happen simultaneously in two sensors installed side by side, the first dual-sphere SG (CD029) was manufactured in 1998. Basically, the dual-sphere sensor is two single sphere sensors mounted one over another with a distance of about 20 cm. There are small differences in the weight of two spheres and the coil winding. In the pre-processing stage, the measurements from the two spheres are treated separately, as from two instruments. These two time series could later be combined in the following ways: two series are compared to detect the offsets, which may not be detected in the pre-processing stage; the two signals can be merged into one signal, by choosing the slices of signal with less disturbances. Another application is after pre-processing the data, the difference of the two series can be used to determine the gravity gradient, as long as the vertical distance of the two spheres is well determined. Even though the amount of offsets is largely reduced because of the improvement of instruments (Kroner et al., 2004), the possibility of getting gravity gradient value from two spheres is still of great interest for researchers. Another advantage of the dual sphere design is lower noise in second heavier sensor: The instrumental noise power $P(\omega)$ for an accelerometer is $P(\omega) = 4k \cdot T \cdot b/m^2$, where m is the mass (GWR Instruments, 2011). From this formula, we can say, increasing the sphere mass can help reducing the noise. The newly introduced lower sphere is 17 g, comparing to the 4.3 g upper sphere.

2.4 Data quality

In the early years of SG, the drift is usually modeled as the sum of exponentials and a low degree polynomial(Boy et al., 2000). For recent models, the drift can be modeled as an exponential and a linear drift in the following period. A SG and an AG can be placed side by side to determine the drift value. The SG gives a continuous time series and the AG provides the gravity values at some discrete time. The SG series is adjusted to fit the AG data, which serves as a reference. This method is an optimal way, since the major part of hydrological and tectonic influences are contained in both measurements. But the tiny difference of these influences on two kinds of instruments may still make precise determination of drift complicated. Since there is no instrument with the same level of accuracy as SG for frequency lower than 1 mHz, it is impossible to compare the measurements of SGs with a reference to evaluate the precision of the instrument. The development of dual sphere OSG has helped estimating the precision of SG.
Table 2.2 compares the three types of gravimeters: the GWR OSG which is used in this thesis, the absolute gravimeter FG-5 and spring-based gravimeter CG-5. The GWR OSG can achieve the highest accuracy of 0.1-0.4 nm$\cdot$s^{-2}, which is about $1/10^{11}$ of the gravity on earth surface. The nominal drift is 30 nm$\cdot$s^{-2}/year (this value may vary from a few nm$\cdot$s^{-2}/year to about 100 nm$\cdot$s^{-2}/year depending on different OSG types and different characters of the superconducting spheres). The drift of spring gravimeter is about 200 nm$\cdot$s^{-2}/day. Note the different time scales used in expressing the drift of OSG and spring gravimeter - day and year. GWR OSG has advantages in measuring the long period gravity variation, considerding the low instrumental drift and the highest measurement accuracy.

	Superconducting Gravimeter (GWR OSG)	Absolute Gravimeter (FG-5)	Spring-based relative Gravimeter (Scintrex CG-5)
Drift	30 nm$\cdot$s^{-2}/year	0	200 nm$\cdot$s^{-2}/day
Accuracy	0.1-0.4 nm$\cdot$s^{-2}	20 nm$\cdot$s^{-2}	50 nm$\cdot$s^{-2}

Table 2.2: *A comparison of three types of gravimeters*

Chapter 3

Black Forest Observatory (BFO) and Strasbourg Observatory (ST)

3.1 BFO

3.1.1 General information about BFO

The mine 'Grube Anton' (where BFO now sites) dates back to 1770. In 1970 the observatory was built at the site of the abandoned mine 'Anton'. The construction work of the observatory takes 2 years and the costs were paid by the Volkswagen (VW) Foundation. The observatory opened in 1972. Since the beginning the observatory (BFO) is jointly managed by the following institutes:

- Institute of Geophysics, Karlsruhe Institute of Technology (KIT)
- Institute of Geodesy, Karlsruhe Institute of Technology (KIT)
- Institute of Geophysics, Stuttgart University
- Institute of Geodesy, Stuttgart University

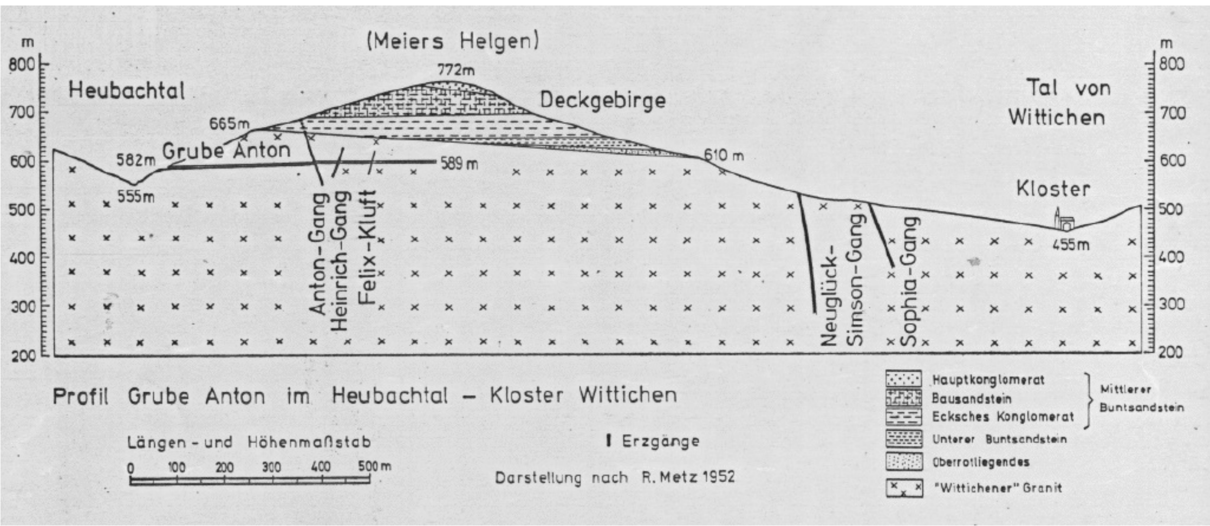

Figure 3.1: *Geology of BFO (http://www.bfo.geophys.uni-stuttgart.de/Geology.html). The instruments are installed in a former silver mine on granite base at depth of about 170 m below the surface and at distance of up to 600 m from the entrance.*

As it is shown in figure Figure 3.1, instruments are installed in a former silver mine on granite base at depths of up to 170 m below the surface and at distances of up to 600 m from the entrance. As shown in Figure 3.2, two airlocks along the main aisle provide thermal stable environment and also contribute to attenuation of air pressure fluctuations.
Here is a list of instruments at BFO, which are related to this research:

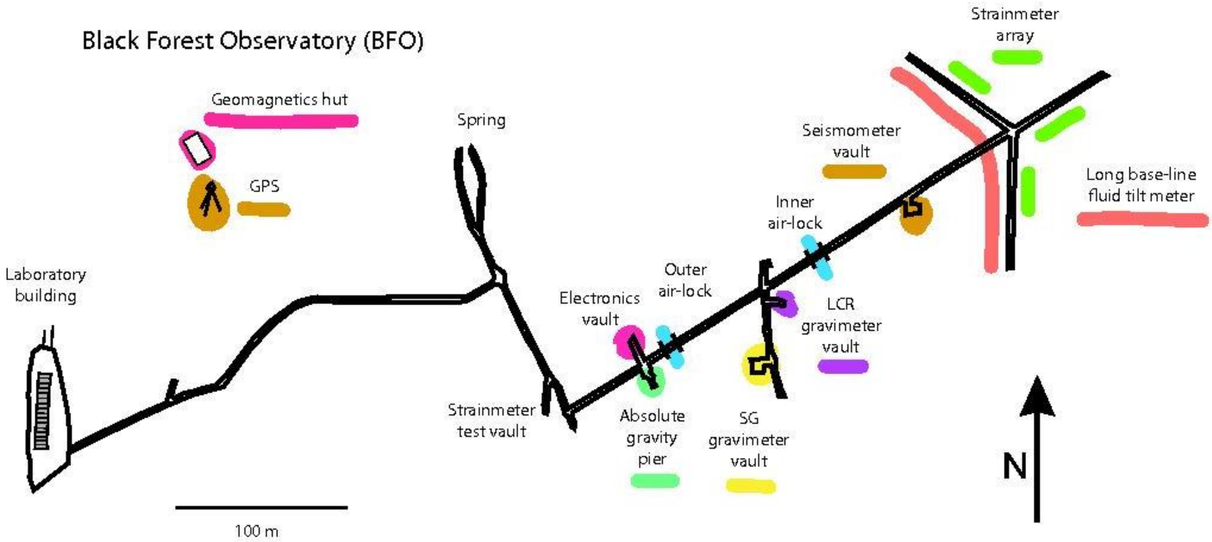

Figure 3.2: *Instruments at BFO (http://www.bfo.geophys.uni-stuttgart.de/BFO_walk3.html)*

- ET-19 La Coste&Romberg gravimeter
- STS-1 three component seismometer
- STS-2 three component seismometer
- Superconducting gravimeter GWR SG-056
- GPS
- Microbarograph
- Paroscientific Microbarometer
- Thermometer
- Windspeed sensor
- Rain gauge

3.1.2 The location of BFO

The geographic coordinates of the BFO laboratory building are (Google Earth): 48°19′44.24″ North, 8°19′23.13″ East. The station building is on one side of the Heubach Valley. Heubach is a small stream located about 50 m from the entrance of the mine. Figure 3.3 shows the position of station building (point A), which is close to the entrance of the silver mine.

Figure 3.3: The location of BFO (Google Earth). The entrance of the silver mine is close to point A. The mine is extending eastwards from the entrance.

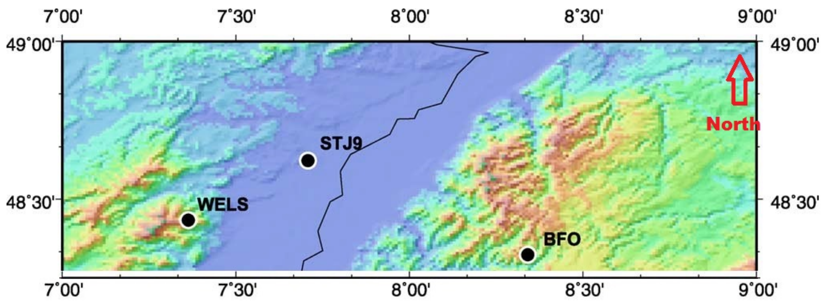

Figure 3.4: The topography in BFO-ST area (Amalvict et al., 2006). The black line is the German-France border in the area of the Rhine Graben. ST is located in the Rhine alluvial plain and BFO is located in Heubach valley of the Black Forest.

3.1.3 Site noise of BFO

The nearest town is called Schiltach, which is 5 km away and has a population of about 4000. The town is connected by Bundesstrasse 294 and 462 without busy traffic. There are train connections to Freudenstadt and Offenburg every hour. The SG is located in a branch of the mine (Figure 3.2). The instrument is about 400 m from the entrance of the mine, where the station building is located. The hard rock mountain cover of about 150 m acts as a natural shield for the instruments. The nearest noise source is the 400 m away station building. These facts ensure the signal from SG at BFO has low background noise.

3.1.4 Site stability of BFO

As shown in Figure 3.1, the Heubach valley has the granitic basement rock covered with the sedimentary cover ('Deckgebirge') and the ore carrying dykes (Anton Gang, Heinrich Gang, Felix Kluft). Most instruments are installed in the granite base. There is no clay layer nor gravel layer in a 150 meter radius space centered in the SG. This reduces the very local hydrological effect, which is the most hard to model part of the whole hydrological signal. The sedimentary cover of the mountain may have a strong effect on the observation. It is of interest to further investigate the influence of the sedimentary cover when addition information is available. The stream Heubach (to the west of the observatory) may also generate a signal, even though the rate of flow is not massive.

3.2 Strasbourg Observatory (ST)

3.2.1 General information about ST

The temporal variations of the gravity are observed with the superconducting gravimeter GWR C026 within the global network GGP (Global Geodynamics Project). The C026 came into operation in the summer of 1996. The Strasbourg Observatory operates also an absolute gravimeter FG5 #206 Micro-g. Since late 1999, the site also has a permanent GPS (Global Positioning System) to acquire information on tectonics. A weather station is in operation since May 2005, and this provides useful information for modeling of the atmospheric and hydrological effect. In order to observe the water table variation at ST, a gauge was installed in 1987 in a well under the station (50 m depth).

3.2.2 The location of ST

Strasbourg Observatory is located at 48°37′18″ North, 8°41′2″ East in an old fort about 10 km Northwest from Strasbourg. The station is 340 m away from the regional road D31 and 1 km away from the nearest town Mittelhausbergen. 3 km away is the train cargo station with the most heavy traffic in Strasbourg area and also the high way A 4. Figure 3.5 shows the location of ST (point A).

Figure 3.5: *The location of ST (Google Earth). The dense rail tracks in the northeastern part is the train cargo station. The southeastern part is the suburb of Strasbourg. ST is surrounded by farmland.*

3.2.3 Site noise of ST

Considering the relative short distance to noise source (city of Strasbourg, town Mittelhausbergen, train cargo station) comparing with BFO, it is expected the anthropogenic background noise of ST would be higher than at BFO.

3.2.4 Site stability of ST

ST faces complicated hydrological situation due to two sources. The station covers an area of 60 m $\times$ 60 m, which is surrounded by farmland. The foundation is made up of unconsolidated alluvial sediments of the Rhine River. The agricultural activities would without doubt generate a strong signal, both attraction and the loading effect due to the elasticity of the clay foundation. The massive water flow of the 10 km away Rhine River contributes to the seasonal variations.

Chapter 4

Data Processing

4.1 SG data

GWR SG-056 at BFO started operating in October 2009. Until the beginning of 2013, about three and a half years' data have been acquired. The SG data from Strasbourg Observatory are obtained with the superconducting gravimeter GWR C026. The SG at ST is in continuous operation since the summer of 1996. The common period of the two stations from 1st October 2009 to 31st December 2012 has been used in this study. At the beginning of 2010, a major manipulation of instrument has been carried out at ST, which caused massive disturbances on the gravity record. Therefore only the data from 1st February 2010 to 31st December 2012 have been used in most comparisons with data from BFO.
The GGP (Global Geodynamics Project) files are from private communication with Dr. Rudolf Widmer-Schnidrig. The monthly data with sampling interval of 1 minute start from the first minute of the month and last to the beginning of the next month. An overlap with the next month's data is introduced to ensure the continuity of the whole data series. The size of monthly GGP file is about 1.6 Mb. The monthly data files are firstly merged to create continuous series for both gravity value and air pressure. From the data merging to the end of the third iteration, the data processing is done using the software TSOFT version 2.1.6 (Vauterin and Van Camp, 2011), which is popular in the field of SG data processing.

4.2 The 'raw' data

Between 2009 and 2013, 6 SG stations have joined the GGP network, and adding the already existing stations, there are currently 31 stations all around the world in operation. Even though there are few stations in the Southern Hemisphere and not enough stations in the vast Asian part of the Eurasian continent, we have already stations as far North as Ny Alesund (78.93° North) and as far South as station on Antarctica continent – the station Syowa (68.01° South) operated by Japanese scientists. Researchers from BKG and GFZ have also built and operated station in South America (Station Concepcion, Chile) and station in Africa (Sutherland, South Africa). There is a large amount of GGP data available on GGP-ISDC (Information System Data Center). People can refer to website http://www.eas.slu.edu/GGP/ggphome.html for more details about GGP and the data. Figure 4.1 and figure 4.2 show the stations at the beginning of 2013 world wide and in central Europe.

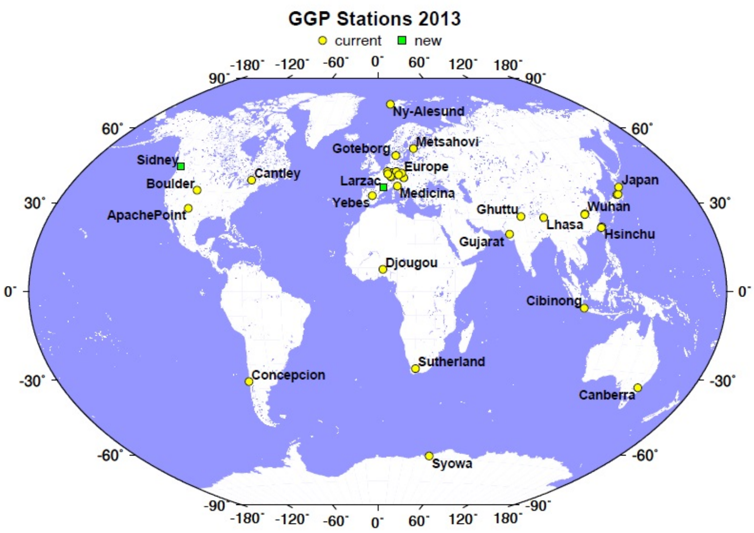

Figure 4.1: *GGP stations at the beginning of 2013 worldwide (http://www.eas.slu.edu/GGP/ggphome.html). The GGP network extends to all five continents.*

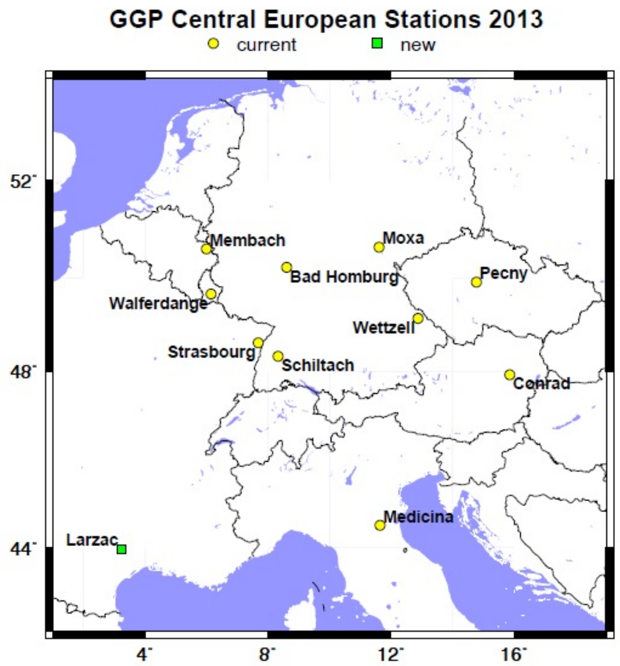

Figure 4.2: *GGP stations at the beginning of 2013 in central Europe (http://www.eas.slu.edu/GGP/ggphome.html). Central Europe is the only region with dense SG arrays at the beginning of 2013.*

The data acquisition systems of SGs typically record two groups of data, the gravity variation and the air pressure. The sampling interval of gravity data is typically 1 second and the auxiliary data is typically in 1 minute interval. As the very high frequency signals are of no interest to us, the minute data in GGP format is used in this research. To convert gravity record from 1 second to 1 minute sampling interval, a zero phase filter and a digital decimation are applied. The gravity data and the air pressure data (also with 1 minute interval) are combined with the time scale. And a header is added with some additional information.

```
Filename              : B1100200.GGP
Station               : Black Forest Observatory, Schiltach, Germany
Instrument            : GWR SG-056_L
Time Delay (sec)      :      9.65       0.15        nominal
N. Latitude (deg)     :   48.32983   0.00005       measured
E. Longitude (deg)    :    8.32728   0.00010       measured
Elevation MSL (m)     :   589.200     0.010        measured
Gravity Cal (uGal/V):    -40.066     0.030        measured
Pressure Cal (Pa/Pa):      1.000     0.100         nominal
Author                : widmer@geophys.uni-stuttgart.de
yyyymmdd hhmmss  gravity(V) pressure(hPa)
C*****************************************************
77777777
20100201 000000    3.017633   934.243
20100201 000100    3.023142   934.240
20100201 000200    3.028555   934.240
20100201 000300    3.033738   934.245
20100201 000400    3.038657   934.252
20100201 000500    3.043467   934.256
20100201 000600    3.048304   934.265
20100201 000700    3.052964   934.273
20100201 000800    3.057312   934.270
20100201 000900    3.061575   934.267
20100201 001000    3.065815   934.274
```

Figure 4.3: *The beginning of data file B1100200.GGP of GWR SG-056 (lower sphere) at BFO. The upper part is the file header which includes Filename, Station information etc.. The lower part shows the beginning of data record which starts from 00:00:00 1st Feb. 2010.*

Figure 4.3 is an example of the GGP data file for SG-056 lower sphere at BFO. The header includes Filename, Station information (name, coordinates, elevation, gravity calibration factor and air pressure calibration factor) and the units of gravity and pressure used in the recording. For the Filename B1100200.GGP, B1 stands for the lower sphere of SG-056 (B2 stands for the upper sphere respectively), and 1002 stands for the year of 2010 (10), February (02). The last two digits (00) mean that it is the raw data in GGP format. As mentioned before, only a decimation filter and a zero phase filter are applied to the second data to get the minute data, thus it has gaps, steps, spikes. There are two conventions here: firstly, in the following paragraphs of this thesis, 'raw data' or 'raw gravity' means the raw data from GGP files (1 minute sampling interval data with offsets), not the 'true' raw data directly from the digitizer of SG in sampling rate of 1 second; secondly, the gaps, steps, spikes are generally called offsets. Figure 4.4 shows the plot of raw gravity channel of file 'B1100200.GGP' in software TSOFT. The steps are not visible on this scale, but the spikes and gaps at the end of this month are clearly visible. The first gap is from 17:00 26th Feb 2010 to 14:00 27th Feb 2010. Considering the air pressure recording is not affected during this period, it is most likely this gap is caused by a strong earthquake. This can be verified using the earthquake database of Earthquake Hazards Program - USGS. When an earthquake happened, it took maximum 20 min for the waves to reach the station, and normally the waves of strong earthquakes exceed the recording range of the digital voltmeter. The result is a clipped signal from a period of a few minutes to a few days. It finally appears in the GGP file as flagged values. Generally the waves will not cause permanent damage to the instrument, so the data recording will recover as soon as the amplitudes of waves drop down below the recording limit. In the case of power failure, a gap in gravity channel happens simultaneously with the gap in air pressure channel, and the failure would not cause continuous spikes following the gaps.

Until now, the gravity value is still in unit of Volt. It can be easily converted into value in

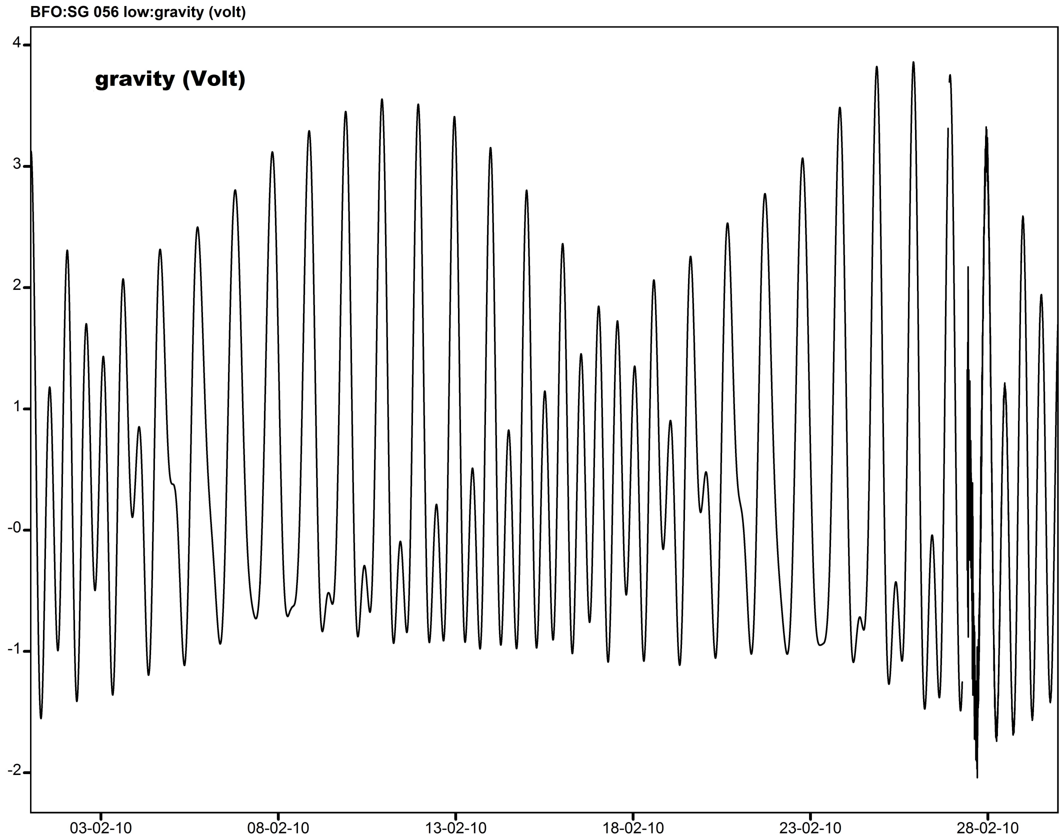

Figure 4.4: *A screenshot of gravity channel of the file shown in figure 4.3 - data file B1100200.GGP in software TSOFT (SG-056 lower sphere). Disturbances occurred on 27th Feb. 2010. The time scale (x-axis) is from 1st Feb. to 2nd Mar. 2010. The raw gravity measurements range from -2 Volt to 4 Volt.*

unit of gravity by multiplying with the gravity calibration factor from the file header. Due to the different weights and other characters of two spheres at BFO, different calibration factors must be applied (-40.066 μGal/Volt for the lower sphere and -80.006 μGal/Volt for the upper sphere).

$$g(\text{nm/s}^2) = g(\text{volt}) \cdot \text{GCF} \tag{4.1}$$

where GCF is the gravity calibration factor.

4.3 Remove-restore technique

4.3.1 The model for observed data

There are a variety of signals in the raw gravity (data from GGP file). Some are of interest for us and some are not the subject of discussion in this thesis.

$$g_{\text{raw}} = g_{\text{offsets}} + g_{\text{atmo}} + g_{\text{tides}} + g_{\text{loading}} + g_{\text{polar}} + g_{\text{drift}} + g_{\text{residual}} \tag{4.2}$$

g_{raw} refers to the raw measurement from the GGP files. g_{offsets} includes the gaps, steps and spikes of instrument origin and also external disturbances. g_{atmo} is the atmospheric effect on the gravity observation, which is a combination of the direct attraction and the atmospheric loading effect. g_{tides} is the gravitational effect of the solid earth tides and the ocean tides. g_{loading} specifies the effect of water movement in shallow areas of the continental shelves. g_{polar} refers to the annual and Chandler polar motion. g_{drift} includes the drift of the instrument and also the very long period tides which can not be modeled in the component g_{tides}. The typical referred gravity residual contains the hydrological effect and the tectonic deformation effect. In addition, the noise of the instrument and the error of mismodeling are also contained in g_{residual}.
In the case of gravity data processing, signals which are not related to the research topic should be removed at first. For example, the modeling of hydrological effect is a widely studied topic recently, and this effect has a magnitude of 50-100 nm/s^2. And the solid earth tides dominate g_{raw} with an amplitude of 1000-1500 nm/s^2. The hydrological effect would be concealed when the solid earth tides are not removed.

4.3.2 The necessity of remove-restore technique

The remove-restore technique is, in simple words, first subtracting (removing) the nominal corrections for some known effects, such as the solid earth tides and the air pressure correction, and then the offsets in the data can be fixed, finally the corrections applied in the first step are added (restored). The ideal result is that all offsets and disturbances are perfectly corrected and other signals remain unchanged in the restored signal. Figure 4.5 shows the whole work flow of three iterations using remove-restore technique.

The reason why the offsets are corrected in such a circuitous approach is again the massive difference in the magnitudes of all the components of g_{raw}. Figure 4.6 is an example of a gap which needs to be filled. The upper figure shows g_{raw}, and the lower figure shows the residual after removing the solid earth tides and the atmospheric effect. As mentioned before, the raw data g_{raw} is dominated by the solid earth tides with an amplitude of about 1000 nm/s^2. For example, when it is intended to fill the gap from 06:35 27th February to 09:54 27th February directly from g_{raw}, a straight line is drawn from the last data point before the gap to the first data point after the gap. In this process, there is an uncertainty of about 100 nm/s^2. This is surely not acceptable, because the uncertainty is even larger than the amplitude of the hydrological signal (50-100 nm/s^2), where one focus of this thesis lies. Otherwise, if the dominated part of g_{raw} (g_{tides}) is removed in advance, the variation of the signal in three hours can be reduced to a few nm/s^2 (as shown in the lower figure). Under such condition, when the same approach of gap filling is carried out, the uncertainty of correction is about 1-2 nm/s^2. In this way,

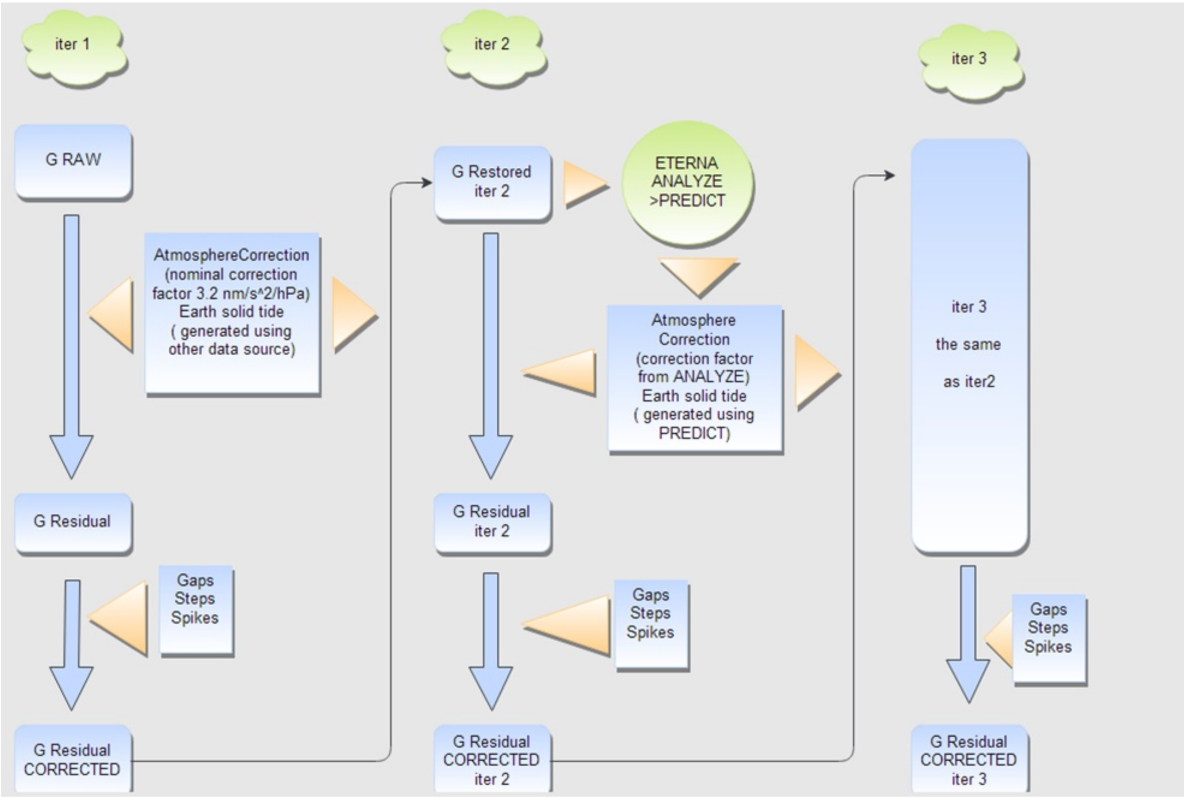

Figure 4.5: *The whole work flow of remove-restore technique. Three iterations of remove-restore technique have been applied.*

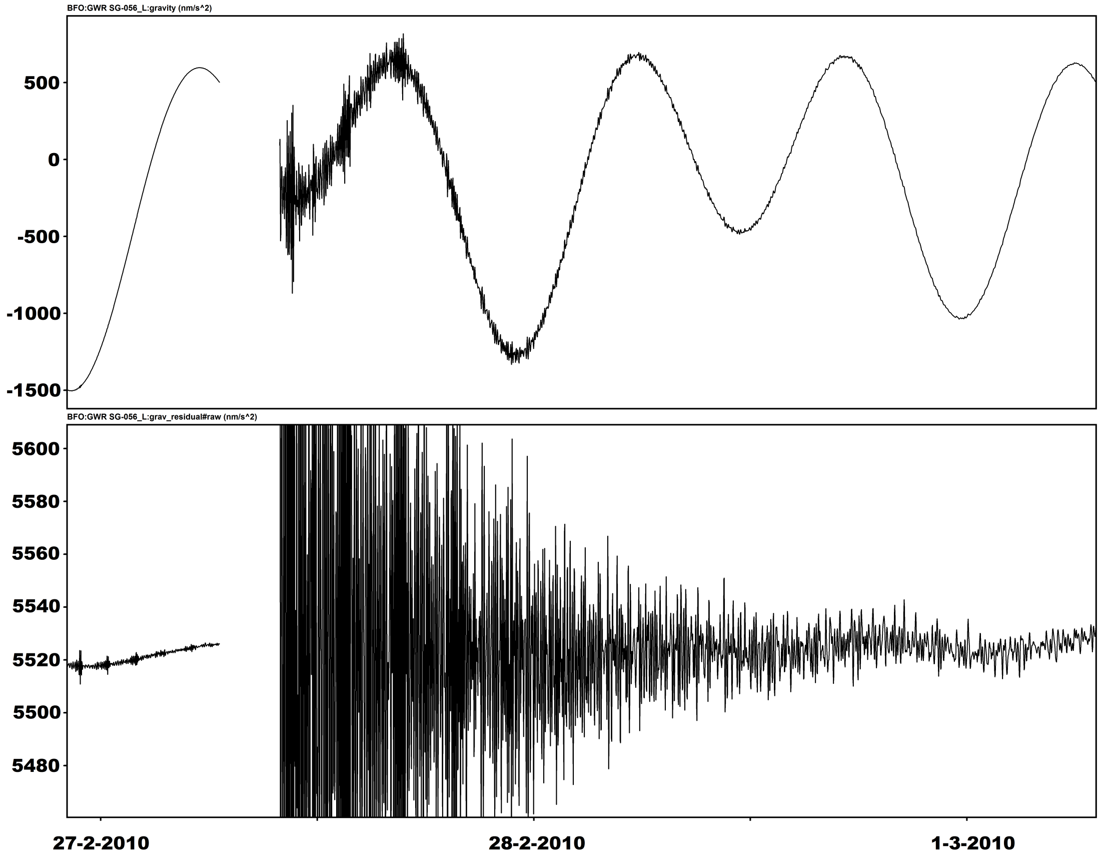

Figure 4.6: *A gap in February 2010 (SG-056 lower sphere). The upper panel shows the raw gravity. The lower panel shows the gravity residual after correcting for the solid earth tides and atmospheric effect. Note the different scales of the upper panel and the lower panel. (unit: nm/s^2)*

the uncertainty is significantly reduced and the accuracy in data processing is ensured. The mechanism of improving correction accuracy for steps and spikes is similar, thus it will not be discussed here in detail. Moreover, in most cases, some small steps and spikes can not even be detected from g_{raw} without removing the solid earth tides.

4.3.3 Remove the solid Earth tides and the atmospheric effect

The optimal situation when correcting for the offsets is that only offsets and noise are contained in the gravity residual – all other effects are removed in advance, so that the correcting operation can be done easily. But there are difficulties in reality. Some of the effects can not be perfectly modeled in this stage. 'Not perfectly modeled' means the modeling accuracy can not satisfy the quality requirement of the whole processing workflow. The modeling ambiguity of the hydrological effect amounts to 10-20 nm/s^2, thus it is left in g_{residual} and kept until the last step of the work flow (not corrected before removing offsets). g_{polar} and g_{drift} can be evaluated in this stage with a relative high accuracy, but they would not be removed. This decision is made by carefully judging and weighing the advantage and the disadvantage of removing these components. g_{polar} contains the annual and Chandler polar motion (435 days period) and appears like smooth damped sinusoidal wave. The hourly variation of the polar motion correction is about 0.1 nm/s^2. In most cases, the offsets should not exceed period of a few days, so the variations of the polar motion correction could be treated as a straight line in the period of an offset. In addition, the gaps and spikes are also corrected with a straight line, thus correcting for g_{polar} would not improve the accuracy significantly in this regard. On the other hand, any means of modeling a geophysical phenomena would introduce error. Based on the above considerations, it is preferred that the polar motion effect is not removed in this stage. This is also true for drift, which is exponential in the first half a year after installation and becomes linear after the first half a year. Finally only the solid Earth tides and the atmospheric effect need to be removed.

Unlike g_{raw}, the channel of air pressure has only gaps that need to be corrected for. Since the pressure variation would look like red noise, there is not enough evidence which can be used to recognize the sudden change of pressure value as steps or spikes. So there is only one type of offsets – gaps. It is difficult to generate data in a gap period. For a gap of a few hours or shorter, it is reasonable to fill the gap with a linear interpolation from the beginning point to the ending point of the gap. For longer period gap, data from meteorological service would be helpful. These data are usually in 1 hour interval and a simple linear interpolation can be applied on the 1 hour interval data before filling the gap. The tide data is from Dr. Rudolf Widmer-Schnidrig. It is a preliminary model from analyzing data from other instruments (for example, the collocated seismometer or spring gravimeter). This tidal model will be improved in the second iteration of data processing, which will be discussed in details later.

How to model the atmospheric effect is a widely studied topic. There are in general four kinds of approaches with different complexities and calculation amounts. Single admittance factor approach uses the station air pressure measurement and a single constant admittance factor. Frequency-dependent admittance approach replaces single admittance factor by variable admittance function of frequencies. The 2-D approach convolves the surface air pressure grids of the whole Earth surface with a Green's function and the 3-D approach includes even the vertical variation of air density distribution. In remove-restore process, the removed air pressure effect will be restored in the later steps, so the pressure model error should not have de facto influence on the final restored signal. The model error may have an influence on the

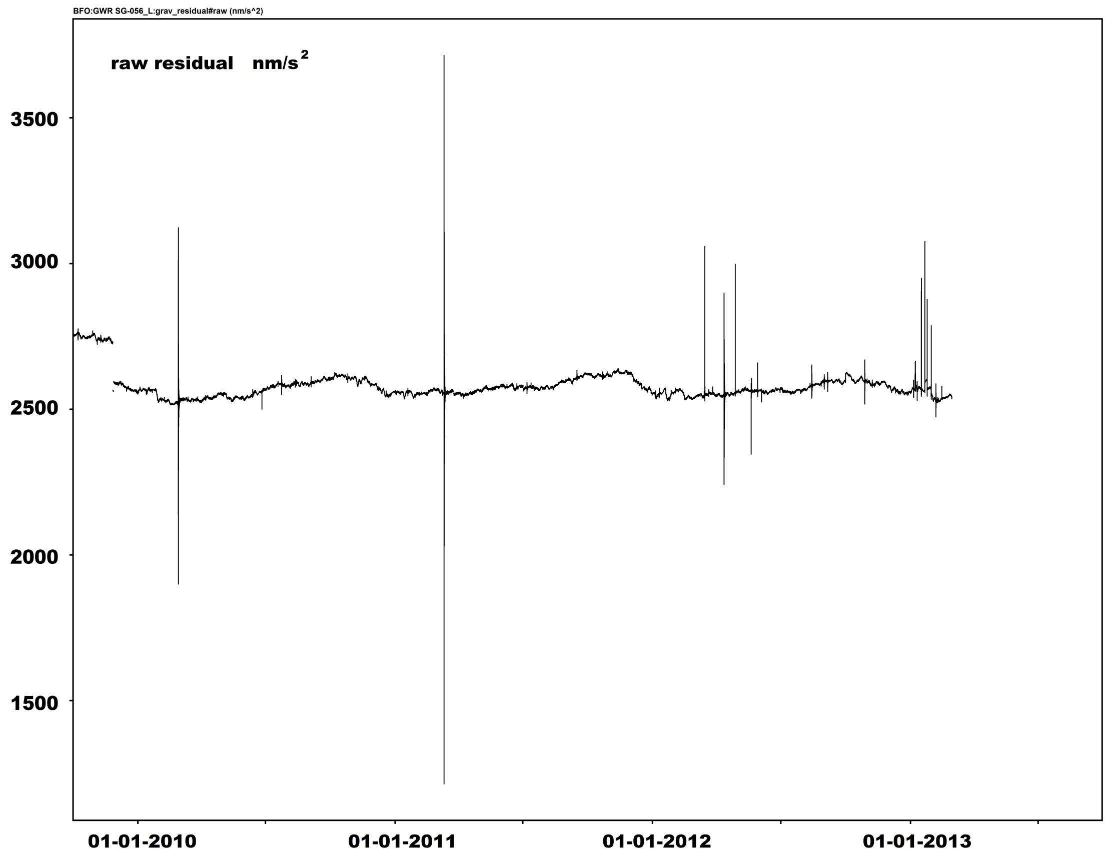

Figure 4.7: *The gravity residual of SG-056 lower sphere after removing the solid earth tides and the atmospheric effect. The spikes of instrumental origin or earthquake oscillation can amount to a few thousand nm/s*^{2}*, which should be corrected to make the variations of gravity residual clearer.*

offset correction, but it can be ignored considering the small magnitude. In the first iteration of remove-restore technique, the nominal factor of 3.2 nm·s^{-2}/hPa is applied.

$$g_{\text{residual raw}} = g_{\text{raw}} - g_{\text{tide}} + 3.2 \cdot P \tag{4.3}$$

g_{raw} is the gravity value after the gravity record from GGP file is multiplied by the GCF (Gravity Calibration Factor), g_{tide} is the tide effect from external tide model, and P is the local air pressure measurement (unit: hPa) from the GGP files and -3.2 is the nominal factor in unit of nm·s^{-2}/hPa. Figure 4.7 shows the gravity residual after removing the solid earth tides and the atmospheric effect. Large steps and spikes happen continuously. The annual cycle of the gravity residual is hidden in the raw gravity residual. The large variations in February 2010 (as also shown in figure 4.11), in March 2011 and in April 2012 are all due to earthquakes. A step of about 200 nm/s^2 happens on 26th Nov. 2009 (the smaller step after this huge step will be shown in figure 4.10).

4.3.4 Remove the offsets

4.3.4.1 The correctors in TSoft

Removing the offsets is the most time-consuming part of data processing. TSoft uses the concept of correctors for the removal of offsets on a data channel. A corrector can be one of the following objects (Vauterin and Van Camp, 2011):

1. A linear interpolation. This interpolation replaces the values in an interval with linear function. Two nodes are used to determine the starting value and the ending value of the corrector.
2. A cubic interpolation. This interpolation replaces the values in an interval with a third degree function. Two of the four nodes are used to determine the starting and ending value and the other two control the shape of the corrector.
3. A step. A step adds a constant value to all the points after the ending point of the corrector, and the data points in the period of the corrector are replaced by a constant value, which equals to the starting value of the step corrector.
4. A gap. All the points in the range of the corrector are flagged and replaced by a space hold.

The node points and the connecting lines are the main components of the corrector. The corrector introduced can be further edited by changing the positions of nodes. All the correctors are initially in inactivated state. When a certain function needs to be applied, the corrector must be activated in advance. Figure 4.8 and figure 4.9 are three correctors in unapplied state and in applied state respectively.

When the user uses the automatically detecting offsets function, an offsets is detected and a proper corrector is created at the location of the offset. The automatic procedure is usually problematic, because of the complexity of the offsets. Each corrector that is defined on a curve can have two states. The unapplied state ensures further editing the automatically generated corrector. In this case of unapplied state, the data points still have their raw values. And in

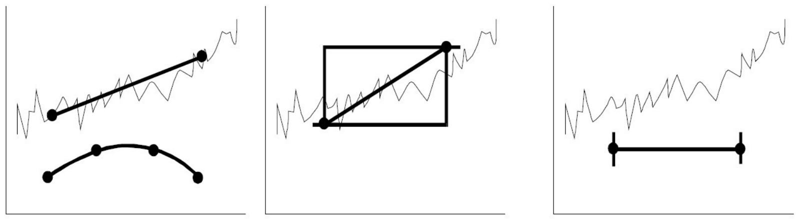

Figure 4.8: Graphical representation of the different correctors in unapplied state. Left: linear and cubic interpolations; middle: step; right: gap. (Vauterin and Van Camp, 2011)

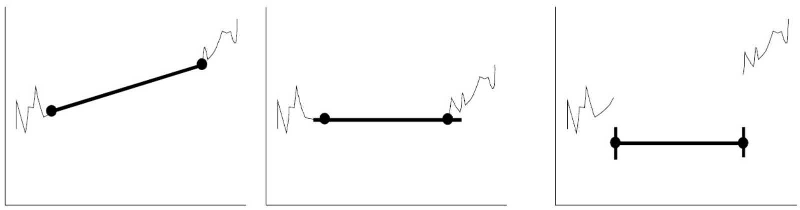

Figure 4.9: Graphical representation of the different correctors in applied state. Left: linear interpolation; middle: step; right: gap. (Vauterin and Van Camp, 2011)

the case of applied state, the point value is changed, and no further editing of the corrector can be carried out. If the user needs to change the corrector after it is applied, the corrector can be deleted by using <Correctors | Delete selected> and a new corrector could be created.

4.3.4.2 The combined approach

At the beginning of data processing, the automatic algorithm for detection and correction of offsets is used. But the automatic procedure does not save time in reality, because large amounts of automatically generated correctors have errors in correcting for gaps and large steps. Some of the correctors are found automatically displaced by a constant value when a large-size corrector is introduced. This may be because of a program bug. The format 'eterna' does not have the ability to store the corrector information. When a file in TSF format (the format of TSoft) is stored in 'eterna' format, the corrector information is automatically deleted and only the corrected signal is stored. This is a disadvantage for 'eterna' format when one needs to recover the original signal before correctors are applied, but on the other hand, it is an advantage for avoiding the case of automatic displacing of correctors. In practice, the intermediate results are transformed into 'eterna' format and the original files in TSF format act as backup. Due to the nature of the detection algorithms, the best approach is first to detect and correct spikes, then to detect and correct gaps, and finally to detect and correct steps (although this ordering is not necessary)(Vauterin and Van Camp, 2011). In this research, the combined approach, which is a combination of automatic approach and manual approach, is used.
The processing workflow consists in the following steps:

1. **Manually correct the large size offsets.**
   Search the gravity series visually and detect the offsets. In this step, only the large gaps, steps, spikes need to be determined. In some cases, a gap is combined with a steps. This

should be corrected with a step corrector. Figure 4.10 is an example of a gap combined with a steps that happened on 27th Nov. 2009.

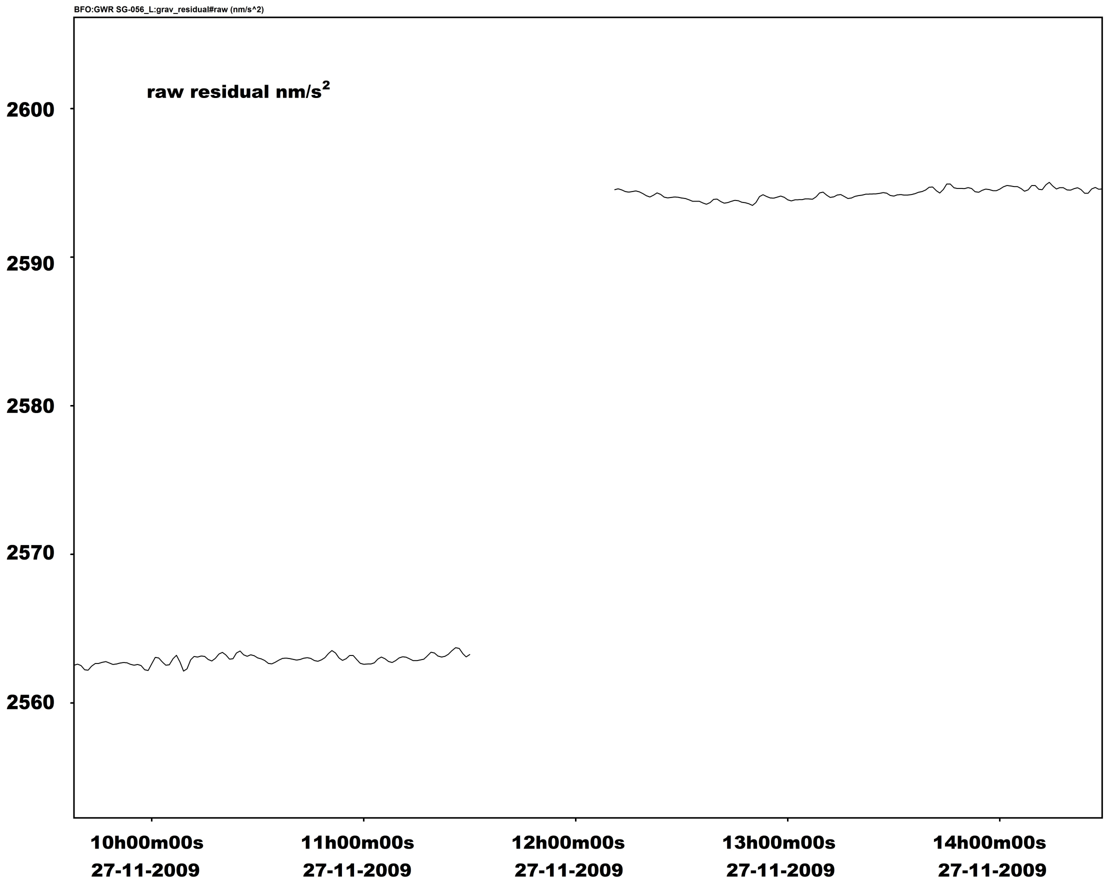

Figure 4.10: *A gap combined with a step that happened on 27th Nov. 2009 (SG-056 lower sphere). There is a significant jump in the period of the gap. In this case, the gap should be corrected with a step corrector, instead of a linear interpolator.*

To determine whether a gap corrector or a step corrector should be applied, the Slope Factor (SF) is introduced.

$$\mathrm{SF} = \frac{g_{\text{ending}} - g_{\text{starting}}}{t_{\text{ending}} - t_{\text{starting}}} \tag{4.4}$$

When SF exceeds a certain threshold, this offset is classified as 'step (combined with a gap)', otherwise as 'gap'. The determination of SF threshold will be discussed in the later section. These large offsets are classified into three sorts (spikes, steps, gaps) and then corrected with corresponding correctors. Then the file is converted into 'eterna' format to avoid possible corrector displacing. The function 'automatic detect gaps' is used to detect and correct all the gaps. Table 4.1 shows the detection settings of spikes and steps in TSoft.

2. **Correct the middle size and small size offsets.**
The parameters of determining middle size offsets are input in the automatic detecting function and the correctors are visually checked and adjusted. Then all the correctors are

	Large size	Middle size	Small size
SPIKES			
Min deviation (nm/s^2)	visible	5	2
Window size	-	20	20
Spike envelope	-	10	5
Ratio	-	3	3
STEPS			
Min deviation (nm/s^2)	visible	10	3
Window size	-	30	30
Exclude w. s.	-	6	6

Table 4.1: *The detection settings of spikes and steps in TSOFT*

applied. The small offsets are corrected in a similar way.
Here comes the problem of classifying the offsets into large size, middle size and small size. Since there is no proper objective factor to classify offsets in different size, the trial-improve strategy is used to determine a series of subjective thresholds for offsets detecting. The determinant of threshold value is the percentage of 'right decision'. The so called percentage of 'right decision' means how many automatically classified steps can be manually determined as steps (not determined as gaps nor spikes), when a certain series of thresholds are applied in the automatic procedure. The way to determine a threshold is as follows:

- step 1: a group of nominal thresholds is applied on a short period of gravity signal (for example, two months' signal). The statistics of 'right decision' is got from the result of offsets classification.

- step 2: one of the parameters in step 1 (preliminarily the 'Min deviation') is changed, and the new statistics are calculated.

- step 3: comparing the results in step 1 and step 2, the parameter is further adjusted towards the trend of improving the percentage of 'right decision'. For example, when a min deviation of 5 nm/s^2 for step detecting (80 % 'right decision') has better performance than a min deviation of 4 nm/s^2, the deviation threshold may be enlarged to 6 nm/s^2. And then the result of 6 nm/s^2 threshold is compared with the result of 5 nm/s^2. If 6 nm/s^2 is again better, a value of 7 nm/s^2 would be applied, otherwise a value between 5 nm/s^2 and 6 nm/s^2 is tried. With this iteration, an optimal value is generated and can be applied to the whole series of 3 years.

The disturbances caused by earthquakes should be dealt with carefully. As shown in figure 4.11, only the gaps should be corrected, the damped oscillation which are the seismic free oscillations of the Earth should be kept in the gravity residual. The upper panel shows the raw gravity residual with the damped oscillation after the earthquake in 27th Feb. 2010. The wave is not fully shown here because of the large amplitude of oscillation. The lower panel shows the gravity residual after correcting for the offsets and the signal is filtered. The amplitude of the oscillation is largely reduced. The amplitude of the oscillation is about 2 nm/s^2. The three hours' gap is filled with a straight line (a linear interpolator). In the case of long period gap with small jump (i.e. the difference of the value at the beginning of the gap and the value at the end of the gap), a linear interpolator is the optimal treatment of the gap. The final step of offsets correction is filtering the residual with a finite impulse response (FIR) filter. The most violent earthquake of the three years' recording occurred on 11th Mar. 2011 and caused one gap. The gaps are filled with straight lines and then the data is filtered. The strong oscillation is reduced to a few nm/s^2 after the filter is applied.

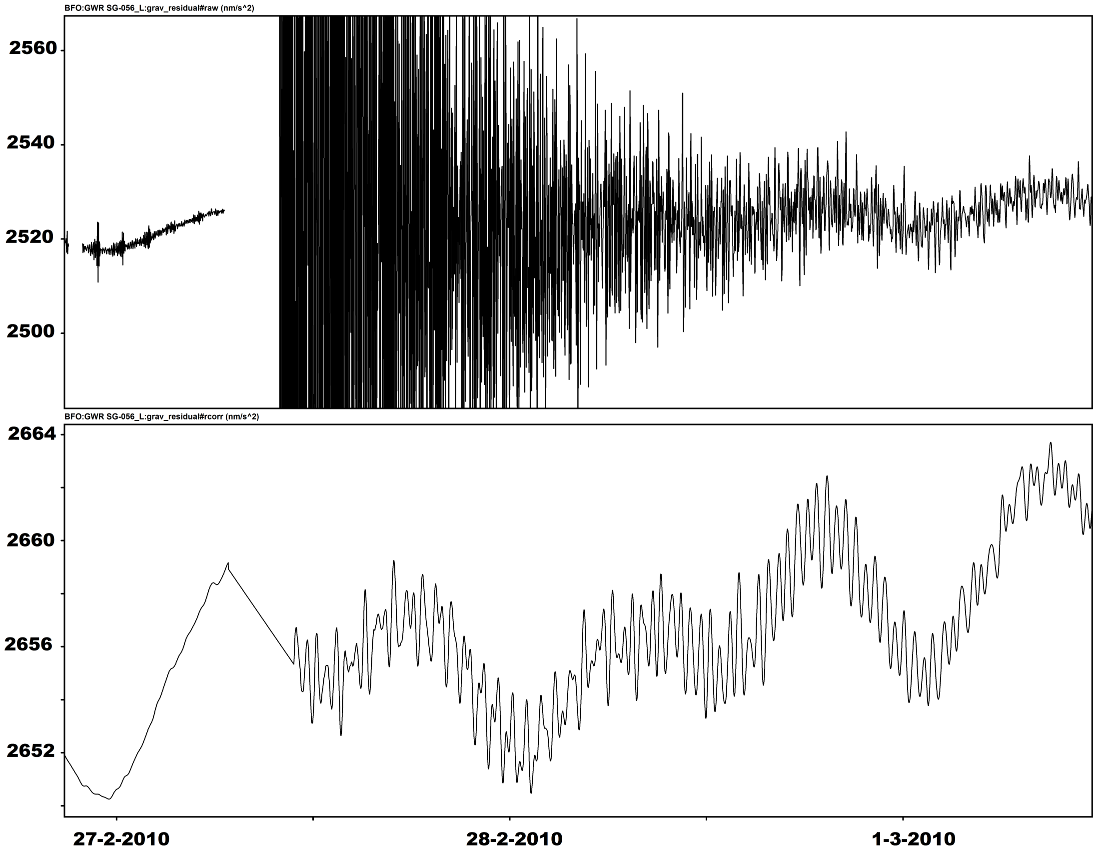

Figure 4.11: *Removing a gap caused by earthquake (unit: nm/s^2, SG-056 lower sphere). The upper panel shows the raw gravity residual with the damped oscillation after the earthquake. The lower panel shows the gravity residual after correcting for the offsets and the signal is filtered.*

After correcting all the offsets in the three years' gravity signal, an annual period variation that dominates the residual can be clearly seen. And this variation has an amplitude of about 50 nm/s^2 for BFO low sphere as shown in figure 4.12. The amplitudes of different years vary in the three and a half year gravity residual.

Figure 4.13 shows some intermediate results of the first iteration (BFO low sphere).

- Channel 1: the gravity series in volt. Massive disturbances occurred in March 2011 and in January 2013, which are also clearly visible in Channel 2 and Channel 5.

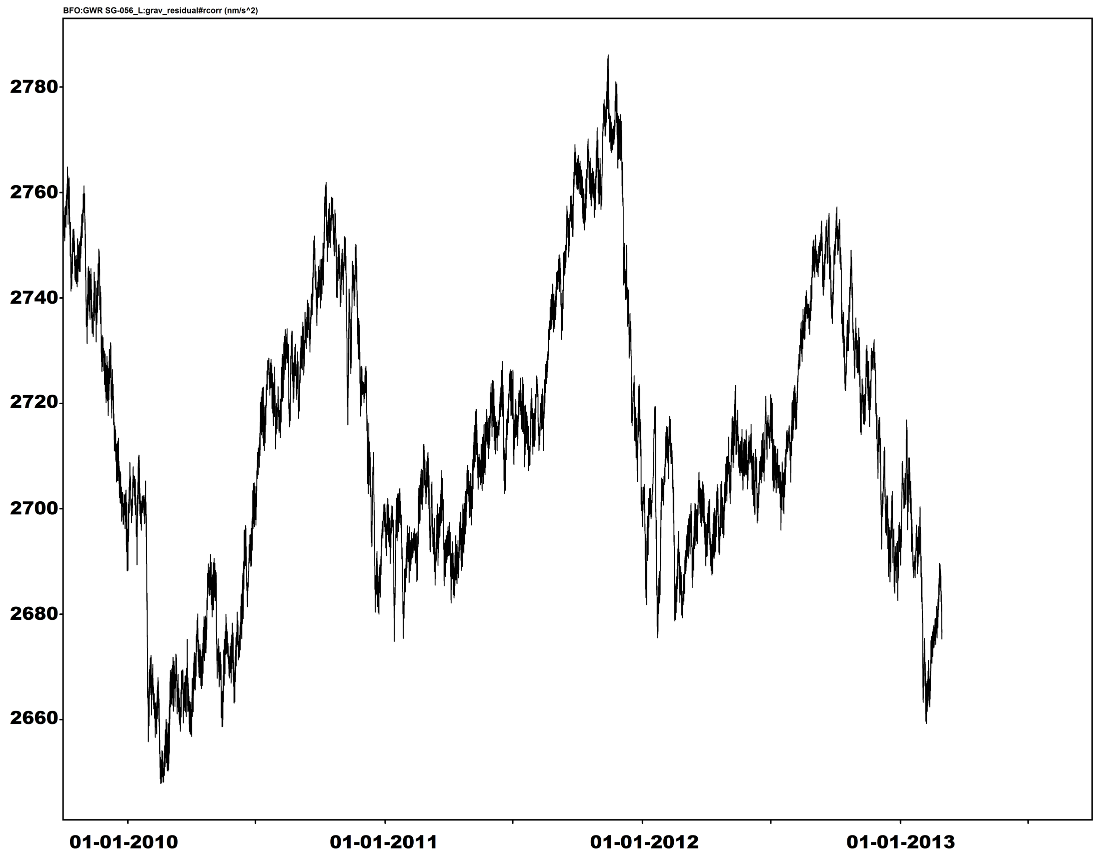

Figure 4.12: *Offsets corrected gravity residual of SG-056 lower sphere (unit: nm/s^2). The annual variation has an amplitude of about 50 nm/s^2. The gravity residual peaks around October and reaches its troughs between January and February.*

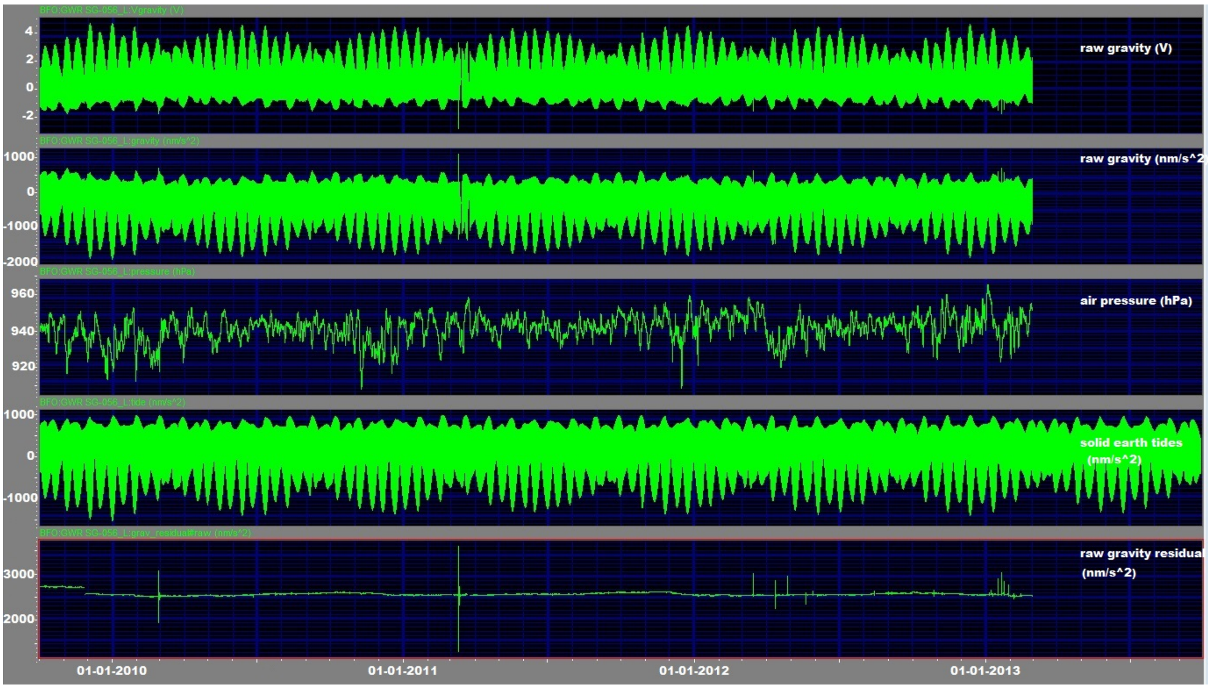

Figure 4.13: *Some intermediate results of the first iteration (BFO lower sphere). They are the gravity series in Volt, the gravity series in nm/s^2, the air pressure in hPa, the solid earth tides in nm/s^2 and the residual after removing the solid earth tides and the atmospheric effect ($g_{residual\ raw}$).*

- Channel 2: the gravity series in nm/s^2. Since the GCF (Gravity Calibration Factor) is negative, the shape looks like an inverted image of Channel 1.
- Channel 3: the pressure series changes in an irregular way (unit: hPa).
- Channel 4: the theoretical prediction of the solid earth tides dominates the raw gravity signal. This is from measurements of a collocated spring gravimeter. Note the similar signal amplitude and shape with Channel 2.
- Channel 5: $g_{\text{residual raw}}$ is the residual after removing the solid earth tides and the atmospheric effect. No clear period is visible, as long as the huge disturbances are not yet corrected.

Figure 4.14 shows the gravity residuals in different processing steps (BFO low sphere, Oct. 2009 - Dec. 2009).

- Channel 1: (top) the gravity residual before correcting for the offsets;
- Channel 2: (middle) the gravity residual after correcting for the offsets;
- Channel 3: (bottom) the corrections for the offsets (Channel 1−Channel 2).

A series of steps happened on 26th Nov. 2009 and continued until 27th Nov. 2009. Two major earthquakes happened on 8th Oct. 2009 and 9th Nov. 2009. These disturbances have been cleared out in the Channel 2.

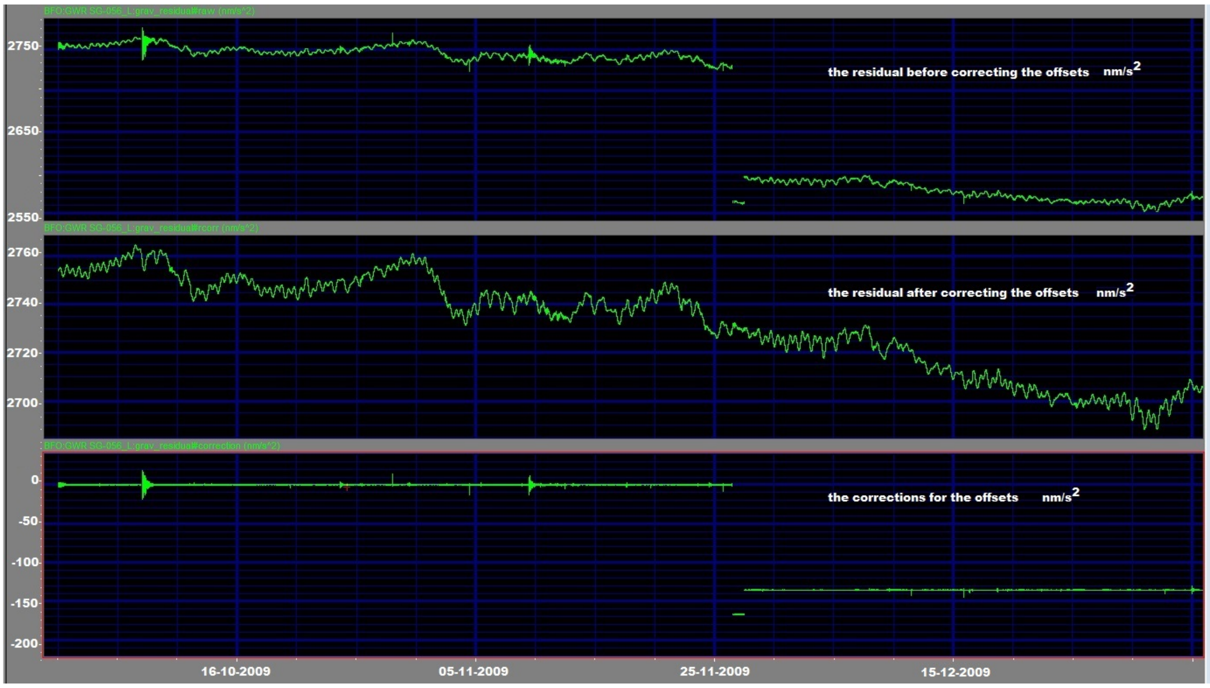

Figure 4.14: *Remove the offsets in 2009 (unit: nm/s^2, SG-056 lower sphere). Three channels are : Channel 1 (top), the gravity residual before correcting for the offsets; Channel 2 (middle), the gravity residual after correcting for the offsets; Channel 3 (bottom), the corrections for the offsets (Channel 1—Channel 2). In channel 2, the steps are corrected and the earthquake oscillations are filtered out.*

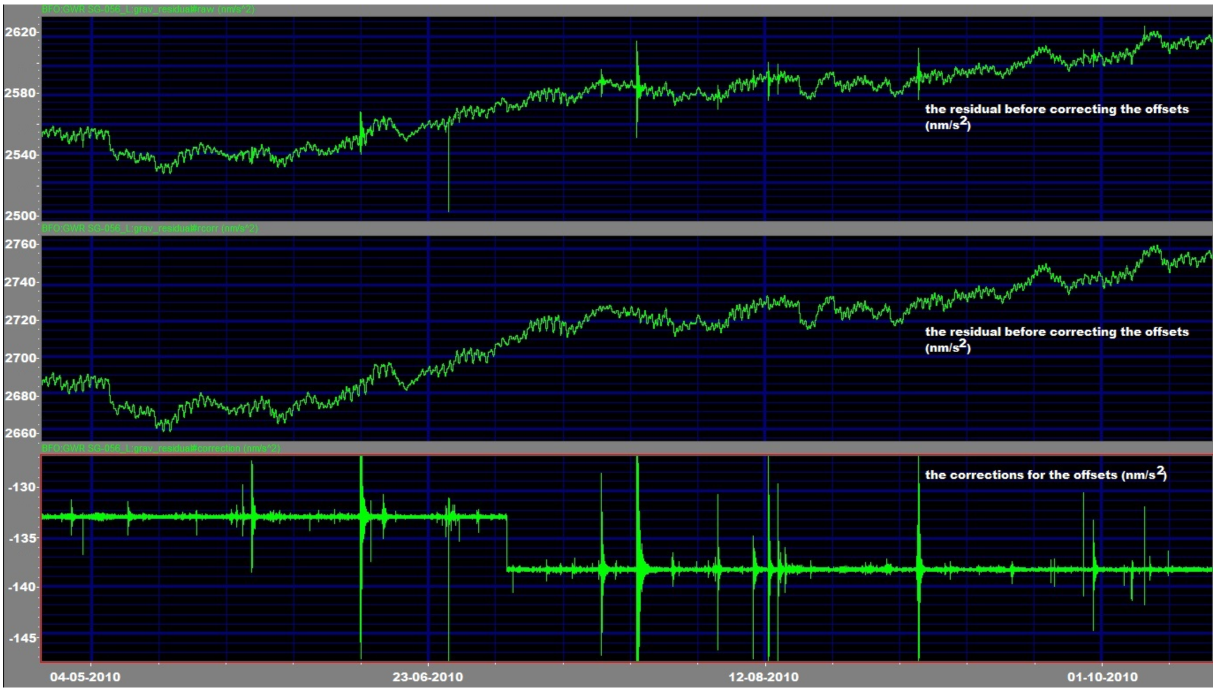

Figure 4.15: *Remove the offsets in 2010 (unit: nm/s^2, SG-056 lower sphere). Three channels are : Channel 1 (top), the gravity residual before correcting for the offsets; Channel 2 (middle), the gravity residual after correcting for the offsets; Channel 3 (bottom), the corrections for the offsets (Channel 1—Channel 2). There are earthquake oscillations, steps and spikes in this period.*

Figure 4.15 is another zoomed in view of the gravity residual before and after correcting for the offsets and the correction for offsets. A step that occurred on 4th July 2010 is corrected and a variety of small oscillations following the earthquakes are filtered out.

4.3.5 Restore the signal

After the offsets are cleared out and the earthquake oscillations are filtered out, the gravity residual on this stage is called $g_{\text{residual corr}}$. Now the next step is to restore the gravity signal. According to figure 4.5, three iterations are done in the data processing. The output of the first iteration $g_{\text{restored iter2}}$ (the result after restoring the removed components in iteration 1) is imported into iteration 2 as the input signal. When restoring the signal, one must make sure the restored signals (the solid earth tides and the atmospheric effect) are exactly the signals removed in the first step.

$$g_{\text{restored iter2}} = g_{\text{residual corr iter1}} + g_{\text{tide}} - 3.2 \cdot P \tag{4.5}$$

And in the removing process,

$$g_{\text{residual raw}} = g_{\text{raw}} - g_{\text{tide}} + 3.2 \cdot P \tag{4.6}$$

$$g_{\text{correction iter1}} = g_{\text{residual raw}} - g_{\text{residual corr iter1}} \tag{4.7}$$

combine these three equations, we can get

$$g_{\text{restored iter2}} = g_{\text{raw}} + g_{\text{correction iter1}} \tag{4.8}$$

This formula is usually used to check the result from iteration 1.

4.4 The second and the third iterations

4.4.1 A brief description of the three iterations

As mentioned in Section 4.3, 3 iterations are done in the data processing to get the final $g_{\text{residual corr iter3}}$. The iteration 1 is already explicitly described in Section 4.3. In short, the atmospheric effect and the earth tides from external data sources are removed to reach $g_{\text{residual raw}}$, then the offsets are corrected and the earthquake oscillations are filtered out to get $g_{\text{residual corr}}$. On the basis of $g_{\text{residual corr}}$, the atmospheric effect and the solid earth tides used in the removing step of the iteration 1 are restored to create $g_{\text{restored iter2}}$, which is the input of iteration 2. The iteration 2 and iteration 3 are similar to iteration 1. The difference is the source of the solid earth tides and the atmospheric correction factor. In iteration 2, the restored signal is imported into the software ETERNA (Wenzel, n.d.), and the program ANALYZE is used to generate the solid earth tides model and a new correction factor for the atmospheric correction. The output of ANALYZE, which is a tidal model, is used to generate a gravimetric tidal series. This new generated atmospheric correction factor and the solid earth tides model are more accurate than the one used in the first iteration. The iteration 3 is similar to the iteration 2.

4.4.2 The solid earth tides

4.4.2.1 An overview of the solid earth tides

The earth tides can be calculated using some models: the model of tidal forcing and the model of Earth's response to the forcing. One of the models is the attraction force model. The attraction forces from astronomical bodies can be evaluated using Newton's law of universal gravitation. Other models are the models of Earth's and ocean's response to the attraction forces. The solid earth's response is usually called body tide, which means the Earth's response without considering the ocean. Ocean model describes the tide loading because of the transportation of ocean water. The solid earth tides and ocean loading are summed up to calculate the total tide effect. The gravity tide $y(t)$ is represented by (Schubert and Price, 2007)

$$y(t) = \int x_T(t-\tau)w_T(\tau)\mathrm{d}\tau + n(t) \tag{4.9}$$

where $x_T(t)$ is the tide force and $n(t)$ is the noise. The function $w_T(\tau)$ is the Earth's response to the tide force. In frequency domain, this equation equals to

$$Y(f) = W_T(f)X_T(f) + N(f) \tag{4.10}$$

$W(f)$ is the 'tidal admittance'. When predicting the tidal gravity $Y(f)$, the admittance $W(f)$ is assumed known. When analyzing the tides, we determine $W(f)$ from tide observations. Figure 4.16 is an overview of the solid earth tides.

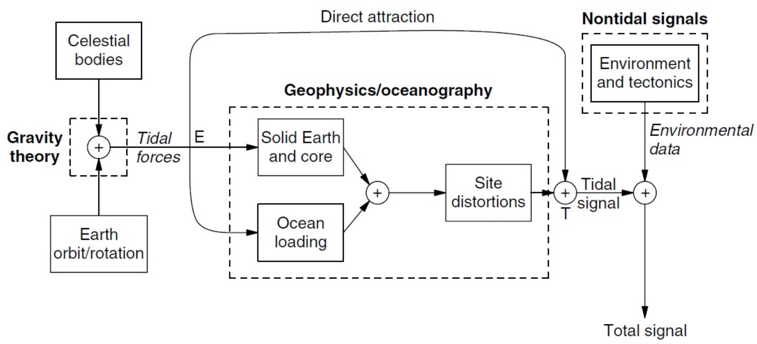

Figure 4.16: *An overview of the solid earth tides (Schubert and Price, 2007)*

4.4.2.2 Analyzing and predicting earth tides

1. **The ETERNA 3.40 software package**
   The software ETERNA 3.40 (Wenzel, 1996) is designed to preprocess, analyze and predict earth tides and calculate the ocean tide loading. This software has a series of programs DETIDE, DESPIKE, DECIMATE, ANALYZE, PREDICT and OCELOAD. The ETERNA 3.40 package contains altogether 21 programs, of which only programs ANALYZE (analysis of earth tide data) and PREDICT (computation of synthetic model tides) are used in this thesis.

2. **The ETERNA format**
   The data files of the ETERNA 3.40 package use the ETERNA format to store high precision tidal measurement. One ETERNA data file consists of one header, one or more parameter parts and one or more data sections.
   Figure 4.17 is an example of the ETERNA files used in the data processing. For more detailed description of the ETERNA format, readers can refer to 'ETERNA 34 manual' written by H. G. Wenzel.

```
FILE                   : BFO_ANALYZ.DAT
STATUS                 : 20130422
CONTENTS OF THE FILE   : GRAVIMETRIC EARTH TIDE OBSERVATIONS WITH
GWR SG-056                          _L at Black Forest
Observatory
STATION:               : Heubach 206 D-77709 Wolfach Germany
latitude: 48.3298N   longitude: 8.3273E    elevation: 589.2m
REGISTRATION PERIOD    : 20091001 03:00 ... 20130228 21:00
AVAILABLE DATA         : HOURLY CALIBRATED GRAVITY VALUES, HOURLY
AIR PRESSURE VALUES

CONVERTED FROM TSF FORMAT
C*****************************************************************
***************
INSTR              1.0000    1.0000     0.000         0
77777777             .000      .000
20091001 050000   279.606   940.267
20091001 060000    53.142   940.671
20091001 070000  -209.560   941.050
20091001 080000  -445.993   941.309
20091001 090000  -597.763   941.478
20091001 100000  -624.108   941.337
20091001 110000  -515.939   941.409
20091001 120000  -293.301   941.113
20091001 130000    -7.698   940.945
20091001 140000   274.977   940.852
20091001 150000   486.733   941.079
20091001 160000   579.149   941.247
20091001 170000   531.535   941.570
```

Figure 4.17: The beginning of file BFO_ANALYZ.dat in eterna format. This file records the 1 h sampling interval solid Earth tides. A 77777777 record marks the beginning of the data section.

   Explanation of data file BFO_ANALYZ.dat in ETERNA format data records: The data section, which starts with a 77777777 record, contains four columns: IDAT, ITIM, Channel 1 and Channel 2.

   - IDAT = data of the record, 20091001 means year = 2009, month = 10 = October, day = 1.
   - ITIM = time of the sample in UTC, 050000 means 5 hrs, 0 min, 0 sec.
   - Channel 1 is usually the earth tide observation (the gravity channel in this thesis, unit: nm/s^2).
   - Channel 2 is the air pressure channel (unit: hPa).

3. **Analysis of the Earth tides using program ANALYZE**
   The program ANALYZE is used to analyze Earth tide observations. The file 'project' defines the project name for ANALYZE. The project name is used to define the input and output files. The program ANALYZE uses the following file name convention (Wenzel, n.d.):

   - control parameter file: 'project name'.ini

- hourly data input file: 'project name'.dat
- print file: 'project name'.prn
- hourly residuals of adjustment: 'project name'.res
- spectrum of residuals: 'project name'.far
- adjusted parameters: 'project name'.par
- normal equation system file: 'project name'.new

4. **The control parameter files 'pn'.ini**

   There exists a default control parameter file given by ETERNA software package. Some default parameters must be changed according to the parameters of stations (like TEXTHEADER – the header of the printed file, STATLATITU – ellipsoid latitude, STATLONITU – ellipsoid longitude, STATELEVAT – ellipsoid height, ...).
   The list of wave groups used for analysis of Earth tides is shown in figure 4.18, with 23 wave groups.

	Frequency from (cpd)	to (cpd)	Amplitude factor	Phase lead (degree)	
WAVEGROUPI=	0.000000	0.001369	1.00000	0.0000	long
WAVEGROUPI=	0.001379	0.004107	1.00000	0.0000	SA
WAVEGROUPI=	0.004108	0.020884	1.00000	0.0000	SSA
WAVEGROUPI=	0.020885	0.054747	1.00000	0.0000	MM
WAVEGROUPI=	0.054748	0.091348	1.00000	0.0000	MF
WAVEGROUPI=	0.091349	0.501369	1.00000	0.0000	MTM
WAVEGROUPI=	0.501370	0.911390	1.00000	0.0000	Q1
WAVEGROUPI=	0.911391	0.947991	1.00000	0.0000	O1
WAVEGROUPI=	0.947992	0.981854	1.00000	0.0000	M1
WAVEGROUPI=	0.981855	0.998631	1.00000	0.0000	P1
WAVEGROUPI=	0.998632	1.001369	1.00000	0.0000	S1
WAVEGROUPI=	1.001370	1.004107	1.00000	0.0000	K1
WAVEGROUPI=	1.004108	1.006845	1.00000	0.0000	PSI1
WAVEGROUPI=	1.006846	1.023622	1.00000	0.0000	PHI1
WAVEGROUPI=	1.023623	1.057485	1.00000	0.0000	J1
WAVEGROUPI=	1.057486	1.470243	1.00000	0.0000	OO1
WAVEGROUPI=	1.470244	1.880264	1.00000	0.0000	2N2
WAVEGROUPI=	1.880265	1.914128	1.00000	0.0000	N2
WAVEGROUPI=	1.914129	1.950419	1.00000	0.0000	M2
WAVEGROUPI=	1.950420	1.984282	1.00000	0.0000	L2
WAVEGROUPI=	1.984283	2.002738	1.00000	0.0000	S2
WAVEGROUPI=	2.002739	2.451943	1.00000	0.0000	K2
WAVEGROUPI=	2.451944	7.000000	1.00000	0.0000	M3M6

Figure 4.18: *The list of wave groups with initial amplitude factors and phase leads. There are in total 23 wave groups. In the '.ini' file for program 'ANALYZE', the amplitude factors and phase leads are set as 1 and 0 respectively.*

4.4.2.3 Generating a new tide series using ETERNA software package

As described in Section 4.3, the solid earth tides used in the first iteration are from spring gravimeter observations. We prefer to use a tidal model derived from the BFO-SG data itself in iteration 2 and iteration 3. So the restored gravity from iteration 1 is input into the software package ETERNA in iteration 2.

Firstly, improved tidal parameters and meteorological parameter (used for atmospheric correction) are generated using program 'ANALYZE'.
The following files are prepared as the input into the program 'ANALYZE' (BFO as an example):

- **BFO_ANAL.DAT**
  It is converted from the output file of the restored gravity channel in TSF (TSoft format). The header contains the general information of the station and the data record part contains two channels: the restored gravity, the air pressure (identical to the raw measurement from GGP file except gaps are filled). For BFO, the restored period from 1st Oct. 2009 to 28th Feb. 2013 is used. But for ST, only the period from 1st Feb. 2010 to 10th Feb. 2013 is used, since the residual of ST in Jan. 2010 is strongly affected by the manipulation and thus contaminated.

- **BFO_ANAL.INI**
  The configuration file is written according to section 4.4.2.2.

- **myrun.bat**
  The batch file is created with the route to find the necessary input files.

- **PROJECT**
  The file PROJECT provides the project name 'BFO_ANALYZ'.

When all these files are prepared and stored under one route, type in the route of program ANALYZE in MS-DOS window and execute the program.
The program generates files: ANALYZE.PRN, BFO_ANAL.FAR, BFO_ANAL.PAR, BFO_ANAL.PRN, BFO_ANAL.RES. Of all these comprehensive analysis results of the restored gravity, adjusted tidal parameters, regression coefficient (atmospheric correction factor) from the file 'BFO_ANAL.PRN' is most useful in the later data processing.
Secondly, the improved tidal parameters and the meteorological parameter generated using program ANALYZE is input into program PREDICT to generate a new tide series for BFO.
The following files are prepared as the input into the program 'PREDICT':

- **RUN_BFO.INI**
  The configuration file is written according to Section 4.4.2.2. And the adjusted tidal parameters (the result from program ANALYZE) is used as the input of program PREDICT. The parameter INITIALEPO is set as 2009 10 1 and SAMPLERATE is set as 60 (60s - 1 min interval series). PREDICSPAN is set as 35040 (35040 hours equals to 4 years). So 1 minute interval tidal series from 1st Oct. 2009 to about 30th Sept. 2013 would be generated.

- **myrun.bat**
  The batch file is created under the route to find the necessary input files.

- **PROJECT**
  The file PROJECT provides the project name 'RUN_BFO'

The output files are RUN_BFO.PRD and RUN_BFO.PRN. RUN_BFO.PRD contains the new solid earth tide series which can be used in iteration 2. This improved solid earth tide series from 'PREDICT' and the new adjusted atmospheric correction factor from 'ANALYZE' will improve the accuracy of the tide correction and the atmospheric correction respectively.

Table 4.2 is a comparison of air pressure correction factors of three measurements in three iterations. We can see the correction factors range from 3.35 nm$\cdot$s^{-2}/hPa to 3.40 nm$\cdot$s^{-2}/hPa

	BFO low	BFO up	ST
Iteration 1	3.2	3.2	3.2
Iteration 2	3.36	3.38	3.39
Iteration 3	3.35	3.40	3.40

Table 4.2: *Pressure factors of three iterations unit: nm·s^{-2}/hPa*

in iteration 2 and iteration 3. Since the difference of correction factors is not significant and the amount of correction factors is limited, it is not proper to come to a conclusion, that ST has a larger correction factor than BFO. The difference of correction factors between iteration 2 and iteration 3 is not significant (about 0.01 nm·s^{-2}/hPa). We can estimate the uncertainty caused by the correction factor variation in the following way. The variation of air pressure at BFO can amount to about 50 hPa in long period (longer than a year), so the uncertainty is 0.01 nm·s^{-2}/hPa $\times$ 50 hPa = 0.5 nm·s^{-2}. This level of uncertainty does not have influence on the correcting process.

Figure 4.19 is a comparison of the solid earth tide signals in three iterations for BFO. *Upper left figure*, the difference of the solid earth tides in iteration 1 and iteration 2 in the time domain; *upper right figure*, the difference of the solid earth tides in iteration 2 and iteration 3 in the time domain; *lower left figure*, the difference of the solid earth tides in iteration 1 and iteration 2 in the frequency domain; *lower right figure*, the difference of the solid earth tides in iteration 2 and iteration 3 in the frequency domain.
We can see the difference of the solid earth tides in iteration 1 and iteration 2 has an amplitude of 8 nm/s^2. In the frequency domain, there exist differences of about 0.8-2.3 nm·s^{-2}·Hz^{-1}, mostly of diurnal and semi-diurnal tides. This is significant improvement, because the modeling error in the solid earth tides has an influence on the quality of the final gravity residual. But the improvement from iteration 2 to iteration 3 is not significant, both in the time domain and in the frequency domain. The difference in the time domain has magnitude of about 0.1 nm/s^2, which is far below the commonly accepted SG accuracy in the time domain (1 nm/s^2). In the frequency domain, the difference is about 0.006-0.009 nm·s^{-2}·Hz^{-1}, which is also negligible. It can be inferred that, a fourth iteration would not benefit the data processing quality since it would not make any improvement either in the solid earth tides and the atmospheric correction.

4.4.3 Polar motion effect

The polar motion, consists of the Chandler Wobble with a period of about 435 days and a yearly circular motion of the rotation axis of the Earth relative to the crust, is one of the important signal after the tides are corrected. The detection of polar motion effect with a gravimeter was first successfully done in 1980s (Richter, 1983). If a body (with certain mass m) is revolving around a point, there is a trend that this body keeps the direction of motion (moving in the direction of a straight line, according to Newton's first law of motion). A force towards the revolving center is needed to constantly change the direction of motion, thus keep the circling motion. This can be understood in another way: in a non-inertial frame, there exists a force towards the opposite direction of the revolving center. This force in the non-inertial frame

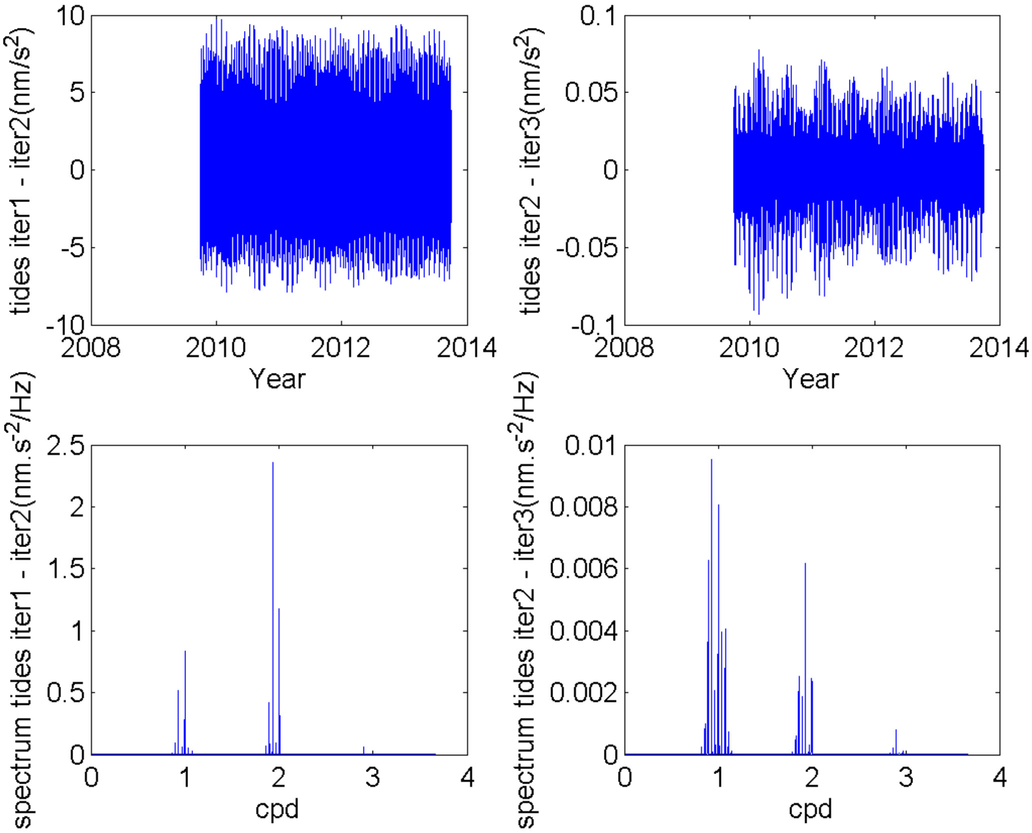

Figure 4.19: *The differences of tide series between Iteration 1 and Iteration 2 and between Iteration 2 and Iteration 3 of BFO. Upper left: the difference of the solid earth tides between Iteration 1 and Iteration 2 in the time domain; upper right: the difference of the solid earth tides between Iteration 2 and Iteration 3 in the time domain; lower left: the difference of the solid earth tides between Iteration 1 and Iteration 2 in the frequency domain; lower right: the difference of the solid earth tides between Iteration 1 and Iteration 2 in the frequency domain.*

is the so called centrifugal force. As shown in figure 4.20, its direction is outward, from the revolving center and perpendicular to the rotation axis. The magnitude of the outward force is $\delta g = \omega^2 r$. This is the same case of Earth's centrifugal force. For all the bodies static referring to the Earth, the rotation period is 1 day. The moment arm r is the distance from the body to the spin axis, thus a function of the latitude. The location of the rotation axis is not fixed inside the Earth. This motion of the rotation poles is termed polar motion. Polar motion changes the latitude of the measurement station (of course, also changes the longitude for most cases), thus it has an influence on the centrifugal force sensed by the SG sphere. Another variable in the formula $\delta g = \omega^2 r$ is the angular velocity of Earth rotation ω. The quantification parameter for the angular velocity is LOD (Length Of Day). The effect of variations in LOD on δg is about two orders of magnitude less than that of polar motion (Xu et al., 2004).

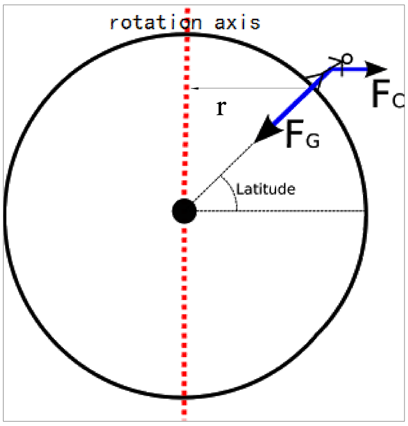

Figure 4.20: *Centrifugal force on Earth's surface. This figure shows the centrifugal force F_C of a person rotating with the Earth around the rotation axis (red dashed line). The moment arm r is the distance from the body to the spin axis, which is a function of 'Latitude'. The direction of the centrifugal force is outward, from the revolving center and perpendicular to the rotation axis.*

The polar motion effect is clearly visible in the gravity recordings after the atmospheric effect and the Earth tides are removed. This is an outstanding feature of SG instruments and is only possible due to their very low instrumental drift. Our intention is correcting the polar motion to see a clearer signal of hydrology, not extracting the polar motion signal from this series. Therefore, the high accuracy polar orientation data from the International Earth Rotation Service (IERS) are used to model the effect at specified position. Today, the best method to observe polar motion are based on space geodesy and the results are published by IERS. We use IERS Earth Orientation Parameters (EOP) to predict and remove polar motion effect. Figure 4.21 shows the EOP from Jan. 2012 to Oct. 2013. It is defined as the disparity of the Earth's instantaneous rotational axis from the CIO (Conventional International Origin). The unit used in this figure is mas (milliarcseconds). On the Earth's surface, there exists a simple relation: 100 mas = 3.09 m.

This following formula builds up a bridge to convert the amplitude of polar motion $(m1, m2)$ to gravity effect δg (Wahr, 1985).

$$\delta g = 3.90 \times 10^{-9} \sin 2\theta [\cos(m_1 \lambda - \sin(m_2 \lambda)] \tag{4.11}$$

where θ is the co-latitude and λ is the eastward longitude.

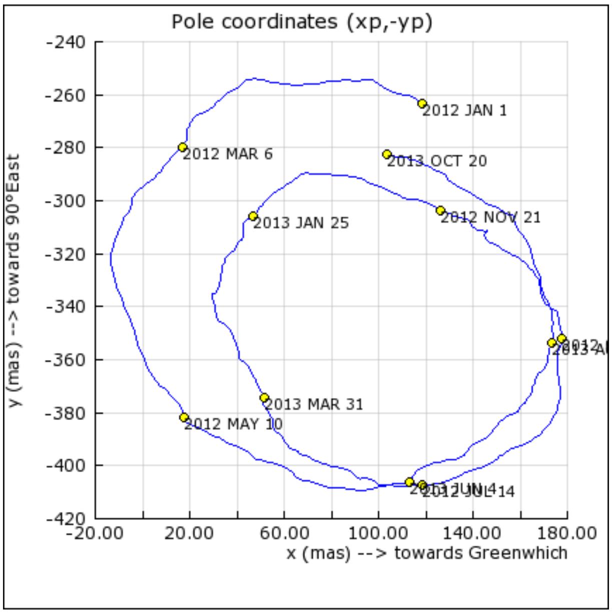

Figure 4.21: *Polar motion from 1 Jan. 2012 (http://hpiers.obspm.fr/eop-pc/). Over recent years, the maximum drift of pole in Y-direction is about 150 mas, which equals to 4.6 m (similar in X-direction).*

A Matlab script (Hartmut Wziontek, personal communication, 2013) is used to generate a polar motion gravity effect series from 2009 to 2013 (until the date when polar orientation data is available) with sampling rate 3600 s in TSF format. In TSoft a linear interpolator is used to interpolate it into 60 s sampling interval data. The adopted linear interpolator is suitable, because the polar motion correction is a smooth curve. Since the IERS polar motion observations come from high accuracy geodetic methods, the polar motion effect can be considered error free in this research. From figure 4.22, we can see the polar motion effect is a beat between annual and Chandler wobble with amplitude of about 20-40 nm/s^2.

4.4.4 Drift

The instrumental drift of SG is discussed in section 2.4. Generally, the drift can be modeled by an initial exponential part of approximately half a year followed by a linear drift. There are two kinds of definitions for drift. In one definition, the drift includes only the trend from the instrumental origin. Another definition is that drift contains all the unwanted long period time varying gravity signal, including the secular change of gravity. In our case, the second definition is adopted, because only the signal of annual period and higher frequency signals are of interest. All the long period signals would be removed. There was attempt to correct for the drift using polynomials, but it can not be supported by a geophysical reason. A simple linear fit is applied to the gravity series after removing the polar motion effect. Only the annual signal and signals with higher frequencies are left out after the drift is removed.
Figure 4.23 shows the gravity residuals before removing the drift and the drift components of these signals.

The fit results are as follows:

- drift-BFOlow = 20.96 nm·s^{-2}/year

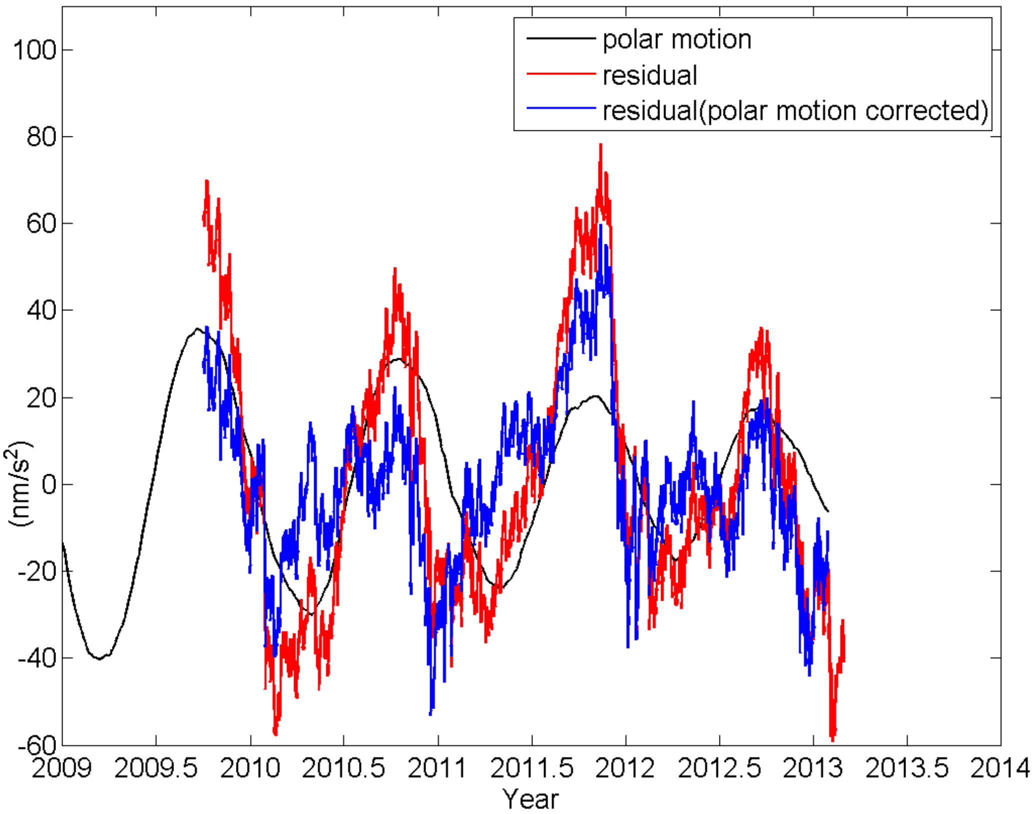

Figure 4.22: *The gravimetric polar motion effect at BFO (unit: nm/s^2). In this figure, the drift is already removed from the gravity residual. The black curve is the gravity effect of polar motion. The red curve and the blue curve are the gravity residuals before and after correcting for the gravity effect of polar motion. We can see the annual variation of the gravity residual is reduced after correcting for the gravimetric polar motion effect.*

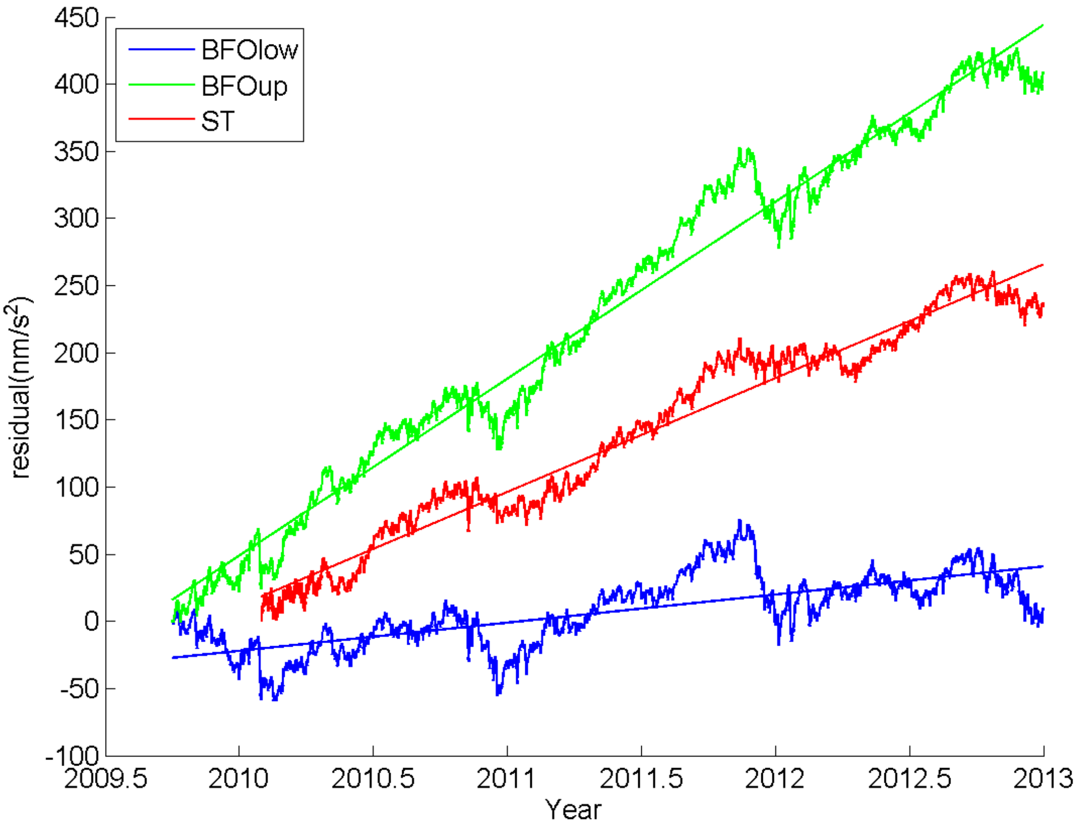

Figure 4.23: *Gravity residuals before removing the drifts and the drift components of these signals (unit: nm/s^2): BFO lower sphere (blue), BFO upper sphere (green) and ST (red). The drift is estimated by a linear fit. The drift of BFO upper sphere is the largest.*

- drift-BFOup =131.71 nm·s^{-2}/year
- drift-ST = 84.76 nm·s^{-2}/year

Only the stable period of signals are used in the linear fit. Stable here means the period without major disturbance (Jan. 2010 for ST) and the part not suitable for a linear fit (first half year's measurements of BFO). The signals used are Apr. 2010 - Dec. 2012 for BFO and Feb. 2010 - Dec. 2012 for ST.
The result of linear fit for ST is 84.76 nm·s^{-2}/year, which is not far from the SG calibration experiments using an absolute gravimeter by Amalvict et al. (2002) (79.19 $\pm$ 0.05 nm·s^{-2}/year). Considering in our fit the tectonics and all other effects are taken into account, this difference is acceptable. The comparison at BFO using AG carried out by Dr. Rudolf Widmer-Schnidrig gave estimation of the drifts: BFO low sphere 0.6 nm·s^{-2}/year, BFO up sphere 128 nm·s^{-2}/year in 2011. Comparing to the estimation in this thesis based on three years data, there is a difference of about a few nm·s^{-2}/year. The relative linear drift fits well (111 nm·s^{-2}/year comparing to 115 nm·s^{-2}/year (R. Widmer-Schnidrig, 2012)).

4.5 Gravity residuals

After removing polar motion effect and drift from the gravity residual of iteration 3, we finally get the 'real' gravity residual, which is dominated by the hydrology signals. From this point on, the term 'gravity residual' refers to the 'real' gravity residual, not to be confused with the intermediate residual before correcting polar motion effect and drift. Note that the gravity residual contains also the modeling errors of the previously removed effects (the atmospheric effect, the solid Earth tides, etc.).

Figure 4.24 shows the gravity residuals of *BFO low* (blue line), *BFO up* (green line), *ST* (red line) and the difference of the residual *BFO low* and *BFO up* (black line).
We can see, all the three residuals show clear annual cycles. The values of *BFO low* and *BFO up* are extremely close after the first half a year. The difference limits to less than 10 nm/s^2. The difference of first half a year looks like an exponential function. This may be because of the different factors A in the two drift functions for two spheres (drift $= A \cdot \mathrm{e}^{-t/\tau}$), where τ is the period.
The small spikes and steps of difference of the residuals *BFO low* and *BFO up* come from the treatment of offsets when correcting the raw gravity residuals. The difference between ST and BFO is more significant, but there are many similar variations of the residuals in some events like the sudden drop of the residuals in October 2010 with similar sizes for three observations. In general, the highest values of residuals occur in Fall and lowest values occur in Winter or Spring, and the decreasing rates of the residuals from Fall to Spring of the next year are much faster than the increasing rates from Spring to Fall.
A sine curve is fitted to each of the three years residuals.

$$Residual = R(t) = A\cos(\omega \cdot t + \phi) \tag{4.12}$$

The fitting parameters are shown in Table 4.3.

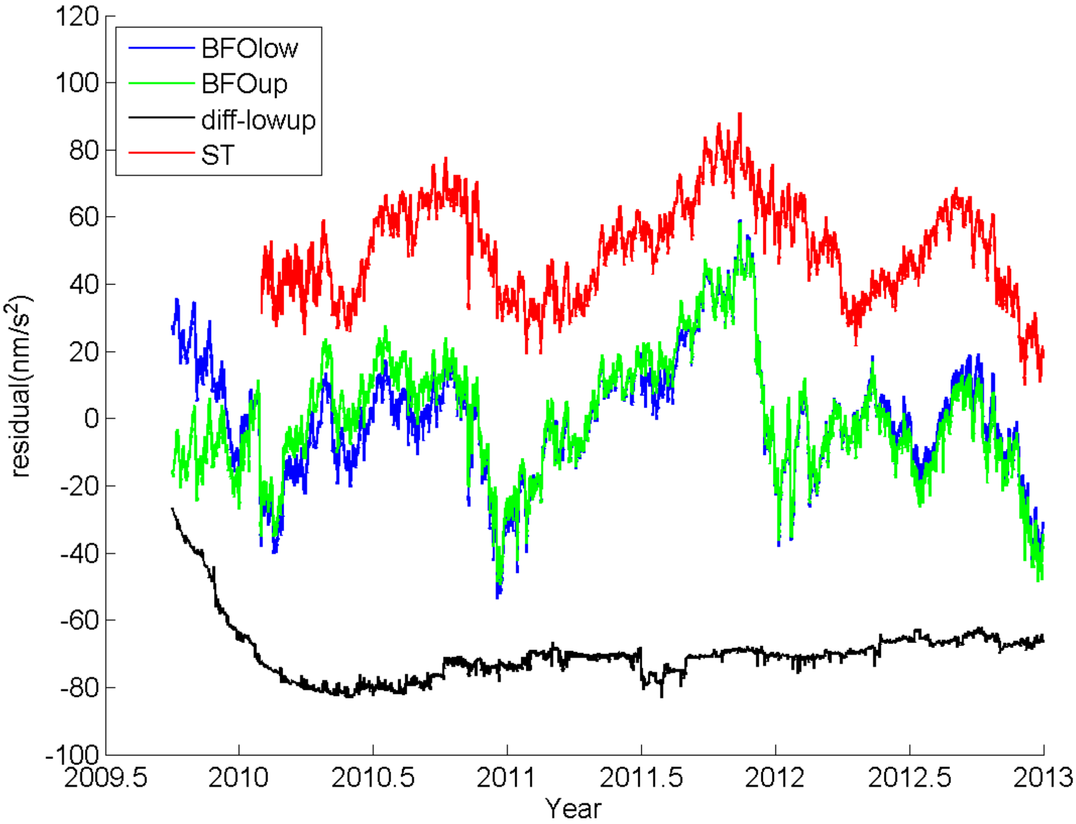

Figure 4.24: *Gravity residuals after removing the linear drift and the difference between the two spheres at BFO (black curve) (unit: nm/s^2). The values of BFO low (blue curve) and BFO up (green curve) are extremely close after the first half a year. The difference between ST (red curve) and BFO is more significant, but there are many similar variations of the residuals in some events.*

	BFO low	BFO up	ST
Amplitude (A) nm/s^2	14.31	13.68	12.68

Table 4.3: *The fitting parameters of residuals*

The amplitude of sinusoid fit for ST residual is smaller than the other two residuals. The residual value from Winter 2011 to Spring 2012 is quite high for BFO, and this abnormality is not clearly shown at ST.
After removing the the atmospherical effect, tides, offsets, the polar motion effect and the instrumental drift, we are now in a position to look at the remaining signal in the residual: the hydrology.

Chapter 5

Hydrology Effects

In this thesis, the hydrological effect is set apart from other effects, because it is perhaps the most complicated correction dealt with. It was a long process, before the hydrological effect on gravity measurement was fully realized in the history of SG. In the first 20 years since a SG was installed at UCSD, the researchers focused on atmospheric effect and tides. For the last 10 years, the hydrological gravity signal becomes the most widely studied topic. The gravity effects from precipitation, water level variation, soil moisture and so on are called hydrological effect. But the hydrological effect can not be simply understood as sum of all these effects, because all these quantities interact with each other. It is problematic to separate the different components that contribute to the hydrological effect. Simply summing up these effects would lead to double counting some parts of the effects. Once the Earth tides, the atmospheric effect, the polar motion effect and the drift are removed, hydrological signals dominate the gravity residual. The hydrological effect is complicated in at least two aspects. The first is some hydrological quantities are not easy to assess. Of all the hydrological quantities, the ground water level is somehow easy to assess with a well close to the instrument. The measurement of soil moisture is not an easy job. The second is the spatial inhomogeneity of most components. Comparing to air pressure, the hydrological quantities are extremely inhomogeneous in different scales, from a few meters to thousands kilometers. Since some measuring methods can only acquire information at single point by their very nature, the measurement should be done by arrays of sensors to acquire a relatively accurate description of the mass distribution.
The local ground water table variation effect can be simplified as a Bouguer plate of thickness h and porosity ϕ. Its effect on gravity is (Crossley, 1998)

$$\mathrm{d}g = 2\pi G\rho\phi h = 0.42\phi h \tag{5.1}$$

where ρ is the density of water. The soil porosity ϕ can only be estimated in very low accuracy. When analyzing the hydrology models, two methodologies are adopted by different groups of researchers. Some focus on the correlation between the observed local hydrological quantities and the gravity residual. The precipitation, soil moisture and ground water level are extensively investigated in the area near a station and these researches show good hydrology - gravity correlation. Recently, a deterministic approach is being deployed to calculate the direct Newtonian attraction. Another methodology consists in using global hydrological models (e.g. GLDAS) to evaluate both Newtonian attraction and loading effect. The accuracy of these models are limited in two dimensions: the highest sampling rate of these data is once every 3 hours and the finest available grid size is limited to 0.25°. The low sampling rate would not cause great trouble, since we are not interested in high frequency signals. But the spatial resolution 0.25° equals to about 19 km in East-West direction and 28 km in North-South direction at 48° N where our two stations are located at. It is not hard to imagine that there are spatial variations

of hydrological quantities within such an area.
In this thesis, not only the hydrological models are discussed, experiments are also done on the precipitation data measured at station BFO. This gives encouraging results in correcting the short period (a few days) variations from the gravity signal.

5.1 Water cycle

Before discussing the hydrological effect and precipitation effect in details, it is necessary to understand the hydrological conditions of the two stations. Water exists in three states: liquid, solid (ice, snow) and gaseous (water vapor). The most important water storage bodies around the instruments are: soil below and above the instruments, vegetation, water aquifer and the rivers in the vicinity of the stations. Water cycle can be further divided into two cycles: biological cycle and global cycle. Biological cycle, just as its name implies, means the entry of water into living beings and then returns to the environment. The terrestrial plants absorb water from the ground and part of the water returns to the environment through transpiration, and another part goes back to soil when in Fall the leaves fall down. Only small percentage of water stays in the plants for longer period but finally somehow is absorbed by the environment. The pumping up effect of plants (mass transportation) has been identified in gravity observations in recent years. The global water cycle does not involve life. The water in the atmosphere is transported onto the ground in the form of precipitation (rain or snow). Most of the water goes into deep layer of the ground through infiltration, other parts go into streams in the form of surface runoff. Precipitation increases the height of the water table and the soil moisture. The streams join the rivers and finally go towards the sea. The transportation between the different bodies and the transformation between the different states ensure the balance of water in long term.

The infiltration of water into the underground and its redistribution are very complex processes. Generally the fundamental equation of hydrology is valid (Harnisch and Harnisch, 2002)

$$P = R_0 + E + (A - C) \tag{5.2}$$

P - precipitation, R_0 - surface runoff, E - evaporation, A - accumulation of water in earth, C - consumption.
According to equation 5.2, the precipitation is the only input of the water system, which can be considered as the engine of the water cycle. A precipitation event leads to rise in water table level and increasing of soil moisture. Both have a direct Newtonian attraction on the SG. The runoff depends on the local topography. High ground slope (BFO) leads to higher speed of water runoff. Evaporation depends on many factors, such as temperature, illumination, wind speed etc.. The accumulation around the station depends on what kind of geologic fabric underground the station is situated in. Soil, sand and granite have totally different characters in porosity. The ground at BFO can be classified as granite with low porosity, thus has lower water retaining capability than the soil base at ST. Consumption depends on the flora and fauna covering the ground of the station. Different sorts of flora and fauna lead to varied characters in water transportation speed and the magnitude of variation (evergreen vs. deciduous plant). Considering the multitude of influence factors of hydrological modeling and the complexity of modeling the transformation of these factors, the following conclusions can be drawn: it is infinitely complex to give an accurate model of the water distribution in the ground, and

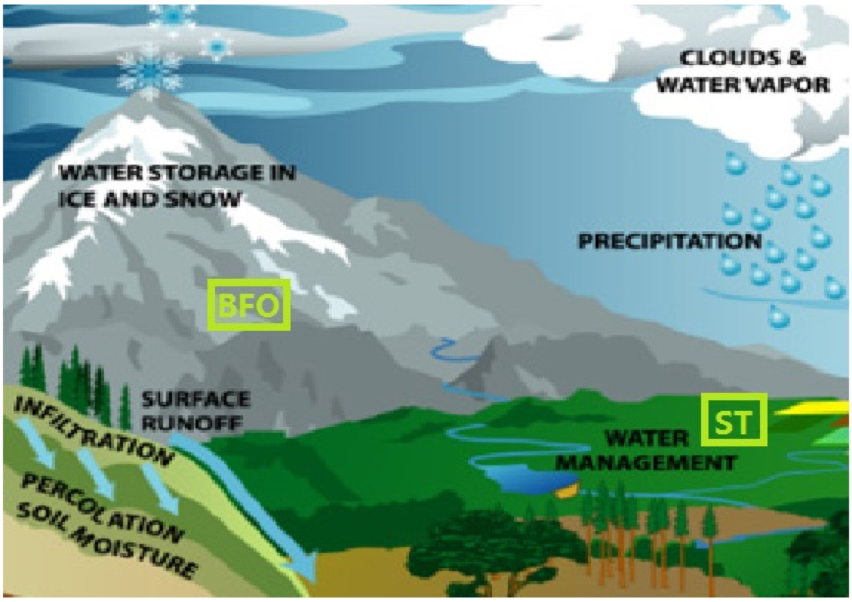

Figure 5.1: *Water cycle (http://gpm.nasa.gov/education/articles/nasa-earth-science-water-cycle). Water exists in three states: liquid, solid and gaseous. The transportation between different bodies and transformation between different states ensure the balance of water in long term. The OSG at BFO is located in a rock mountain and ST is on the alluvial plain of the Rhine river.*

moreover to quantify the gravity influence seems to be nearly impossible. Therefore statistic models are preferred. The quality of these models can be controlled and improved somehow with the help of basic principles of hydrology (Harnisch and Harnisch, 2002).

5.2 Hydrological models

Three hydrological models (GLDAS, ERA-interim, ECMWF operational) are involved in the comparison with gravity residuals. Jean Paul Boy (EOST, Strasbourg) has calculated the hydrological effects from three models at the 36 GGP sites http://loading.u-strasbg.fr/. The hydrological effects are represented in three channels: 1, the local channel, which is the effect of a Bouguer plate with diameter of 0.10° or 0.25° centering at the gravimeter; 2, the non-local channel, which is the effect excluding the local part; 3, the total channel, which is the sum of local effect and non-local effect.

	GLDAS	ERA-interim	ECMWF operational
spatial resolution (degree)	0.25	0.7	0.15
temporal resolution (hour)	3	6	6

Table 5.1: *The spatial and temporal resolutions of hydrological models. Different hydrological models have different spatial resolutions and temporal resolutions.*

The spatial and temporal resolutions of hydrological models are shown in table 5.1 (Boy, n.d.). Hydrological effect estimations are downloaded from http://loading.u-strasbg.fr/GGP/hydro/ in 3 sub-directories corresponding to the different models (GLDAS, ERA interim or ECMWF operational).

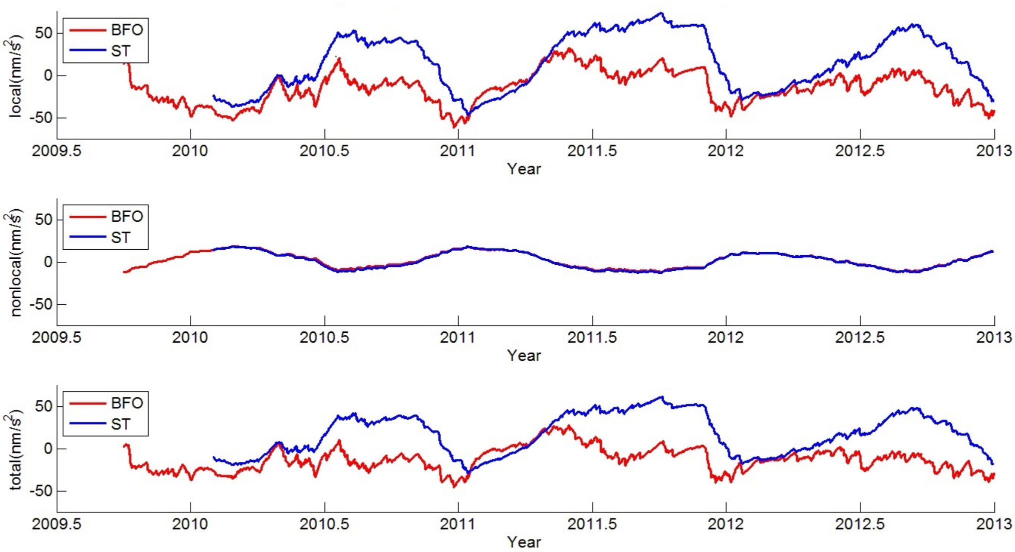

Figure 5.2: *Predicted gravity effects for the local, non-local and total components of GLDAS hydrology model. The upper panel: the local hydrological effect; the middle panel: the non-local hydrological effect; the lower panel: the total hydrological effect. (unit nm/s^2)*

When Mr. Jean Paul Boy calculated the hydrological effects, he assumed all the 36 stations are above ground stations, no matter whether it is true. This means that the water bodies are below the SG sensors (Boy, n.d.). In our cases, BFO and ST are both underground stations, thus an inverse sign should be given to the local channel. Hydrological models show the local effects (inverse sign), the non-local effects and the total effects (local (inverse sign)+ non-local) of GLDAS model at BFO and ST (Figure 5.2). The non-local effects are similar for two stations. The difference is about 2-3 nm/s^2 maximum. Comparing to local effects, non-local effects have less energy in high frequencies. And it is also clear, that the variation of non-local effect (30 nm/s^2) is much smaller than the local effects (100 nm/s^2 for ST and 70 nm/s^2 for BFO). For the local effects, the difference of two stations is more significant. Note that the variations of the local effects are quite similar to the character of gravity residuals described in section 4.5, the highest values of local effects occur in Fall and lowest values occur in Spring, and the decreasing rate of the correction from Fall to Spring is much faster than the increasing rate from Spring to Fall. The local effect and non-local effect are 180° out of phase, so when the local and non-local components are added up to create the total effect, the variation sizes are reduced, comparing to the local effects.
We use the standard deviations of the hydrological effect series as measure of their variabilities. The mathematical definition of standard deviation is as follows. Let X be a time series with mean value (or expectation) μ:

$$X = [x_1, x_2, x_3, ..., x_n] \tag{5.3}$$

$$E[X] = \mu = \sum_{i=1}^{n} x_i p_i \tag{5.4}$$

where p_i is the probability corresponding to x_i, and $E[X]$ is the expected value of X. If x_i are equally likely ($p_1 = p_2 = p_3 ... = p_n$), $E[X]$ is the average of X (our case). The standard deviation is

$$\sigma = \sqrt{\frac{1}{n}[(x_1 - \mu)^2 + (x_2 - \mu)^2 + (x_3 - \mu)^2 + ... + (x_n - \mu)^2]} \tag{5.5}$$

Three hydrological models (GLDAS, ERA-interim, ECMWF operational) give different predictions of the local and non-local effects. But there are much more in common than difference for these models (as shown in Figure 5.2, Figure 5.3 and Figure 5.4): the variations of local effects are always higher than the non-local effects; for both stations, the non-local effects have similar variations (actually not only the variation amplitudes are similar); adding non-local effects to local effects reduce the sizes of variations; ECMWF operational model has higher estimations of local variations than the other two models.

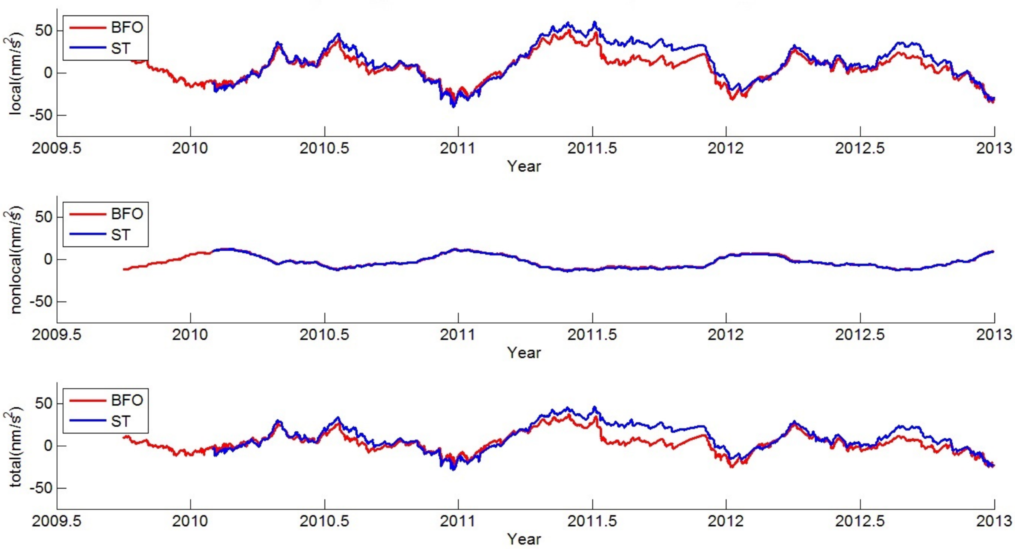

Figure 5.3: *Predicted gravity effects for the local, non-local and total components of ERA-interim hydrology model. The upper panel: the local hydrological effect; the middle panel: the non-local hydrological effect; the lower panel: the total hydrological effect. (unit nm/s^2)*

The difference between GLDAS hydrological effects of two stations is much more significant than the other two models. Considering the different grid sizes of different models (GLDAS 0.25°, ERA-interim 0.7°, ECMWF operational 0.15°) and the short distance from BFO to ST (50 km equals to 0.45°), these two stations may be located in the same grid of ERA-interim model, thus the correction value would only depend on the distance to the grid center.

Since the differences of non-local effects are not significant for the two stations, it is not a major concern to include or exclude non-local effects when we comparing the correcting results of the two stations (the non-local effects would be mostly canceled out when calculating the difference of two stations).

Table 5.2 gives an idea of the magnitudes of the different components and the differences between different models.

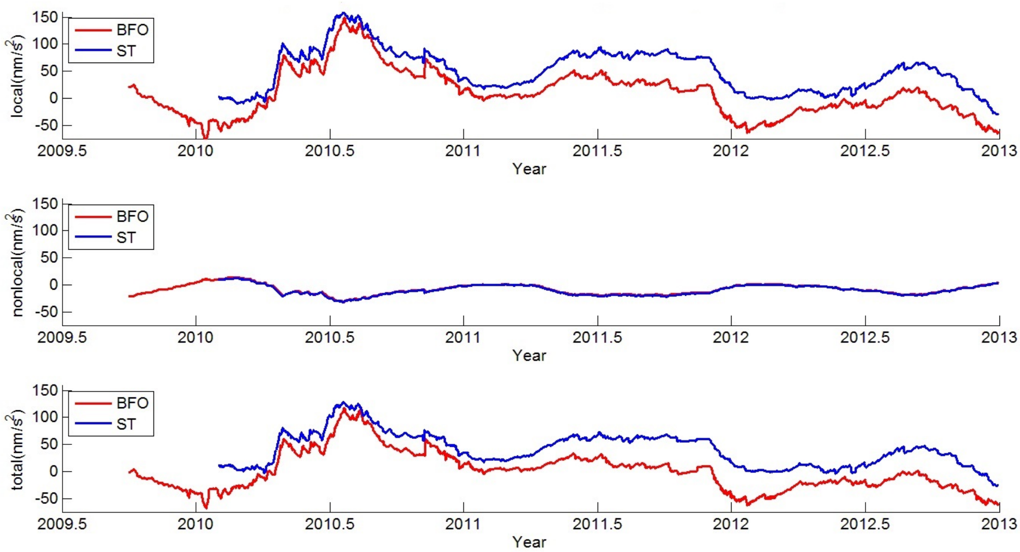

Figure 5.4: *Predicted gravity effects for the local, non-local and total components of ECMWF operational hydrology model. The upper panel: the local hydrological effect; the middle panel: the non-local hydrological effect; the lower panel: the total hydrological effect. (unit* nm/s^2*)*

	GLDAS		ERA		ECMWF	
	BFO	ST	BFO	ST	BFO	ST
local	19.3	32.9	16.6	21.6	43.4	39.8
nonlocal	9.0	9.5	7.1	7.2	9.4	9.4
total	14.0	23.8	11.6	15.3	36.3	31.6

Table 5.2: *The standard deviations of the hydrological effect series (unit* nm/s^2*)*

5.3 Hydrological corrections based upon hydrological models

Figure 5.5 gives a view of the three hydrological models. In most months, the gravity residual and hydrological effects of GLDAS and ERA-interim models almost coincide. The year 2011 sees significant disparity of gravity and hydrological signals, which may be caused by the very local uneven distribution of precipitation around a year. Hydrological models may have problem with modeling the very local meteorological anomalies – continuous strong rain events in summer and continuous dry months in spring and winter. The ECMWF operational model has larger disparity with gravity residual in most months. For ECMWF model, there is a peak of modeled effect in summer 2010, but this is not shown in the residual gravity. The reason is unclear.

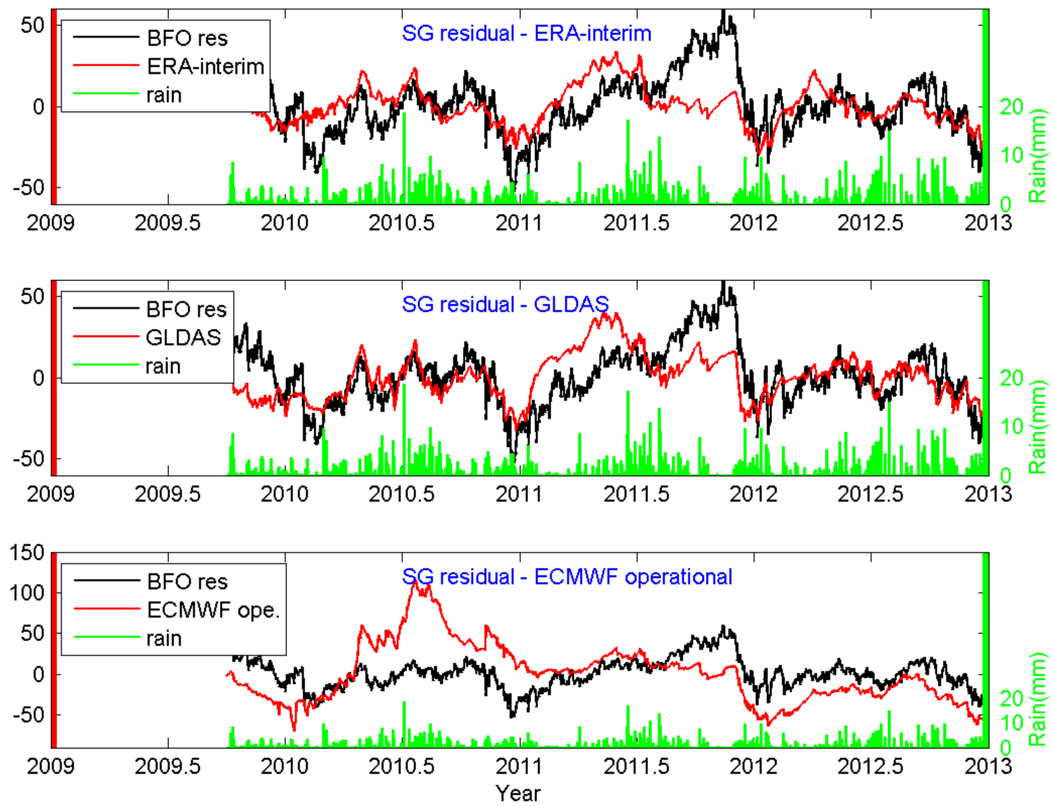

Figure 5.5: Comparison of three hydrological models at BFO (unit nm/s^2). The black curves are the gravity residual. The red curves show the local hydrological effects of three different models. The green lines are hourly precipitation data. For models ERA-interim and GLDAS, the gravity residual and hydrological effects agree in most months. The gravity effect of ECMWF has the largest deviation from the gravity residual.

The standard deviations of the remaining signals calculated for each station individually are shown in table 5.3. Even though the standard deviations are compared here, this does not imply that the smaller standard deviation of the remaining signal means higher correction performance. As can be seen from table 5.3, there are four cases where applying both the local and non-local corrections leads to an increased standard deviation compared to the local correction only case. Note that, the increasing values of these two cases are not so significant as the decreasing of the other four cases. The standard deviation of ECMWF operational remaining signal is almost double the size of the other two models remaining signals. It is believed that GLDAS and ERA-interim models give better results. The subsequent analyses are focused on GLDAS and ERA-interim models.

	GLDAS		ERA		ECMWF	
	BFO	ST	BFO	ST	BFO	ST
residual	18.6	14.5	18.6	14.5	18.6	14.5
residual - local hydro.	14.7	25.1	15.8	20.5	41.0	34.3
residual - total hydro.	16.6	17.2	17.4	17.2	36.5	27.2

Table 5.3: *The standard deviations of the remaining signals (unit nm/s^2, using hourly data). The row which begins with 'residual' shows the standard deviations of BFO and ST residuals as references. The following two rows are the standard deviations of remaining signals after hydrological correction.*

Figure 5.6 shows the residual difference of two stations before and after removing the hydrological effects. As the difference between the two spheres at BFO are small, BFO-low is taken as a representative of station BFO.

The residuals plotted in figure 5.6 are computed like this:

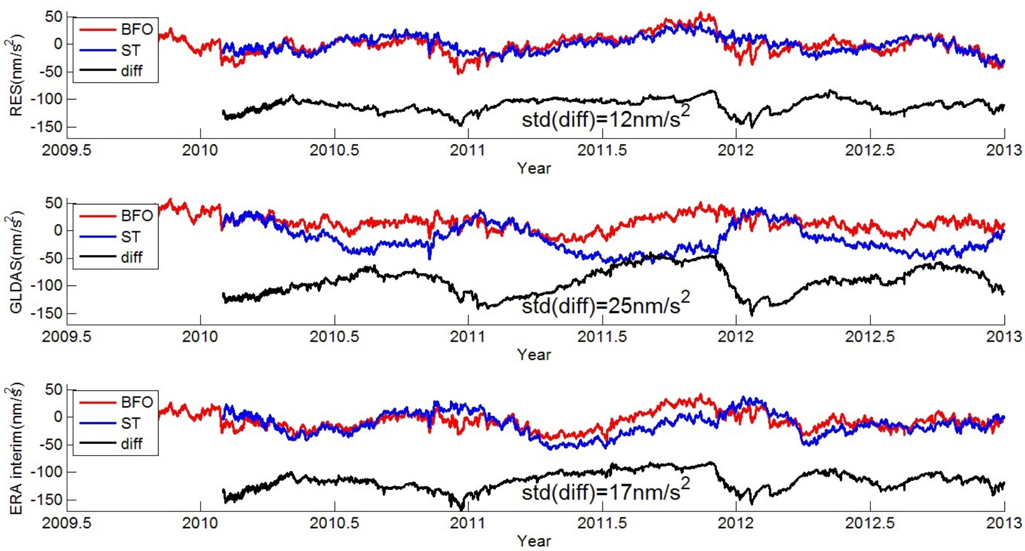

Figure 5.6: *The difference of two stations' residuals before and after removing hydrology effects (unit: nm/s^2). In the upper panel, the red and blue curves are the gravity residuals before correcting for local hydrological effects of BFO and ST. The black curve represents the difference of these two gravity residuals. In the middle panel, the red and blue curves are the gravity remaining signals after correcting for local hydrological effects of BFO and ST using GLDAS model. The black curve represents the difference of these two remaining signals. In the lower panel, the red and blue curves are the gravity remaining signals after correcting for local hydrological effects of BFO and ST using ERA-interim model. The black curve represents the difference of these two remaining signals.*

$$res(\text{diff}) = res(\text{BFO}) - res(\text{ST}) \quad (5.6)$$

$$\sigma(\text{diff}) = \sigma(res(\text{diff})) \quad (5.7)$$

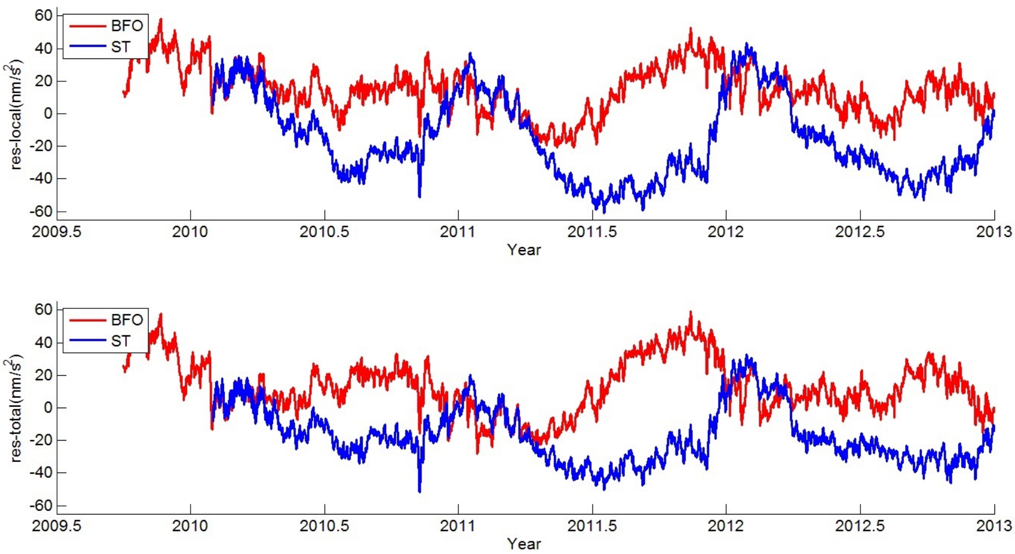

Figure 5.7: *Remaining signals after correcting for GLDAS hydrological effects (unit: nm/s^2). The upper panel shows remaining signals after correcting for local hydrological effects using GLDAS model for BFO (red curve) and ST (blue curve). The lower panel shows remaining signals after correcting for total hydrological effects using GLDAS model for BFO (red curve) and ST (blue curve). The standard deviations shown in columns 1 and 2 of table 5.3 give an idea of the annual variations.*

In a theoretical view, the local hydrological signal of BFO accounts for most of the gravity residual (the same for ST), and the local components of BFO and ST hydrological signals are by nature different. When the dominant different components (the local hydrological signals) are removed, it is expected that the difference of the remaining signals would be reduced. But the real situation shows the opposite behaviour. In figure 5.6, the gravity residuals of the two stations coincide in most months, but after removing the local hydrological effects using GLDAS or ERA-interim model, the differences increase. This increasing difference between the residuals of BFO and ST is also reflected in the standard deviations of the differences $\sigma(\text{diff})$. $\sigma(\text{diff})$ is 12 nm/s^2 before correcting the local hydrological effects, and increases to 25 nm/s^2 (GLDAS) and 17 nm/s^2 (ERA-iterim) respectively. Moreover, the difference of the two stations has a stronger annual component after removing the GLDAS local effects. This suggests that GLDAS may have a systematic annual error. And it is not proper to judge the performance of the two hydrological models by simply comparing the differences of the two stations' remaining signals.
Figure 5.7, figure 5.8 and figure 5.9 compare the remaining signals after correcting for local hydrological effects and total hydrological effects. For ERA-interim model, the remaining signals

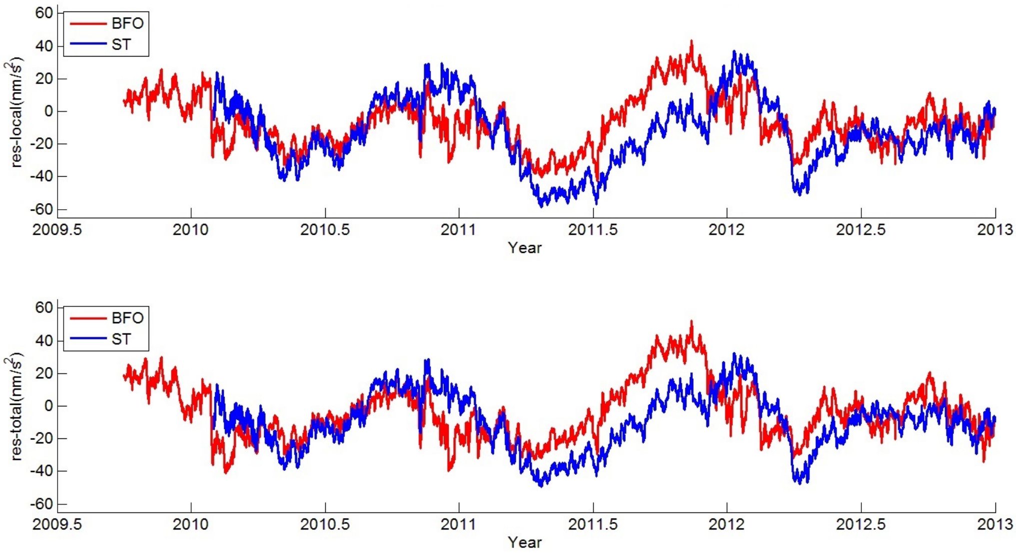

Figure 5.8: *Remaining signals after correcting for ERA-interim hydrological effects (unit: nm/s^2). The upper panel shows remaining signals after correcting for local hydrological effects using ERA-interim model for BFO (red curve) and ST (blue curve). The lower panel shows remaining signals after correcting for total hydrological effects using ERA-interim model for BFO (red curve) and ST (blue curve). The standard deviations shown in columns 3 and 4 of table 5.3 give an idea of the annual variations.*

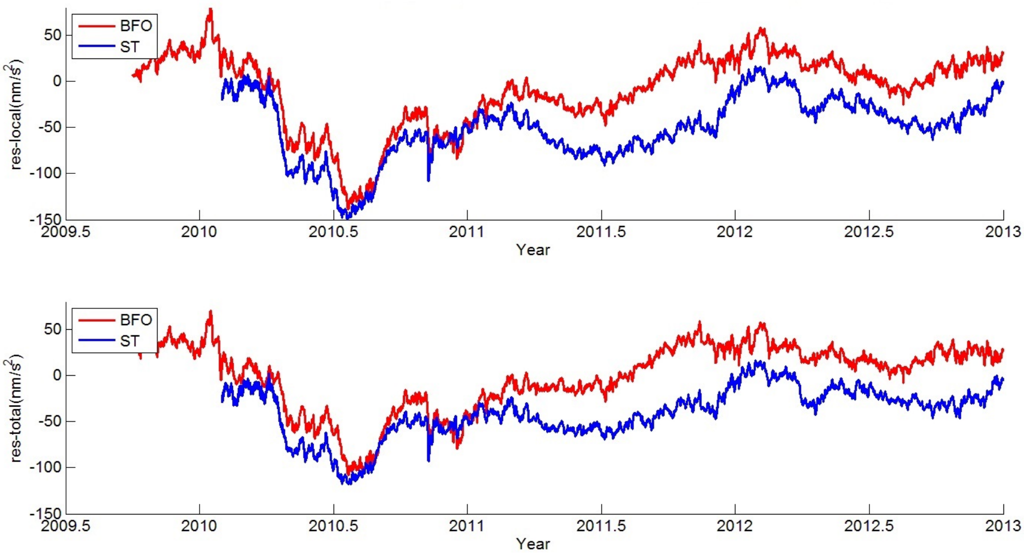

Figure 5.9: *Remaining signals after correcting for ECMWF hydrological effects (unit: nm/s^2). The upper panel shows remaining signals after correcting for local hydrological effects using ECWMF model for BFO (red curve) and ST (blue curve). The lower panel shows remaining signals after correcting for total hydrological effects using ECWMF model for BFO (red curve) and ST (blue curve). The standard deviations shown in columns 5 and 6 of table 5.3 give an idea of the annual variations.*

of two stations have no big difference, and for GLDAS model, the disparity is massive. In the summer of 2010, the gravity residuals seem to be over corrected by the ECMWF model.
We have two options to correct the hydrological effects. As discussed in Section 5.1, the local effects have much larger size than non-local effects. We can correct only the local effects from the gravity residual, or correct the local and non-local effects (i.e. total effects). When the purpose of removing the hydrological signal is to evaluate the remain of tectonics and other modeling errors, it is obvious that the total effects should be corrected. But if the research purpose is to compare the performance of two stations, it is preferred to leave the non-local effect in the remaining signal. There are two reasons: any kind of modeling introduces error, to remove the non-local effects would increase the uncertainty before comparing the two stations; the non-local effects are similar for both stations, considering the short distance between two stations. It is clear that correcting the non-local effect does have an influence on the remaining signals, but its influence on the difference of the remaining signal is not significant. In a practical view, involving the non-local component or not would not cause big difference, because as discussed in section 4.1 the difference of two stations is about 2-3 nm/s^2 maximum.

	σ(residual)	σ(residual$-$GLDAS)	σ(residual$-$ERA interim)
local	12.2	$24.9^{(1)}$	$16.6^{(2)}$
total	12.2	$24.4^{(3)}$	$16.5^{(3)}$

Table 5.4: *The standard deviations of the differences of the gravity residuals between BFO and ST before and after removing the local or the total hydrological effect (corresponding to figure 5.6). The first column σ(residual) is the standard deviations of the gravity residual difference before correcting for any hydrological effects (unit nm/s^2).*

The difference between the residuals at BFO and ST is analyzed in table 5.4. It shows the standard deviations of the remaining signals after removing the local hydrological signal or removing the total hydrological signal. These standard deviations (denoted by the σ-operator) in table 5.4 are calculated using the following formulas:

$$\text{value (1)}: \quad \sigma(\text{resGLDASlocal}) = \sigma(\text{(BFOres-BFOGLDASlocal)-(STres-STGLDASlocal)}) \tag{5.8}$$

$$\text{value (2)}: \quad \sigma(\text{resERAlocal}) = \sigma(\text{(BFOres-BFOERAlocal)-(STres-STERAlocal)}) \tag{5.9}$$

$$\text{value (3)}: \quad \sigma(\text{resGLDAStotal}) = \sigma(\text{(BFOres-BFOGLDAStotal)-(STres-STGLDAStotal)}) \tag{5.10}$$

$$\text{value (4)}: \quad \sigma(\text{resERAtotal}) = \sigma(\text{(BFOres-BFOERAtotal)-(STres-STERAtotal)}) \tag{5.11}$$

$\sigma()$ means the operator of standard deviation defined in equation 5.5. The expressions in the brackets are the differences of the two stations remaining signals after correcting the gravity residuals with local or total effects corresponding to different models. For example, ((BFOres-BFOERAlocal)-(STres-STERAlocal)) means, firstly, the gravity residuals of BFO and ST are corrected by the corresponding local effects of the ERA-interim model, and then the difference of the remaining signals is calculated.

5.4 Hydrological corrections based upon station recorded precipitation data

As discussed in section 5.1, precipitation is the only input into the water system, when no artificial transportation of water is conducted (e.g. the pumping experiment at Wettzell, from 15th Sept. 1999 to 16th Sept. 1999). Precipitation comes in the form of rain (liquid) or snow (solid) (excluding the rare case of hail). These two water states have different runoff periods.

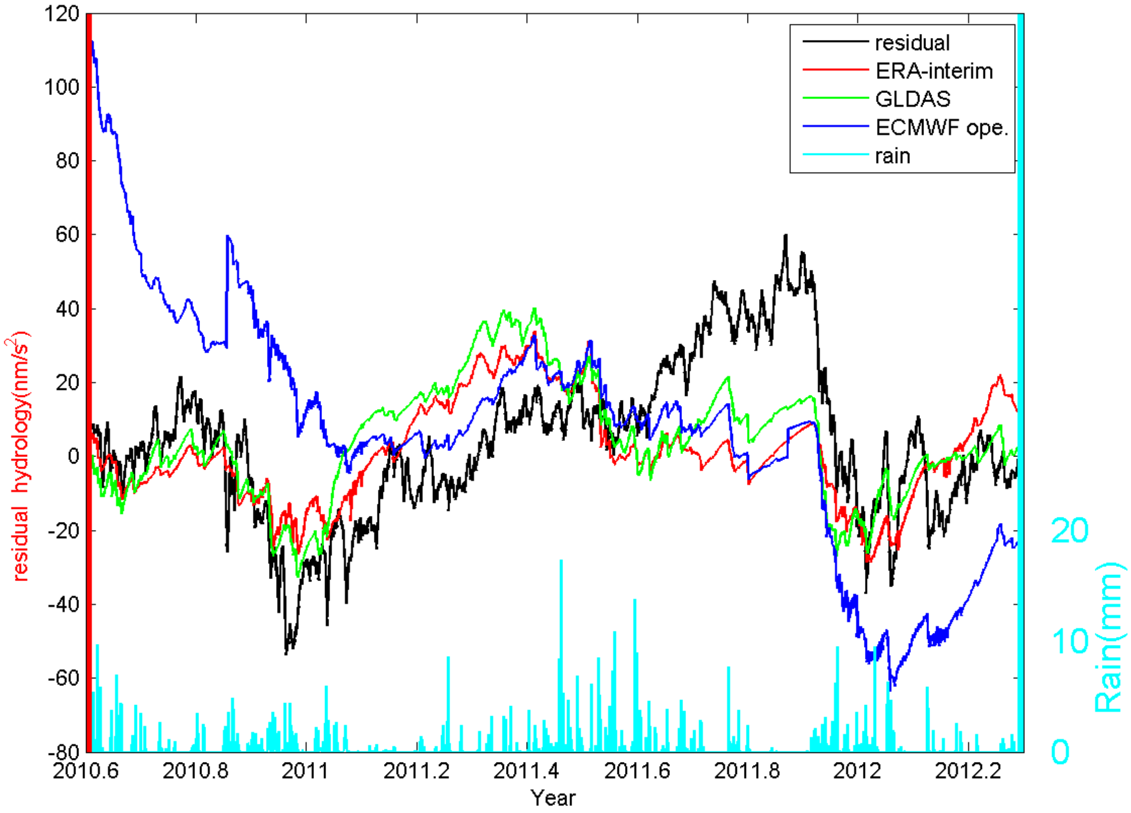

Figure 5.10: *The gravity residual and hydrology models in 2011 at BFO. The black curve represents the gravity residual. The red, green and blue curves are the gravity effects of local hydrological models ERA-interim, GLDAS and ECMWF operational models. The cyan lines are plotted using hourly precipitation data. There are two dry periods in spring 2011 and autumn 2011 at BFO. The latter dry period caused decrease of gravity residual.*

Figure 5.10 shows the two dry periods in spring 2011 and in autumn 2011 at BFO. There is a long dry period from October to December. This results in that the gravity residual drops from $+50\,\mathrm{nm/s^2}$ to $-10\,\mathrm{nm/s^2}$. There is also another dry period from February to early March in 2011, but the gravity residual does not decrease in this period. Temperature is the decisive factor here. The temperature in the dry period Feb.-Mar. is on average below zero. The snow from winter 2010 still stays on the ground surface, thus no decreasing trend is found from this period. And for period Oct.-Dec., the temperature is above 0. The preceding period from Aug.-Sept. is again not wet, so the accumulated effect is that there is a sudden drop of gravity

residual in December.
A heated rain gauge was installed at BFO to measure the precipitation (both rain and snow) in 1 minute interval. Because of the different runoff periods for water and snow, we do not expect the precipitation to have a linear relationship with gravity. So the precipitation data must be first convolved with an exponential function, as the rate of runoff decreases exponentially. The minute data would be summed up for each individual hour.
The following equations are used to evaluate the influence of precipitation (Harnisch and Harnisch, 2002):

$$F_{\mathrm{i}} = (1 - \mathrm{e}^{-(t_{\mathrm{i}}-t_{\mathrm{j}})/T1}) \times \mathrm{e}^{-(t_{\mathrm{i}}-t_{\mathrm{j}})/T2}; \tag{5.12}$$

$$F = \begin{bmatrix} F_1, & F_2, & F_3 & \ldots & F_{\mathrm{n}} \end{bmatrix} \tag{5.13}$$

$$\mathrm{d}g = 2\pi\rho G(Rh * F) \times 10^6 \tag{5.14}$$

$\mathrm{d}g$ is precipitation perturbance ($\mathrm{nm/s^2}$). F is called the damping filter. F_{i}: the factor of a rain event at the time t_{j} has the precipitation contribution at time $t_{\mathrm{i}}(t_{\mathrm{i}} > t_{\mathrm{j}})$. Rh: hourly rain accumulation series (unit: mm). F is a function of time and $Rh * F$ denotes the convolution of F with Rh. $T1$ and $T2$ are called the damping periods. $T1$ describes the accumulation, i.e. the rate water infiltrates into ground. $T2$ describes the consumption, i.e. the rate of evaporation and in-ground run-off of the water. Note that this is not a comprehensive model of all the facts, for example, the influence of runoff rate discussed in Section 5.1 is not included. Many factors may have an influence on the damping period ($T1$, $T2$). The air temperature variation would be an example of an unaccounted parameter. Higher temperature in summer would undoubtedly lead to higher evaporation rate, thus it is expected damping period is shorter in summer than in winter. When the temperature is below 0°C, the precipitation comes in form of snow. The frozen ground in winter prevents the water loss by decreasing the underground water run-off. It is suggested to introduce varied consumption damping periods $T21$, $T22$, $T23$. $T21$ is for temperature above 15°*C*; $T22$ for temperature between 0°C to 15°C. T23 for temperature below 0°C. A long period model ($T1 = 4$h, $T21 = 300$h, $T22 = 600$h, $T23 = 4800$h) and a short period model ($T1 = 1$h, $T21 = 40$h, $T22 = 80$h, $T23 = 1000$h) have been tried on precipitation data from Wettzell (Harnisch and Harnisch, 2002). The damping periods influence the amplitudes of the modeled gravity effect. However, it has to be considered that no irreversible long-term accumulation occurs. The greater values of damping periods used in the long-term model result in more pronounced gravity anomalies as compared with the short-term model (Harnisch and Harnisch, 2002). In this thesis $T1$ is set as 4 hours, and T2 varied from 2 days to 30 days. Note T2 is not adjusted depending on the outside air temperature (Harnisch varied T2 depending on air temperature in her experiment). In other words, a constant damping period T2 (for example, T2 = 2 days) is used for the whole three years' period, as long as the 2 days period is chosen.

Figure 5.11 shows the convolved rain effect at BFO using damping period 2 days, 4 days, 6 days, 8 days. The precipitation event in the beginning of 2012 has an effect of 40 $\mathrm{nm/s^2}$ (8 days damping period) or 20 $\mathrm{nm/s^2}$ (2 days damping period). It is clear that longer damping periods help accumulating of gravity correction. And these effects decline to approximately 0 after a long dry period (e.g. spring 2011 and autumn 2011).

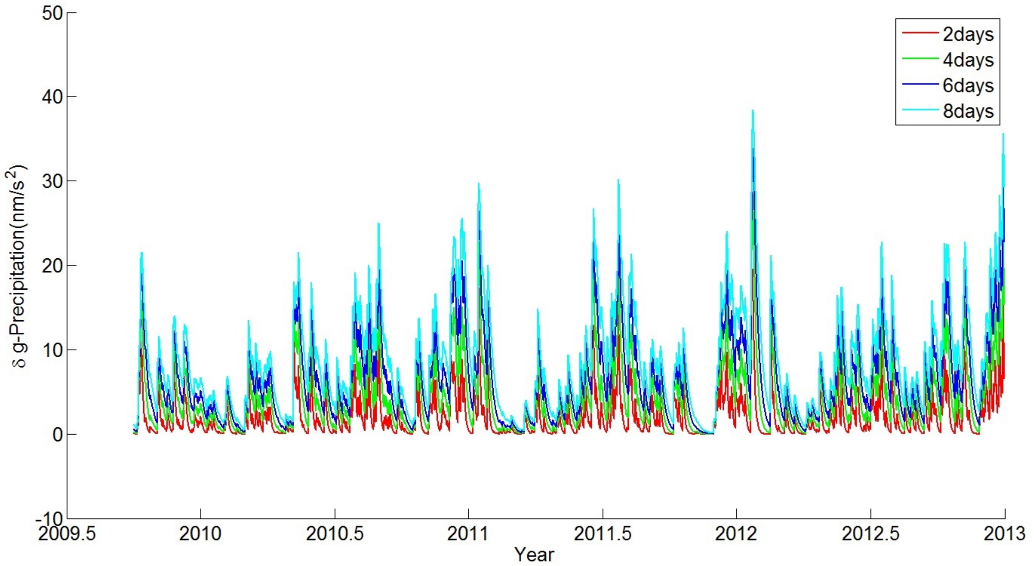

Figure 5.11: *The convolved rain effect at BFO calculated using equations 5.12, 5.13 and 5.14 (unit: nm/s^2). Different colors represent different damping periods T2 used in equation 5.12. Note for convolved rain effects, there is no long period component. In other words, no gravity effect of precipitation can last for longer than a few months using our model.*

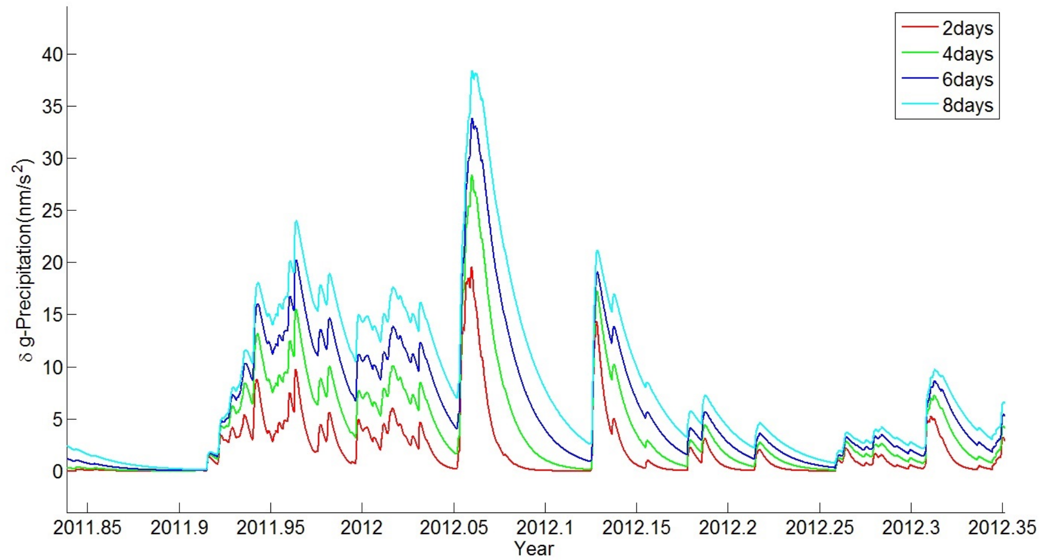

Figure 5.12: *Details of the convolved rain effects in winter 2011 at BFO (a zoomed in view of figure 5.11). It is shown in this figure that the gravity effects decrease slowly after reaching their peaks. The gravity effect can be as large as 40 nm/s^2.*

Figure 5.12 shows details of rain effects in early months of 2012. A strong precipitation process increases the size of rain effect. And after reaching its peak, it decreases slowly (the decreasing rate depending on the damping period $T2$). If the damping period is long enough, a second precipitation process comes when the rain correction of the first process is still significant, then the effects of these two processes add together. In general, the rain effect does not have a long period component. A simple estimation is after five times the damping period, the magnitude of the rain effect is $e^{-5} \approx 0.67\%$, which can be neglected, so there won't be any precipitation process that can generate observable signal after a few months.
The modeled rain effect is used to correct the gravity residual. To observe the individual effect of rain correction, the hydrological effect described in the previous chapter is not corrected in advance.

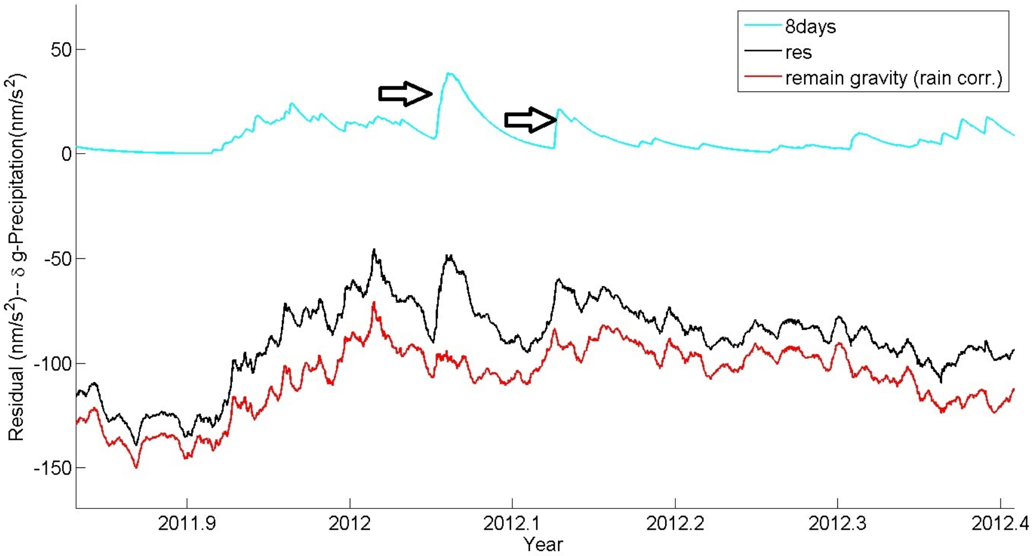

Figure 5.13: *Correcting for the precipitation effect in winter 2011 (unit: nm/s^2). The cyan curve is the modeled precipitation effect using 8 days damping period (T2). The black curve and the red curve are the gravity residual before removing the precipitation effect and the remaining signal after removing the precipitation effect. The cyan curve agrees with the gravity variation quite well.*

Figure 5.13 is again an example of the early months of 2012. The two precipitation corrections with the arrows have the same shapes as the gravity residual. In the remaining gravity after correcting the precipitation effect, the short period variations due to the precipitation processes are almost fully corrected. But precipitation correction does not always have good performance.

In figure 5.14, the gravity variation due to precipitation seems to be over corrected. A shorter damping period would be more proper for this case.

Figure 5.15 gives an idea of the different characters of rain effect and hydrological model. The precipitation correction (upper blue line) has proper estimation of the short period gravity variations. As stated before, the precipitation correction does not have long period term. On the contrary, hydrological models do not have high frequency component, but the hydrological models have excellent performance in a long period (period longer than 1 month). A combined

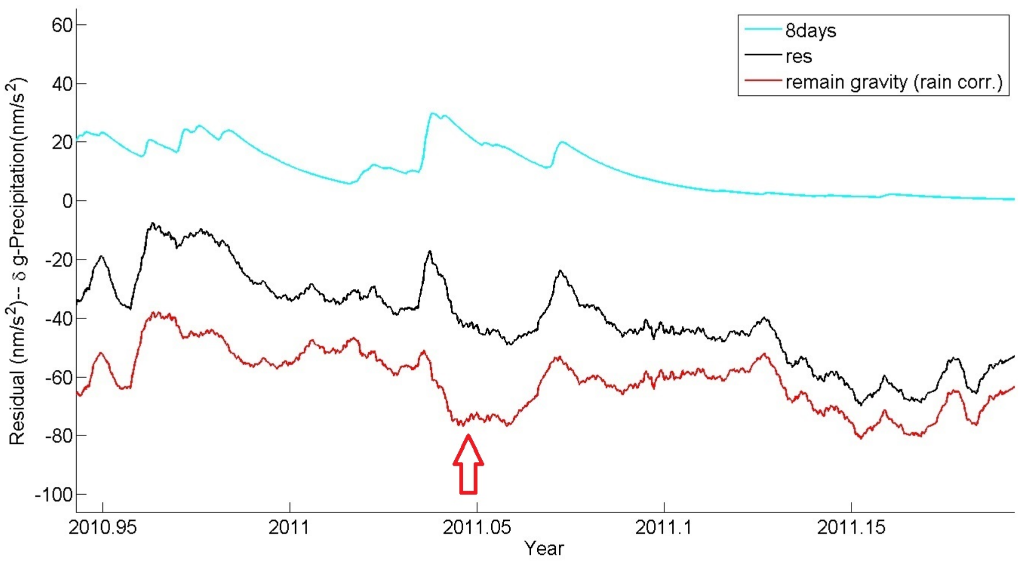

Figure 5.14: *Correcting for the precipitation effect in spring 2011 (unit: nm/s^2). The blue curve is the convolved rain effect with 8 days damping period (T2). The black curve is the raw gravity residual and the red curve is the remaining gravity after removing the rain effect. Note that the red arrow points to the period that seems to be over corrected.*

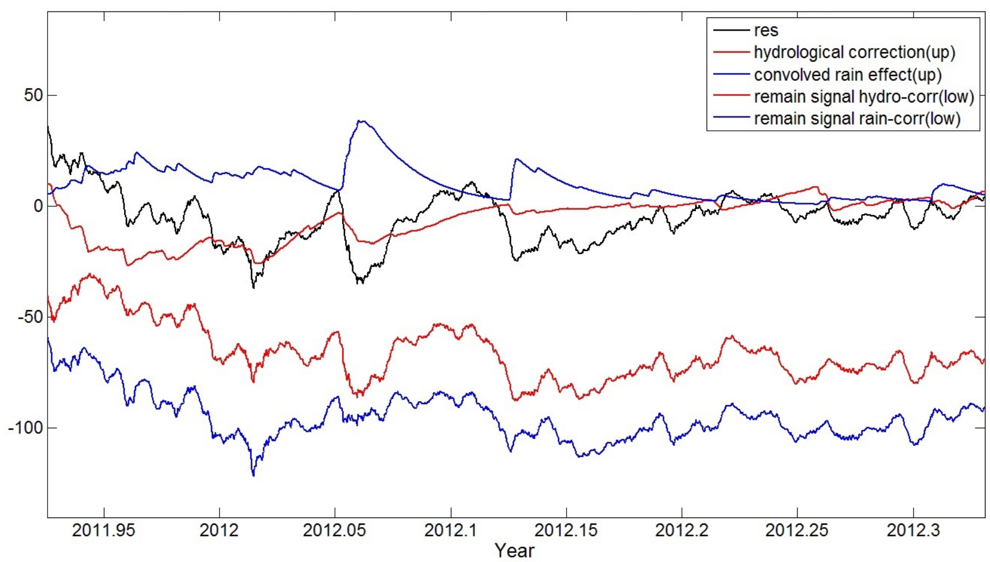

Figure 5.15: *The different characteristics of rain effect and hydrological models (unit: nm/s^2). The three upper traces are the raw gravity residual from BFO (black line), the convolved precipitation effect (blue line) and the GLDAS hydrological model (red line). The two lower traces are the remaining signals after correcting for the convolved precipitation effect (blue line) and after correcting for the GLDAS hydrological model (red line).*

correction including the hydrological models and local precipitation effect may give better result. But this was not successfully tried here.

5.5 Comparing the precipitation effect and hydrological models in the frequency domain

Figure 5.16 shows the amplitude spectrum of gravity residual, GLDAS hydrological model and the rain effect from 0.05 cpd (20 days period) to 0.4 cpd (2.5 days period). Gravity residual has more energy in this period. Rain effect and hydrological model has similar behavior near 20 days period.

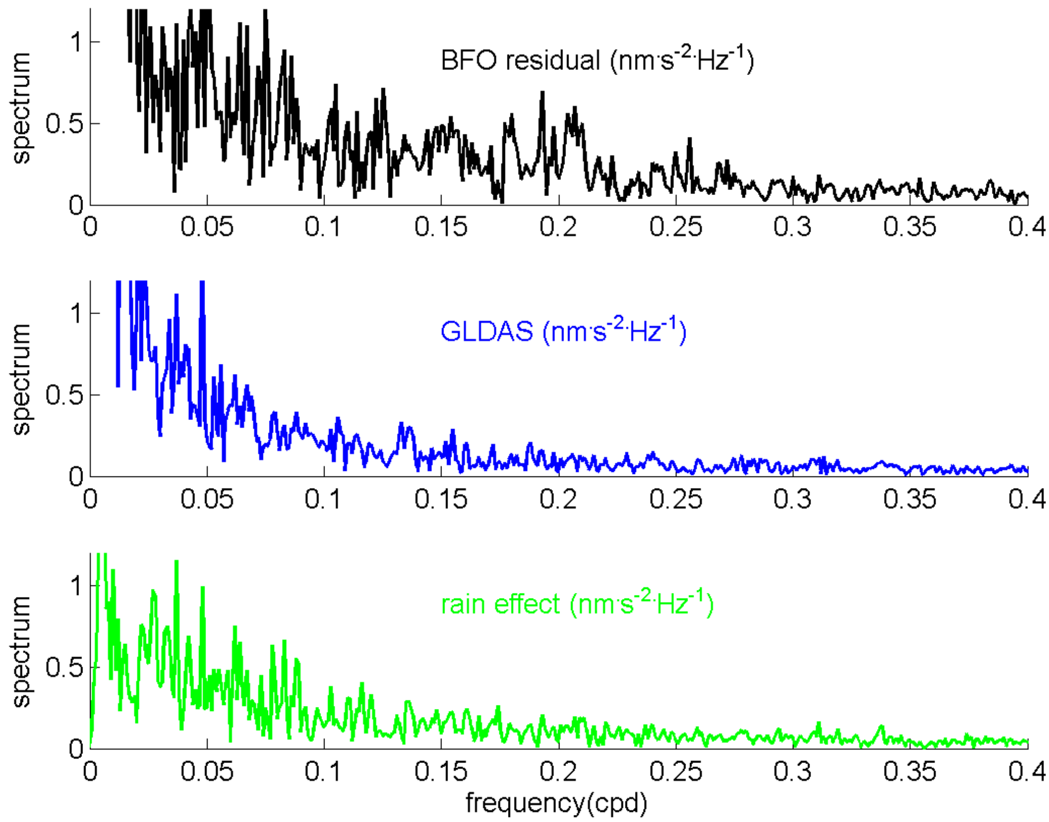

__Figure 5.16:__ Comparing the gravity residual, the precipitation effect (8 days damping period) and the hydrology model (GLDAS model) at high frequency (BFO). Gravity residual has more energy in the period from 0.05 cpd (20 days period) to 0.4 cpd (2.5 days period).

In comparison, figure 5.17 gives an idea of the spectrum at low frequency. Both gravity residual and hydrological model have strong signals in these frequencies, but rain effect has little energy. The spectrum of gravity residual and hydrological model peak between 1 year and 3 years and have the same magnitude. In the period from 3 months to 1 years the spectrum of gravity residual and hydrological effect almost coincide. The lower panel shows the spectrum

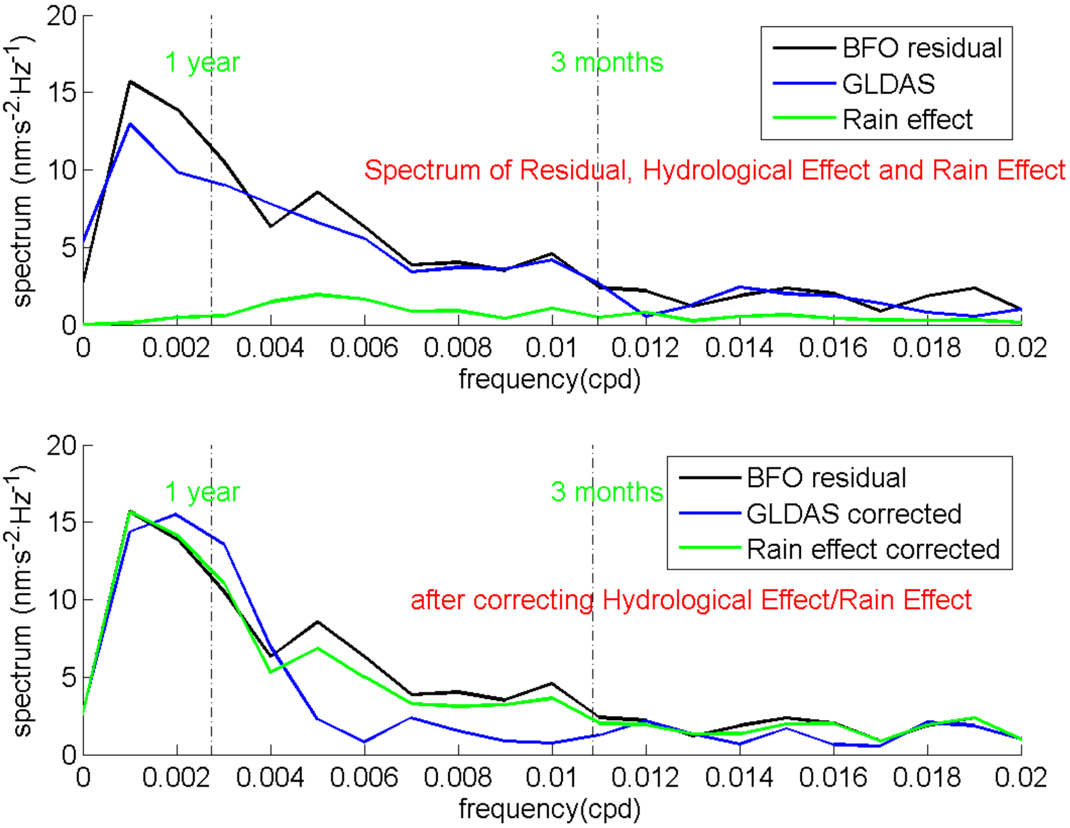

Figure 5.17: *Comparing the gravity residual, the precipitation effect (8 days damping period) and the hydrology model (GLDAS model) at low frequency (BFO). The upper panel compares the spectrum of gravity residual with the spectrum of GLDAS hydrological model and convolved rain effect. The lower panel compares the spectrum of gravity residual with the spectrum of remaining signals after correcting for GLDAS hydrological model and after correcting for convolved rain effect separately. Correcting for the hydrological effect helps reducing the gravity residual in period from 3 months to 1 year.*

after removing hydrological effect or rain effect. It is clear that hydrological model corrects the most residual between 3 months and 1 year, and the rain correction reduces the signal only a little bit. However, the rain correction has no effect at the long period part (longer than 1 year). And the residual after correcting hydrological effect at 1 year period is even enhanced.

Figure 5.18 shows the difference of two stations. BFO residual has higher amplitudes at long

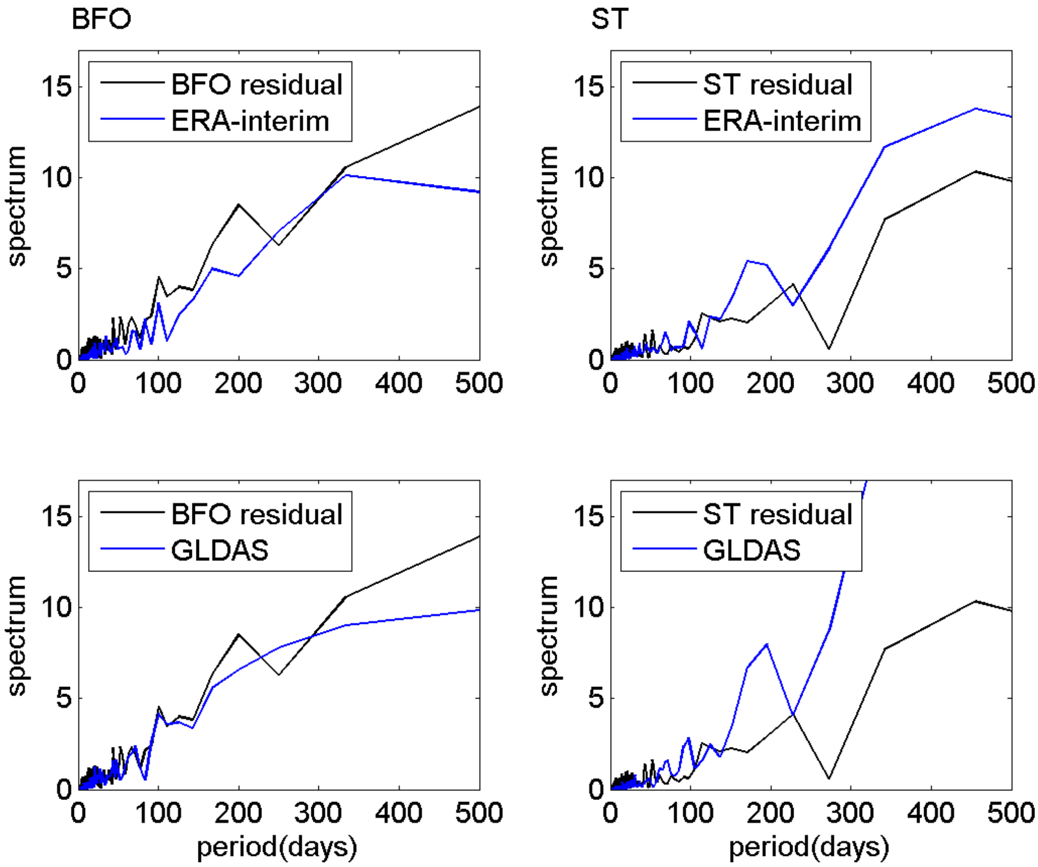

Figure 5.18: The spectrum of SG residuals and hydrological effects (unit: nm·s^{-2}·Hz^{-1}). Upper left: spectrum of gravity residual (black curve) and spectrum of ERA-interim hydrological effect (blue curve) at BFO; lower left: spectrum of gravity residual (black curve) and spectrum of GLDAS hydrological effect (blue curve) at BFO; upper right: spectrum of gravity residual (black curve) and spectrum of ERA-interim hydrological effect (blue curve) at ST; lower right: spectrum of gravity residual (black curve) and spectrum of GLDAS hydrological effect (blue curve) at ST.

period than ST residual. The dominant signals of hydrological models are at 1 year period or longer. At ST, GLDAS hydrological model has better performance than ERA-interim in modeling the gravity residual.

The spectral coherence is introduced to evaluate the relation between two signals. Coherence is a function of frequency. Its value varies from 0 to 1, which indicates how well one signal corresponds to another (the coherence of 1 means 'perfectly correlated' at corresponding frequency). The coherence is defined as follows:

$$C_{xy} = \frac{|P_{xy}|}{P_{xx}P_{yy}} \tag{5.15}$$

where P_{xx} and P_{yy} are the auto-spectral density of x and y respectively, and P_{xy} is the cross-spectral density between x and y. P_{xx}, P_{yy} and P_{xy} are estimated via Welch's method. The calculation is realized using a Matlab function called 'mscohere'. In Matlab function 'mscohere, four parameters 'WINDOW','NOVERLAP','NFFT' and 'Fs' should be defined. 'NFFT' specifies the number of FFT data points used to calculate the PSD or CPSD. In the following calculations, 'NFFT' is set as 2^{10}. 'WINDOW' is an integer, that the signals x and y are divided into sections of length equals to this specified value. It is set identical to 'NFFT'. 'NOVERLAP' specifies the number of overlapping points from one section to the following section. Note it should be an integer smaller than 'WINDOW'. In this thesis, 'NOVERLAP' is approximately 0.8 time of 'WINDOW'. 'Fs' is the sampling frequency of the returned CPSD specified in Hz. In this thesis, 'Fs' is set as 1/3600 Hz. 'NFFT' can also be set as 2^{12}, and using the corresponding set of parameters, the function gives similar results as follows, thus those results are not shown in the following chapters.
The difference of hydrological models can be shown in Figure 5.19. The coherences of gravity residual and hydrological effects are calculated. It is clear that GLDAS has advantage in modeling the long period (longer than 80 days) hydrology component. Between 80 days and 170 days, the coherence of GLDAS and gravity residual range from 0.6 to 0.85 for BFO and 0.65 to 0.75 for ST. Figure 5.20 shows the residual spectrum of two stations more clearly. There are a few similar patterns of two stations' spectrum. The spectrum have local maximum values at about 130 days, 200 days, 450 days periods. At long period, the amplitude of BFO is higher than ST, which is understandable since the BFO residual itself has larger amplitude than ST. For BFO, it seems there is biennial signal in the gravity residual.
So what will the spectrum of remaining signals after removing the local hydrological effects look like? In theory, removing the local hydrological effects will largely reduce the amplitude at longer period (longer than 1 year), simply because the hydrological effects dominate the long period gravity residuals. The results show the reality is much more complicated than the theory. As shown in Figure 5.21, for BFO the remaining signals at period 50-300 days have smaller amplitude than the gravity residual. But the remaining signals at period above 300 days are enhanced. For ST, the decreasing in amplitude after removing hydrological signal is not significant. And removing hydrological effects introduces an increasing in period between 250 days and 450 days.

5.6 Coherence analysis

Now comes the most important question: what are the coherence of two stations' signals before and after removing the hydrological effects.
According to Figure 5.22, the gravity residuals from two stations have strong coherence at period over 30 days. The coherence varies from 0.6 to 0.8. After removing the hydrological effects, the coherence is largely reduced at period of about 90 days - from 0.65 to 0.3. At period of about 170 days (approximately half a year), the coherence is about 0.7.

As we know, the temporal resolution of GRACE is about 15 days to 30 days. We further investigate the coherences at frequencies from 15 days to 30 days. As shown in figure 5.23, the coherence reaches its local maximum value at 5 days (coherence equals 0.97). At 15 days

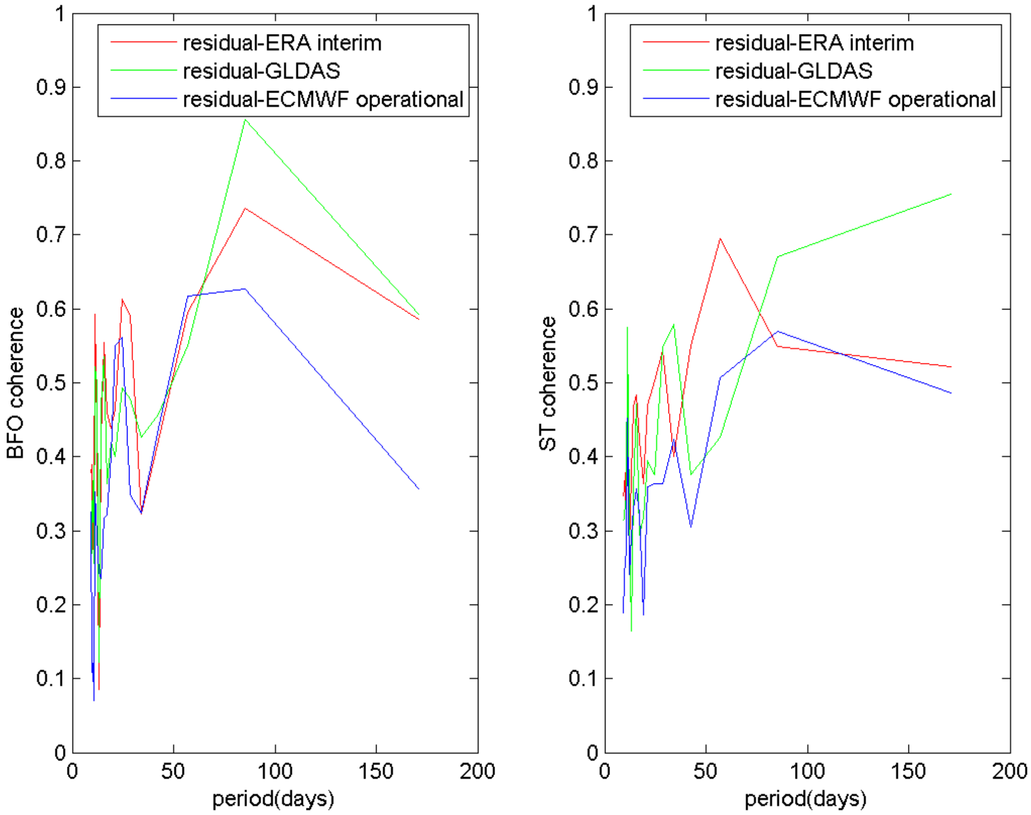

Figure 5.19: *Coherence of SG residual and hydrological effects. The left figure shows the coherence of gravity residual and hydrological effects (different models are represented by different colors) at BFO. The right figure shows the corresponding curves at ST.*

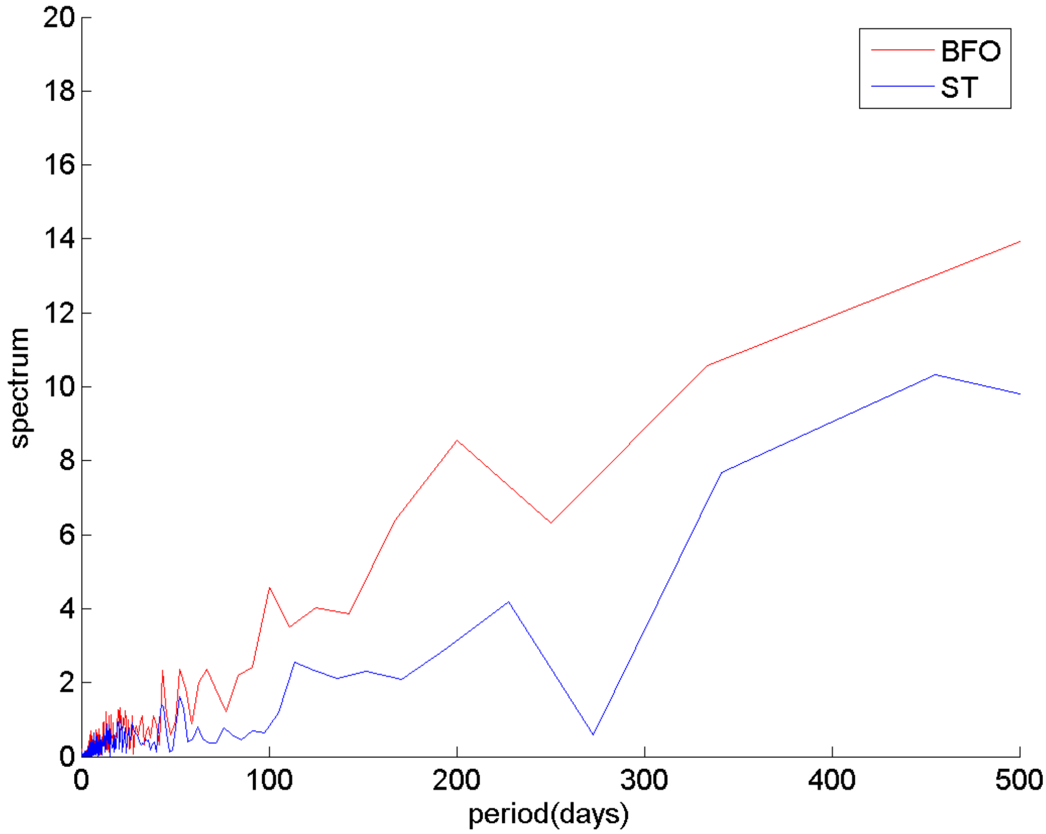

Figure 5.20: *The spectrums of residuals at the two stations (unit: $nm{\cdot}s^{-2}{\cdot}Hz^{-1}$). The spectrums have local maximum values at about 130 days, 200 days, 450 days periods. The gravity residual of BFO has higher amplitude than ST at long period.*

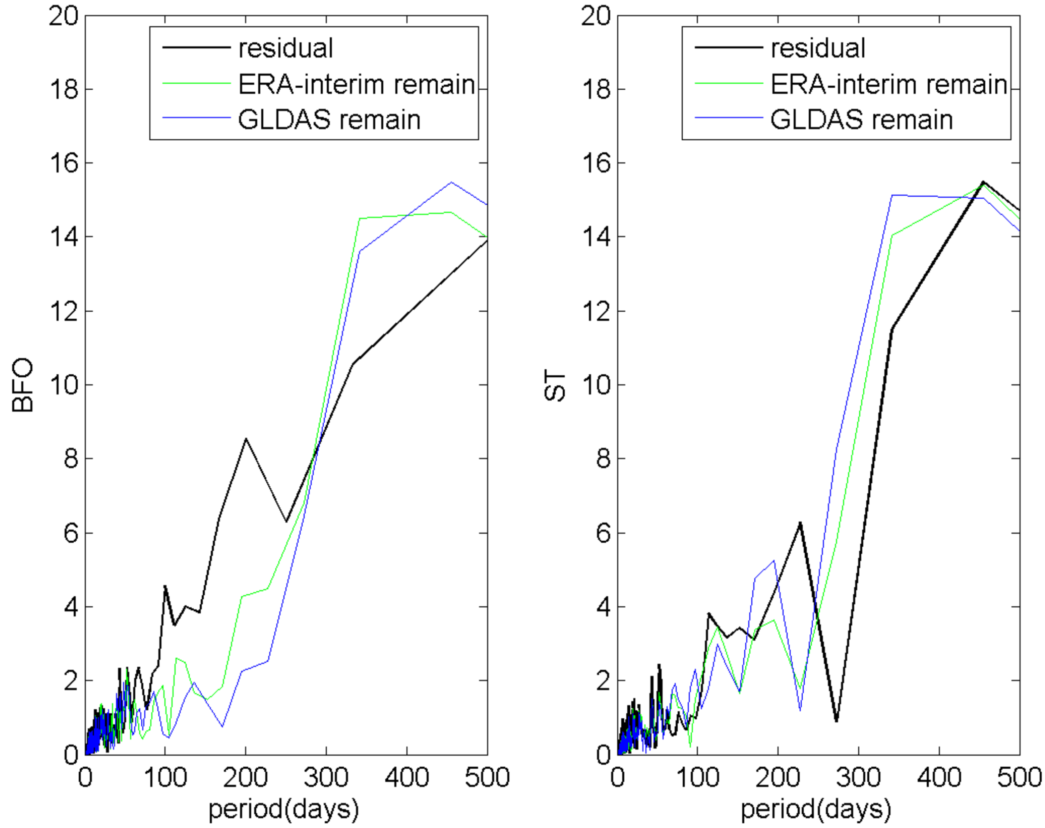

Figure 5.21: *The spectrums of residuals and hydrological effects removed remaining signals at BFO and ST (unit: nm·s^{-2}·Hz^{-1}). The left figure shows the spectrums of the gravity residual (black curve), remaining signals after correcting for ERA-interim (green curve) or after correcting for GLDAS (blue curve) at BFO. The right figure shows the corresponding curves at ST.*

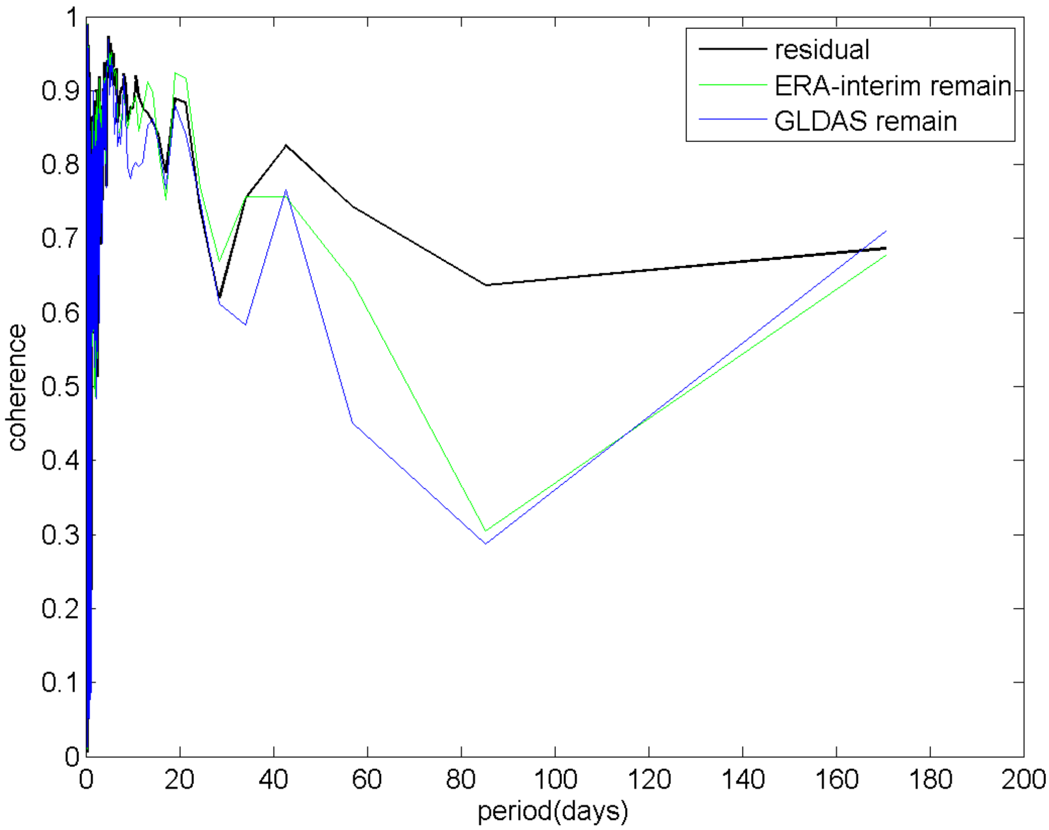

Figure 5.22: *The coherence of BFO and ST residuals before and after removing the hydrological effects. The black curve: the coherence of BFO and ST residuals before removing the hydrological effects. The green and blue curves: the coherence of BFO and ST remaining signals after removing the hydrological effects using ERA-interim or GLDAS model.*

period, the coherence is about 0.84. Another local maximum value appears at around 20 days, and the coherence decreases to about 0.65 at 30 days' period, which can still be considered as strong coherence. Removing the hydrological effects has no significant influence on the coherence between 15 days and 30 days. In general, the residuals and remaining signals show strong coherence from 15 days to 30 days. In most frequencies between 15 days and 30 days, correcting hydrological effect using GLDAS model helps improving the coherence, and when using ERA-interim, the coherence decreases.

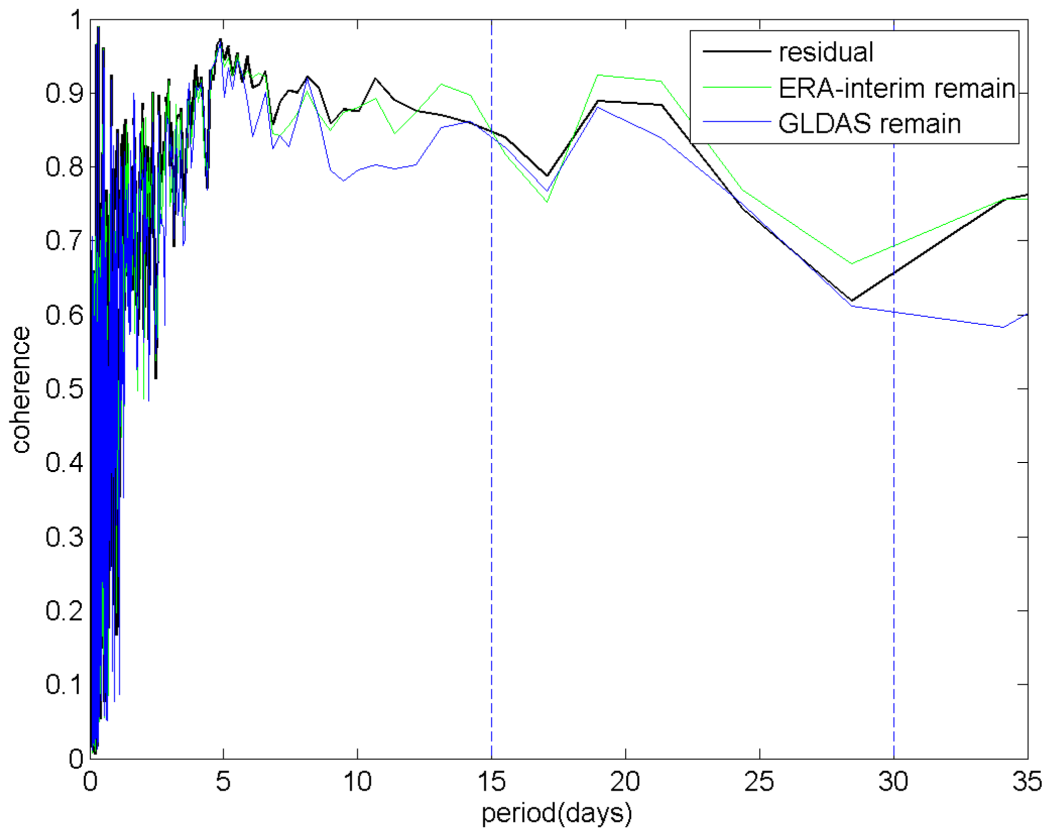

Figure 5.23: *Same as figure 5.22, but for period 0-35 days. The coherence of residuals and hydrological effects removed remaining signals at the two stations. In general, gravity residuals and remaining signals have high coherence at short period.*

5.7 Comparing gravity residuals from SG measurements and GRACE predictions

Mr. Franz Barthelmes (GFZ, Potsdam) helped calculating the gravity disturbances of the two stations from GRACE measurements (monthly solution of gfz-release-05) for the 4 filters DDK2, DDK3, DDK4, DDK5. The details of processing models are described by Dahle et al. (2012). Some of the effects (atmospheric effects, tides,...) are already corrected in these results. The remaining signals are mainly hydrological effects, the same as the SG gravity residuals before correcting the hydrological effects.

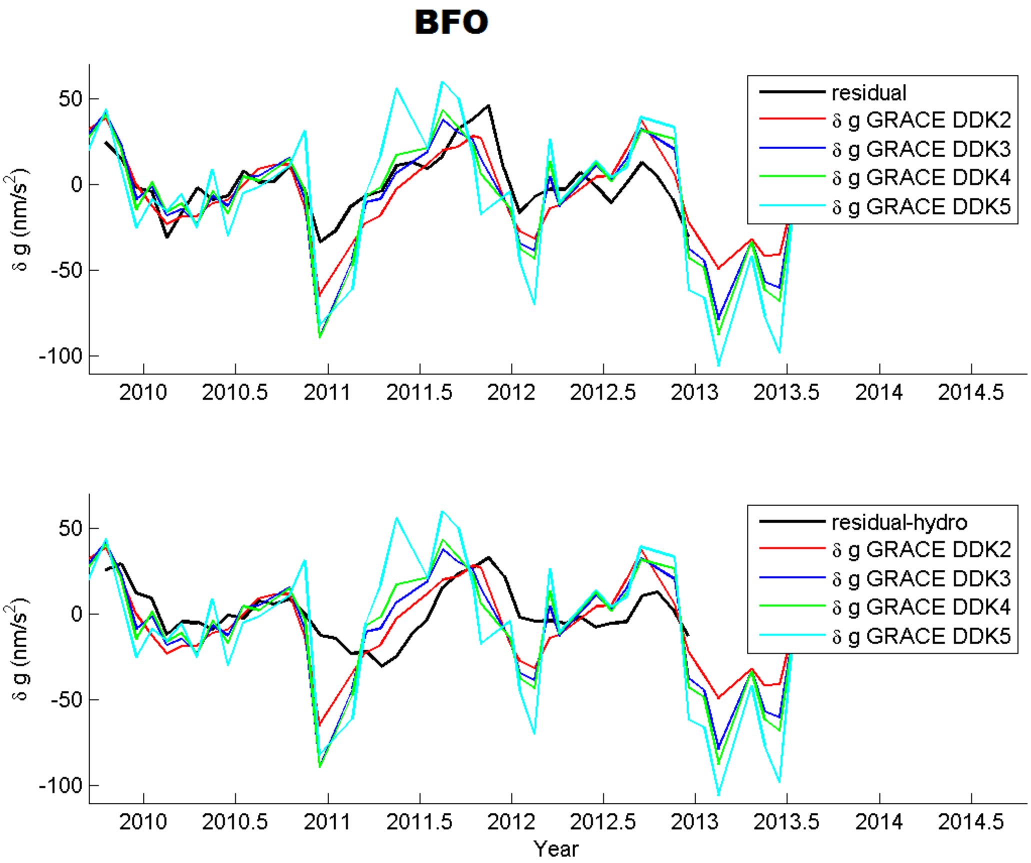

Figure 5.24: *Comparing gravity residuals from SG measurements and GRACE predictions at BFO (unit: nm/s²). The black curves are the gravity residual (in the upper panel) and the remaining signal after correcting for the local hydrological effect using GLDAS model (in the lower panel). The colored curves are the GRACE predictions of gravity variations using different filters.*

Figure 5.24 and figure 5.25 show the gravity residuals from SG measurements and GRACE measurements at BFO and ST respectively. As stated above, it is more reasonable to compare the GRACE results with the SG residuals before correcting the local hydrological effects, as the upper figures show. Different filters give different estimations of the variations. The difference of filters can be as large as 40 nm/s^2. For most months at BFO and ST, the gravity residuals from the two different data sources agree well. Around December 2010, the discrepancies are relative large (amounts to about 50 nm/s^2 for DDK4 solutions at BFO, about 60 nm/s^2 for DDK3 solutions at ST). It seems the residuals from SGs are somehow damped in this period. After correcting hydrological effects for SG residuals, the discrepancies comparing to GRACE solutions increase. The SG residual at ST becomes anti-phase with GRACE residual.

Table 5.5 shows the statistics of gravity residuals (as shown in line 1 in table 5.5), remaining signals after correcting for local hydrological effect using GLDAS model (line 2), the GRACE predictions of gravity variations (lines 3 – 6) and the differences between gravity residual and GRACE predictions (lines 7 – 10). DDK2 has larger filtering radius than DDK3, and DDK3 has

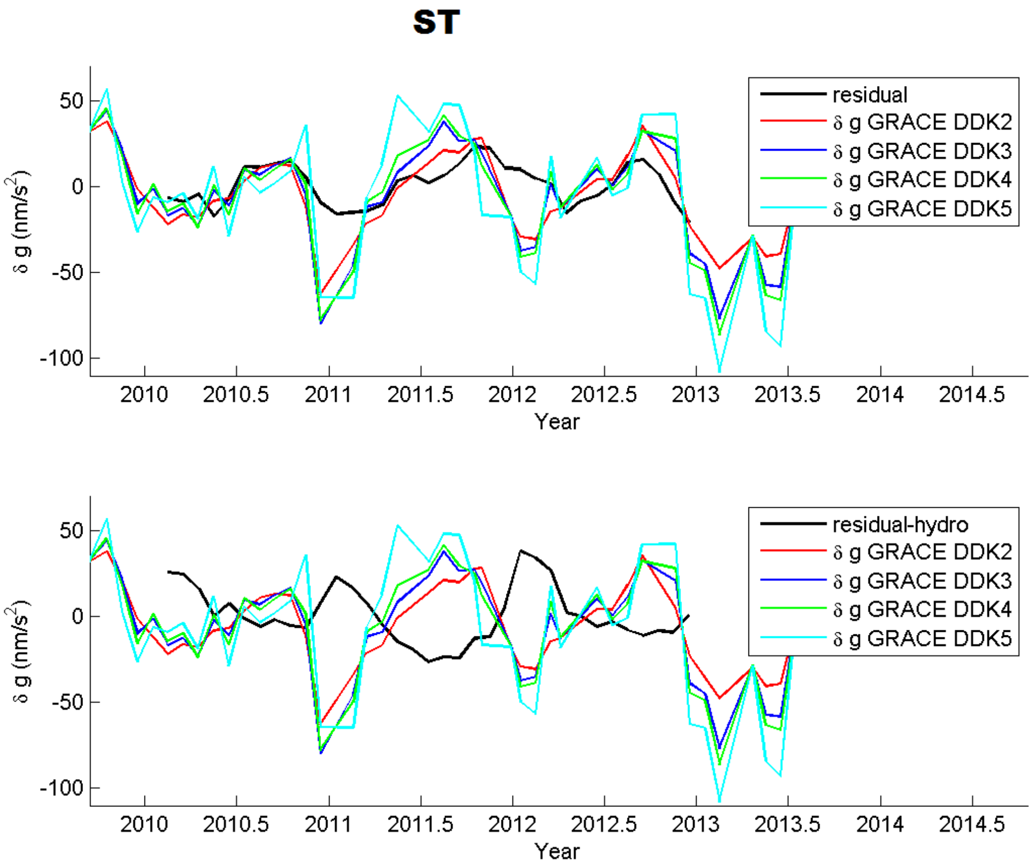

Figure 5.25: *The same as figure 5.24, but for ST (unit: nm/s^2). The black curves are the gravity residual (in the upper panel) and the remaining signal after correcting for the local hydrological effect using GLDAS model (in the lower panel). The colored curves are the GRACE predictions of gravity variations using different filters.*

	BFO	ST
residual	17.3	12.0
hydro. remain	15.3	16.4
GRACE DDK2	24.1	23.7
GRACE DDK3	29.4	29.0
GRACE DDK4	31.0	30.7
GRACE DDK5	38.8	38.5
residual - GRACE DDK2	22.5	24.5
residual - GRACE DDK3	28.6	30.6
residual - GRACE DDK4	31.2	33.1
residual - GRACE DDK5	40.6	42.6

Table 5.5: *The standard deviations of gravity residuals, remaining signals after correcting for local hydrological effects using GLDAS model , the GRACE predictions of gravity variations and the differences between gravity residual and GRACE predictions (unit: nm/s^2, monthly data). Note the standard deviations of gravity residuals and remaining signals are not comparable with the values in table 5.3, since here monthly data series are used and as in table 5.3, the statistics are calculated using hourly data.*

larger filtering radius than DDK4, and so on. In general, larger filter radius in GRACE data filtering leads to smaller standard deviation of the GRACE prediction as shown in table 5.5. And if the GRACE predictions are subtracted from the gravity residuals separately (as shown in lines 7 – 10 in table 5.5), these remaining signals have different standard deviation. The remaining signals corrected for GRACE DKK2 predictions have smallest standard deviations for both BFO and ST. More details about these filter can be found in Kusche et al. (2009). GRACE solutions have larger standard deviations than the gravity residuals.

Chapter 6

Conclusions

From the analysis above, we come to the following conclusions. The measurements of OSG-056 at BFO give excellent results with long period stability. No disturbance which can not be corrected has happened in the three and a half years. The GWR C026 has also stable measurements, except some disturbances in January 2010.
The gravity residuals after correcting for the atmospheric effect and the solid earth tides show clear influence of polar motion. When polar motion effects are further corrected, the residual signal of ST contains linear drift in the period from Feb. 2010-Dec. 2012. And for BFO, in the first half a year (from Oct. 2009 to Mar. 2010), the drift is exponential and after this period, the drift is linear. Our estimates of the drift rates agree well with values published in the literatures. After further corrected for the linear drift components, the gravity residuals of BFO and ST show clear annual variations of 110 nm/s^2 and 80 nm/s^2 respectively, which are dominated by hydrological effects. BFO has larger hydrological signal than ST. This was not to be expected, because of the hydrological settings and the distance from the SGs to the ground surfaces.
The three hydrological models which we have considered here have different estimations of local hydrological effects for the two stations. The non-local hydrological effects are similar for the two stations in all three models, which is not surprising, considering the short distance between the two stations. GLDAS and ERA-interim hydrological models have better performance in explaining the gravity residuals than ECMWF operational model in the time domain as well as in the frequency domain. The local hydrological effects have differences ranging from a few nm/s^2 to 50 nm/s^2 from gravity residuals. The maximum magnitude of deviation has comparable scale to the gravity residual itself. The maximum difference of GLDAS and ERA-interim is about 20 nm/s^2. As there is no higher quality model as a reference, the difference of these two models gives an idea of hydrological modelling accuracy. The gravity variations due to rain events have been modeled with a very simple model. The convolved rain effect fits well with the gravity residual, especially in some massive precipitation events. But as the gravimetric effect of convolved rain model has only short period component, this model can not give a whole picture of rain events' influence on gravity variations for periods longer than 40 days. Considering the relatively large grid sizes of the hydrological models and a lack of in situ hydrological survey, the local hydrological model can not represent the real hydrological situation of the stations with high accuracy, therefore careful investigation of the local hydrological situation is needed when these auxiliary data are available. Correcting the local hydrological effects using models GLDAS, ERA-interim and ECMWF reduces the variations of gravity residuals in the period from 3 months to 1 year significantly. The difference of residuals between two stations is enlarged after correcting for the local hydrological effects. This is caused by the error accumulation when calculating the

difference of not perfectly modelled hydrological corrections.
The coherence between gravity residuals and hydrological effects is strong at periods longer than 70 days. The coherence between the residuals of two stations ranges from 0.65 to 0.9 at periods from 15 days to 30 days. Correcting for the local hydrological effects using GLDAS model or ERA-interim does not improve the coherence from 15 days to 30 days significantly. The SG residuals agree well with GRACE predictions of gravity variations in most months of comparison.
Considering the relative large discrepancy of the two stations' gravity residuals in some period of comparison, whether SG data is suitable for validating GRACE data is still in doubt.

Bibliography

Amalvict, M., Hinderer, J., Gegout, P., Rosat, S. and Crossley, D. [2002], 'On the use of AG data to calibrate SG instruments in the GGP network', *Bulletin d'Information des Marees terrestres* **135**, 10621–10626.

Amalvict, M., Hinderer, J. and Rózsa, S. [2006], 'Crustal vertical motion along a profile crossing the Rhine graben from the Vosges to the Black Forest Mountains: Results from absolute gravity, GPS and levelling observations', *Journal of Geodynamics* **41**, 358–368.

Boy, J. [n.d.], Atmospheric, oceanic & hydrological loading for global geodynamics project sites. http://loading.u-strasbg.fr/GGP/.

Boy, J.-P., Hinderer, J., Amalvict, M. and Calais, E. [2000], 'On the use of long records of superconducting and absolute gravity observations with special application to the Strasbourg station, France', *Cahiers du Centre Européen de Géodynamique et de Séismologie* **17**, 67–83.

Crossley, D. [1998], Comprehensive analysis of 2 years of SG data from Table Mountain, Colorado, *in* 'Proc. 13th Int. Symp. Earth Tides', Obs. Royal Belgique, Brussels, pp. 659–668.

Dahle, C., Flechtner, F., Gruber, C., König, D., König, R., Michalak, G. and Neumayer, K. [2012], 'GFZ GRACE level-2 processing standards document for level-2 product release 0005', *Scientific Technical Report-Data* **12**, –.

GWR Instruments, I. [2011], Observatory Superconducting Gravimeter (OSG). Rev 1.0.

Hager, B. H. [2002], *Essentials of Geophysics*, chapter 2, p. 49.

Harnisch, M. and Harnisch, G. [2002], 'Seasonal variations of hydrological influences on gravity measurements at Wettzell', *Bull. d'Inf. Marees Terr* **137**, 10849–10861.

Kroner, C., Jahr, T. and Jentzsch, G. [2004], 'Results from 44 months of observations with a superconducting gravimeter at Moxa/Germany', *Journal of Geodynamics* **38**(3), 263–280.

Kusche, J., Schmidt, R., Petrovic, S. and Rietbroek, R. [2009], 'Decorrelated grace time-variable gravity solutions by gfz, and their validation using a hydrological model', *Journal of Geodesy* **83**(10), 903–913.

Prothero, W. A. and Goodkind, J. M. [1972], 'Earth-tide measurements with the superconducting gravimeter', *J. Geophys. Res.* **77**(5), 926–937.

R. Widmer-Schnidrig, W. Zürn, P. D. T. F. [2012], The dual-sphere Superconducting Gravimeter at BFO – long-period signals and instrumental drift, *in* 'DGG/EAGE Workshop 2012'.

Richter, B. [1983], 'The long-period tides in the earth tide spectrum', *IAG Symp., 18th IUGG General Assembly, Hamburg* **1**, 204–216.

Richter, B. [1990], 'The long period elastic behavior of the earth', *Variations in Earth Rotation* pp. 21–25.

Schubert, G. and Price, G. D. [2007], *Treatise on geophysics*, Elsevier.

Vauterin, P. and Van Camp, M. [2011], *TSoft Manual*, version 2.1.6 edn, Royal Observatory of Belgium.

Wahr, J. M. [1985], 'Deformation induced by polar motion', *Journal of Geophysical Research: Solid Earth (1978-2012)* **90**(B11), 9363–9368.

Warburton, R. J., Beaumont, C. and Goodkind, J. M. [1975], 'The effect of ocean tide loading on tides of the solid earth observed with the superconducting gravimeter', *Geophysical Journal International* **43**(3), 707–720.

Warburton, R. J. and Goodkind, J. M. [1977], 'The influence of barometric-pressure variations on gravity', *Geophysical Journal International* **48**(3), 281–292.

Wenzel, H.-G. [1996], 'The nanogal software: Earth tide data processing package ETERNA 3.30', *Bull. Inf. Marees Terrestres* **124**, 9425–9439.

Wenzel, H.-G. [n.d.], *Manual ETERNA34*, Black Forest Observatory.

Xu, J.-Q., Sun, H.-P. and Yang, X.-F. [2004], 'A study of gravity variations caused by polar motion using superconducting gravimeter data from the GGP network', **78**(3), 201–209.